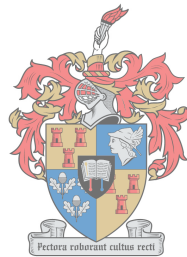# Variable Bandwidth Planar Coupled Resonator Filters Utilizing Tunable Non-Resonant Node Inverters

by

Satyam Kumar Sharma

UNIVERSITEIT
iYUNIVESITHI
STELLENBOSCH
UNIVERSITY

Dissertation presented for the degree of Doctor of Philosophy in Electronic Engineering in the Faculty of Engineering at Stellenbosch University

Supervisor: Prof. Petrie Meyer

December 2018

Declaration

By submitting this dissertation electronically, I declare that the entirety of the work contained therein is my own, original work, that I am the sole author thereof (save to the extent explicitly otherwise stated), that reproduction and publication thereof by Stellenbosch University will not infringe any third party rights and that I have not previously in its entirety or in part submitted it for obtaining any qualification.

Date: . . . . December 2018 . . . .

i

Abstract

Variable Bandwidth Planar Coupled Resonator Filters Utilizing Tunable Non-Resonant Node Inverters

S.K. Sharma

Dissertation: Ph.D.(EE)

December 2018

This dissertation presents a novel design technique for designing microstrip staircase and pedestal substrate integrated waveguide (SIW) filters with tunable bandwidth. The design technique utilizes non-resonant nodes as inverters, allowing the inter-resonator coupling to be varied by varactor diodes.

For the microstrip implementation, a circuit model of the proposed tunable non-resonant node inverter (NI) to be implemented in parallel coupled line staircase filter is presented. Generalized synthesis design equations are formulated and dimensional design charts are presented to aid designers in designing tunable staircase filters using NI. Reconfigurable second order and third order parallel coupled line staircase filters with constant absolute bandwidth are designed and measured.

For the substrate integrated waveguide (SIW) implementation, the proposed tunable non-resonant node inverter is implemented in a T-ridge pedestal SIW resonator based filter topology. A detailed dimensional analysis for integrating NI in T-ridge SIW filters is presented and design charts are formulated. A design procedure is proposed to design NI based T-ridge SIW filters with bandwidth control for a given filter specification. A second order T-ridge SIW filter with tunable bandwidth is designed and simulated.

The designed reconfigurable filters using NI offer significant advantages over most of the other reconfigurable filter designs. The proposed synthesis method comprising of design equations and design charts presents an insight into the dimensional information required to design these filters for a given specification. Further, it reduces the reliance on full wave optimization and thus results in reduced computational cost and design time. The designed and measured prototype filters based on NI demonstrate negligible centre frequency deviation as the bandwidth is tuned. The use of spatial biasing mechanism reduces the complexity of the filter designs as additional biasing circuit is not required to bias tuning elements.

Uittreksel

Verstelbare bandwydte planêre gekoppelde resoneerder filters met verstelbare Nie-Resonante-Nodus omkeerders

S.K. SharmaProefskrif:

Ph.D.(EE)

Desember 2018

Hierdie proefskrif bied 'n nuwe ontwerpstegniek aan vir die ontwerp van mikrostrook- en oppervlak-geïntegreerde-golfleier (OGG)-filters met verstelbare bandwydte. Die tegniek gebruik nie-resonante nodusse as omkeerders en maak dit moontlik vir tussen-resoneerder koppelings om verstel te word deur varaktor diodes.

Vir mikrostrook implementerings word 'n stroombaanmodel van die voorgestelde omkeerder in newe-gekoppelde trap-filters aangebied. Veralgemeende sintese vergelykings word geformuleer en strukturele ontwerpsgrafieke word aangebied om ontwerpers in staat te stel om hierdie klas van filters te ontwerp. Verstelbare tweede en derde orde filters met konstante absolute bandwydte word ontwerp en gemeet.

Vir OGG-implementering, word die voorgestelde tegniek ge-implementeer as 'n gevoude T-rif filter topologie. 'n Detail strukturele analise word aangebied, sowel as 'n ontwerpsprosedure. 'n Tweede orde filter word ontwerp en gesimuleer.

Die gebruik van hierdie tegniek bied beduidende voordele bo meeste ander verstelbare topologieë. Die voorgestelde sintese tegniek, bestaande uit ontwerpsvergelykings en ontwerpsgrafieke, bied ook insig in die strukturele aspekte wat benodig word om 'n gegewe spesifikasie te haal. Dit verminder verder die afhanklikheid op volgolf analise, en dus ook die berekeningskoste en ontwerptyd. Die prototipes demonstreer weglaatbare senterfrekwensieveranderinge met verstelling van bandwydte. Die gebruik van ruimtelike voorspanning verminder die stroombaankompleksiteit.

Acknowledgements

I would like to acknowledge the role of the following people and organizations in making this research work possible:

- I would like to thank my parents for believing in me and supporting my decision to pursue higher studies. Without their motivation and support, this work would have not been possible.

- I would like to express my gratitude to Prof. Petrie Meyer for giving me an opportunity and hosting me in his research group in South Africa. Prof. Meyer introduced me to the world of RF and Microwave engineering which is a gift for a lifetime. He encouraged and allowed me to pursue different courses apart from my main research theme which has broaden my view on the subject. His expertise in microwave networks is unmatched. He has been a perfect mentor, showed confidence in me when I doubted myself. Non-academically, I was inspired by him to improve my fitness level.

- National Research Foundation (NRF) and Department of Electrical and Electronic Engineering, SU, for the financial assistance.

- All the seniors in the research group: David, Theunis, Shamim, Dewald and Elmine with whom I shared the office space. They were always ready to help and made my transition to South Africa easy. I would like to thank Shamim mam for discussions on SIW design and filter queries in general. I would like to thank Elmine for sharing her knowledge on tuning elements and helping me with the varactor samples.

- All the other members of the group for their companionship: Susan mam, Raven, Geomarr, Peter and Leanne.

- Wessel Croukamp and Wynand van Eeden for manufacturing the filter prototypes which worked perfectly. Ms. Anneke Bester for helping me with the measurements.

Dedications

Dedicated to my parents, Sudha and Indresh Sharma.

Contents

CONTENTS **viii**

List of Figures

LIST OF FIGURES xi

List of Tables

Chapter 1

Introduction

1.1 Tunable Filters

Microwave filters are integral parts of the transmitter/receiver sections of modern day wireless systems such as mobile communications, satellite television, wireless-local area networks (W-LANs), radars etc. Filters play vital roles of separating wanted signal frequencies from unwanted signal frequencies in these systems. Wireless broadband technologies are constantly evolving at a rate that will outgrow the available spectrum. As the spectrum is limited, advanced wireless systems are being investigated with intended characteristics of having multifunctional trans-receiver subsystems that can operate in multiple frequency bands, are faster, have reduced interference and have reduced size. These wireless systems demand improved microwave filter designs which are completely reconfigurable and are miniaturized. Present wireless systems suffer from many factors that degrade their performance. With a number of wireless systems utilizing different frequency bands, there is often interference between these bands resulting in problems like frequent call dropping. Limited frequency spectrum results in high call rates and data rates. Bulky size prevents installation of wireless systems in congested places. Reduced board space is always desirable in a wireless system circuit. Design of new tunable microwave filters would help in eradicating these problems, resulting in improved performance of current and future wireless systems. Figure 1.1 shows considerable reduction in the size of the front-end of modern wireless systems with the use of tunable filters.

Over the last couple of decades, a vast number of tunable microwave filters have been proposed in different technologies depending upon the intended application. Tunable filter designs in microstrip, coaxial cavities, waveguide, microwave monolithic integrated circuits (MMICs) and substrate integrated waveguide (SIW) technologies have been investigated. The advent of tunable filters began with the tuning of centre frequency of the filter followed by investigation of tuning the bandwidth, external Q and transmission zero responses of the filter. The centre frequency tuning is achieved by connecting variable reactance elements like p-i-n diodes, semiconductor varactor diodes and micro-electromechanical systems (MEMS) to the resonators of the filter resulting in tunable resonators [1–15]. Centre frequency tuning by integrating active devices to the resonators for loss compensation and improved performance have also been proposed in the litera-
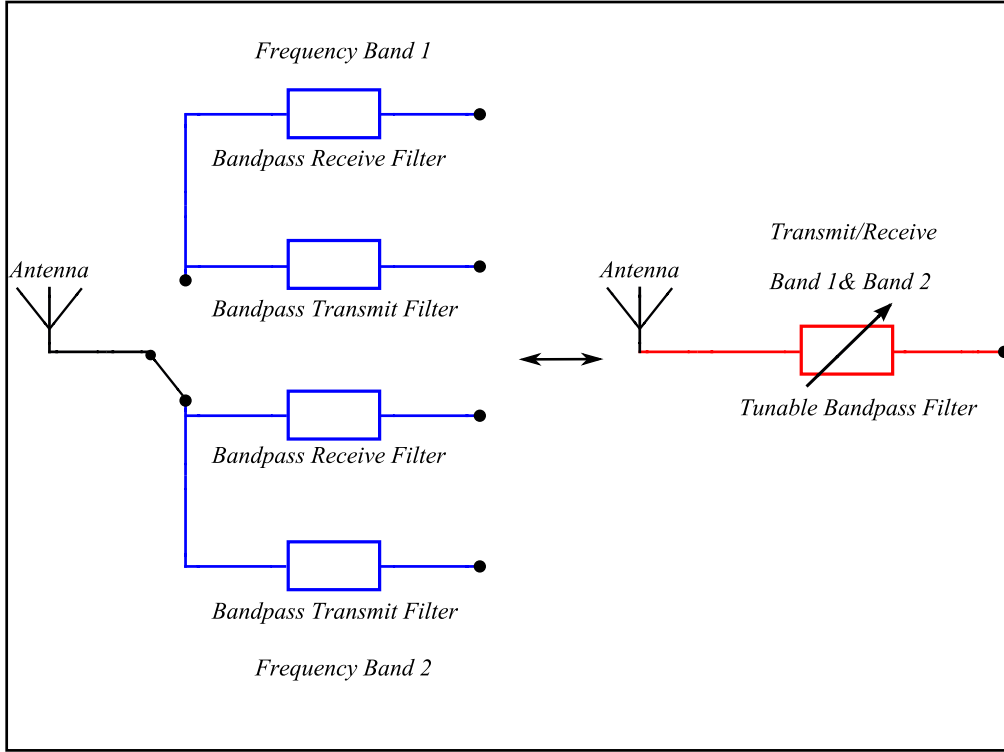
Figure 1.1: Front-End System

ture [16–20].

Most of the current tunable filters suffer from change in bandwidth when tuning the centre frequency. Bandwidth control is more difficult than frequency control, as the inter-resonator couplings need to be adjusted, and not only the resonator frequencies. Bandwidth control has thus far been demonstrated with various mechanisms in different implementation technologies [21–43]. The planar combline filter topology has been a popular choice, due to its inherent small bandwidth variation as the centre frequency is tuned. In [21], a three pole combline tunable filter with centre frequency and bandwidth tuning is presented. The filter consists of three short-ended resonators with varactor diodes attached on the opposite end for centre frequency tuning. A pair of diodes are connected between the first and last resonators in back to back configuration for bandwidth tuning. A pair of transmission zeros are realized because of the non-adjacent coupling between the first and last resonators. In [22], a three pole tunable combline bandpass filter with centre frequency, bandwidth and transmission zero control is presented. The centre frequency is controlled using varactor diodes attached to the resonator of the filter while the bandwidth is controlled by placing two varactor diodes in back to back configuration between the adjacent resonators. Transmission zeros are tuned by placing a pair of varactor diodes at the input and output matching networks. In [23], stepped-impedance resonators are used in a basic combline structure. Absolute passband bandwidth is maintained at nearly constant values within the tuning range, by reducing magnetic coupling due to a larger gap near the short circuit ends of the stepped impedance resonator. Inter-resonator coupling is controlled in [24] with the use of lumped series resonators with controllable slope parameters, attached to planar resonators of a combline filter. In [25], a bandwidth

control subnetwork is proposed to tune inter-resonator couplings in combline filters. The bandwidth control subnetwork comprises of a coupling reducer element connected in shunt between adjacent resonators. The coupling reducer element is made up of a transmission line segment with variable capacitor attached at one end while the other end is short circuited. The length of this transmission line is longer than the adjacent resonators, thus forming a resonator which resonates at a lower frequency, or a detuned resonator at the filter centre frequency. As the variable capacitor is varied, the admittance of the coupling reducer varies between open and short circuited states resulting in variation in bandwidth. For large variable capacitance, highest variable admittance of coupling reducer is obtained, which results in a short circuit condition in between resonators and hence minimum bandwidth is achieved. In [26], corrugated microstrip coupled lines are used in combline structures to design a constant bandwidth tunable filter.

Ring resonators have also been studied to develop reconfigurable filters. In [27], electric and magnetic couplings between ring resonators are varied to realize different coupling coefficients. In [28], centre frequency tuning is obtained by switching between quarter-wavelength and half-wavelength resonators to obtain low-band and high-band modes, whereas, bandwidth is controlled by a combination of electric and magnetic coupling variation. In [29], a ring resonator loaded with two tunable pi-sections operating as open stubs is proposed to implement bandwidth reconfigurability. An even and odd mode frequency analysis is presented for a ring resonator loaded with two open circuited stubs and it is established that for switching the bandwidth from a narrowband to a wideband state, characteristic impedance of the open circuit stub needs to be changed from a higher to a lower value. Further, an analysis is done using EM simulations and an equivalence is demonstrated between an open circuit stub and a pi-section comprising of two p-i-n diodes. Finally, open circuit stubs connected to the ring resonators are replaced by pi-sections loaded with p-i-n diodes. By switching the p-i-n diodes, narrowband (4 pole) and wideband (6 pole) responses are realized. In [30], a mixed combline and split ring topology has been utilized to develop a constant bandwidth tunable filter.

Reconfigurable filters using cross shaped resonators and hairpin resonators have also been investigated. In [31], a wideband reconfigurable bandpass filter based on cross-shaped resonator (CSR) with open circuit stubs is presented. The open stubs consists of stepped impedances of three branches connected through p-i-n diodes. The location of the poles are determined through the on/off states of p-i-n diodes. A narrowband to wideband response is realized using different switching states of p-i-n diodes. In [32], a third order hairpin filter design is presented with centre frequency and bandwidth tuning. Centre frequency tuning is achieved with the help of tunable hairpin resonators with varactor diodes attached to the ends of the resonators. Bandwidth is controlled by attaching varactor diodes between adjacent resonators. Three different tuning elements comprising of semiconductor varactor diodes, BST thin film and BST thick film varactor diodes are analysed and implemented in the designed hairpin tunable filter. Evaluation and comparison of the performance of the three tuning elements in the filter is presented.

Waveguide based reconfigurable filters have been proposed in [33–35]. A two pole tunable substrate integrated waveguide (SIW) filter is presented in [33] where RF MEMS

are utilized as tuning elements. The resonators are tuned by perturbing each SIW cavity with perturbing metallic posts between the top and bottom metal layers. A total of six metallic posts are utilized for fifteen frequency states, out of which, four are for coarse frequency tuning while two are for fine tuning. The placing of the metallic posts in the SIW cavity is analysed using an EM simulator and a constant fractional bandwidth is obtained by placing tuning posts in regions within the cavity where external quality factor shows relatively less variation. In [34], inter-resonator couplings are mechanically tuned using out-of-band resonators between the main resonators. In [35], inter-resonator couplings are changed using varactor diodes positioned between evanescent-mode cavity resonators, while the centre frequency is tuned using piezoelectric actuators attached to the resonators.

1.2 Motivation

Current bandwidth control mechanisms suffer from the following challenges:

- Most of the current solution methods for tuning of bandwidth result in deviation of the center frequency of the filter as the bandwidth is tuned. The available designs present little design information, are suitable only for low order filters and are optimized.

- The external bandwidth control sub-network proposed, comprise of chip inductors, PIN diodes and varactor diodes attached to the filter resonators. These are low Q components and load the resonators. Use of these elements result in a degradation of the transmission performance of the filter.

- Continuous centre frequency and bandwidth control is difficult to achieve in designs using switchable open stubs attached to the main filter resonators.

- The external bandwidth control circuit employs biasing circuitry to implement tuning components, resulting in an increase of the overall complexity of the design of the filter.

There is therefore a need to investigate new filter topologies which have functionality of continuous bandwidth tuning with minimum centre frequency deviation. The filter should have the ability to maintain constant absolute bandwidth (CAB) as well as constant fractional bandwidth (CFB) at different centre frequencies. The tunable filters should have a simple biasing circuitry with reduced losses. A generalized synthesis method to design N^{th} order reconfigurable filters need to be proposed which takes into account the design parameters of the external tuning elements.

1.3 Contributions

In both [25] and [34], bandwidth control is achieved using a form of variable detuned resonator between resonators, respectively for combline and waveguide structures. In this dissertation, a general procedure for bandwidth control of coupled resonator filters is

proposed based on the insertion of tunable non-resonant nodes between resonators. This procedure can be seen to represent a generalization and formalization of the work in [25] and [34]. A new type of tunable inverter which utilizes non-resonant nodes is proposed, and applied for the first time to coupled line staircase microstrip filters, and pedestal substrate integrated waveguide filters.

In order to design tunable microstrip filters based on NI, a detailed dimensional analysis of the NI-structure is performed and the effect of dimensional variation on the coupling coefficient between resonators is studied. A synthesis method is proposed in order to extract dimensional parameters to design microstrip filters based on NI. With the use of NI, the bandwidth control mechanism of the filter is almost completely separated from the resonant frequency tuning of the resonators and results in negligible deviation in centre frequency as the bandwidth is varied. A second order chebyshev filter prototype based on non-resonant node inverter (NI) is designed and measured. Parallel coupled line topology in microstrip technology is chosen for the implementation of the filter. A constant absolute bandwidth (CAB) of 200 MHz (3 dB bandwidth) is maintained across centre frequency tuning range varying from 4.0 GHz to 4.7 GHz. Insertion loss varies between -3.45 dB and -8.60 dB while return loss maintains an approximately constant value of -15 dB. The filter works as an independent bandwidth tunable filter with 3 dB bandwidth varying from 180 MHz to 250 MHz at a constant center frequency of 4.7 GHz with insertion loss minimizing from -4.4 dB to -3.74 dB and return loss improving from -12 dB to -25 dB. The dimensions of the designed filter are 16x44 mm.

Two third order filters are designed and measured. The first third order chebyshev filter based on NI is designed and implemented in microstrip parallel coupled line topology. The filter maintains a constant absolute bandwidth of 210 MHz (3 dB bandwidth) across the entire centre frequency tuning range varying from 3.54 GHz to 4.54 GHz. The insertion loss varies between -4.94 dB to -11.39 dB while return loss varies between -4.3 dB to -11 dB. The filter works as an independent bandwidth tunable filter with 3 dB bandwidth varying from 207.6 MHz to 281 MHz at a constant centre frequency of 5.2 GHz. A second third order filter prototype based on NI is developed with an additional circuitry attached to the feed lines in order to tune the external quality factor of the circuit. As the centre frequency of the filter is varied from 4.05 GHz to 4.75 GHz, a constant absolute bandwidth of 210 MHz (3 dB bandwidth) is maintained across the entire centre frequency tuning range. The insertion loss varies between -5.6 dB to -8.9 dB while a constant return loss of -10 dB is maintained. The filter also works as an independent bandwidth tunable filter at a centre frequency of 4.65 GHz with 3 dB bandwidth varying from 170 MHz to 230 MHz with a constant return loss of -10 dB. The dimensions of the designed third order filters are 18x44 mm.

The proposed non-resonant node inverter is further implemented in substrate integrated waveguide (SIW) technology. A design procedure is proposed and followed to design a second order T-ridge pedestal SIW resonator filter with bandwidth tuning using the proposed NI. The simulated filter response shows a bandwidth increase of 31% from 200 MHz to 262 MHz with negligible deviation in the centre frequency. The simulated response demonstrates significant bandwidth variation with acceptable insertion and re-

turn losses thus validating the design technique.

The original contributions of this thesis can be outlined as:

1. The functionality of non-resonant nodes for the purpose of tuning inter-resonator couplings in coupled resonator filters is formalized and extended. A general tunable non-resonant node inverter (NI) is presented.

2. Implementation of the proposed design procedure in coupled line staircase microstrip second order and third order filter designs.

3. Implementation of the design technique in pedestal substrate integrated waveguide (SIW) based second order filter.

4. A generalized design procedure to implement NI in tunable filters. The design procedure comprises of synthesis design equations and design charts to provide designers with the required dimensional information to design filters based on NI. This prior dimensional insight would reduce the reliance on optimization of dimensional parameters, thus, reducing the computational cost and design time to design filters with bandwidth control using NI.

1.4   Layout of the Thesis

Chapter 2 provides literature review of the fundamentals of coupled resonator filters in order to build a theoretical foundation for the concepts to be introduced in subsequent chapters. Classical filter response functions and their synthesis procedures are reviewed. Transformations from the low pass prototype filter to other classes are outlined. The theory of immittance inverters in coupled resonator filters is reviewed. Derivations of the coupling coefficients for lowpass prototype filters and corresponding band pass filters with immittance inverters is presented. A comprehensive listing of commonly used inverter models in filter network theory is presented followed by a section reviewing external tunable components for microwave circuits. The chapter ends with a section reviewing the use of non-resonant nodes in coupled resonator filter networks.

Chapter 3 presents the main theme of the research work which is based on the theory of non-resonant node inverters in filter networks. Chapter 3 begins with the development of non-resonant node inverters (NI) to be implemented in microstrip technology. A circuit model for the proposed non-resonant node based inverters is developed. A synthesis method comprising of design equations is presented. Dimensional analysis of the NI parameters are studied with the help of an EM simulator and the results are compared with the results of the synthesis method. This is followed by the application of the developed theory to a design example based on second order parallel coupled line microstrip filter. The developed technique of non-resonant node inverter is then implemented in SIW technology. Dimensional analysis of the NI parameters is performed with the help of an EM simulator and a design procedure is proposed. Finally, the proposed design procedure is

utilized to design a second order T-ridge pedestal SIW filter with bandwidth tuning based on NI.

In chapter 4, the prototypes developed for the microstrip filters based on NI are presented. Measured responses of the designed second order and third order filters with tunable frequency and bandwidth are discussed. Measured results of a third order filter with tunable centre frequency, bandwidth and external quality factor are discussed.

Chapter 5 presents the conclusion of the research work presented in the dissertation which is followed by recommendations for the future work.

Chapter 2

Coupled Resonator Filter Theory

In this chapter, a number of basic filter concepts are reviewed in order to facilitate the understanding of the main research work of this dissertation presented in the subsequent chapters. Low pass prototype networks and circuit transformations are discussed. Coupled resonator filters using immittance inverters and corresponding design equations are presented. It is followed by a section discussing the commonly used immittance inverter models in filter networks. A section on tunable elements that are utilized in tunable filters is presented. The chapter ends with a background on the use of non-resonant nodes in coupled resonator filters.

2.1 Classical Lowpass Filter Theory

This section describes the characteristic function and transfer function definitions for classical filter responses like maximally flat, chebyshev response, elliptic response etc. These response functions are synthesized into low pass prototype networks which form the basis to derive other filter networks like bandpass and bandstop. As the filters presented in this dissertation are based on chebyshev filter response, a detailed discussion on chebyshev transfer functions is presented.

2.1.1 Filter characteristic functions and transfer functions

The definitions of characteristic function and transfer function are utilized to study different classes of classical filter responses like the Maximally flat response, the Chebyshev response etc. As shown in figure 2.1, for a doubly terminated network, the ratio of maximum available power,P_{max}, to the power delivered to the load,P_2, is given by [44]:

$$\frac{P_{max}}{P_2} = \left| \frac{1}{2} \sqrt{\frac{R_2}{R_1}} \frac{E}{V_2} \right|^2 = \frac{1}{4} \left| \frac{E}{V_2} \right|^2 \text{ for } R_1 = R_2 \tag{2.1}$$

The transfer function H_s for a lowpass filter network is defined as the ratio of maximum available power to the power delivered to the load,

$$|H(s)|^2_{s=j\omega} = \frac{P_{max}}{P_2} \tag{2.2}$$

8
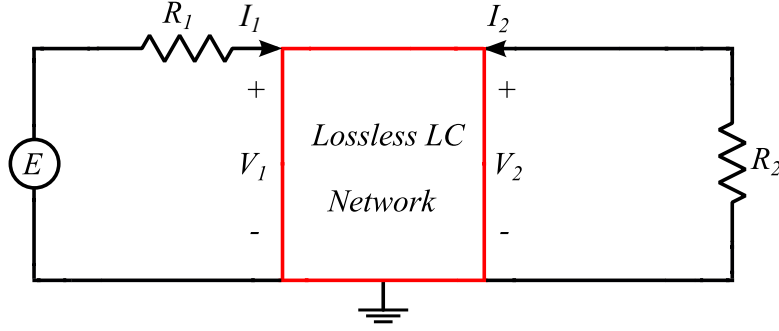
Figure 2.1: Doubly terminated lossless transmission network

The characteristic function $K(s)$ is a rational function in $s = j\omega$ with real coefficients defined as,

$$\frac{P_{max}}{P_2} = 1 + |K(s)|^2_{s=j\omega} \tag{2.3}$$

therefore, the transfer function and characteristic function are related by,

$$|H(s)|^2_{s=j\omega} = 1 + |K(s)|^2_{s=j\omega} \tag{2.4}$$

The characteristic and transfer functions can be described in terms of characteristic polynomials. Firstly, defining the reflection coefficient,

$$|\rho(j\omega)|^2 = \frac{\text{reflected power}}{\text{maximum available power}} = \frac{P_r}{P_{max}} \tag{2.5}$$

and the transmission coefficient as,

$$|t(j\omega)|^2 = \frac{\text{transmitted power}}{\text{maximum available power}} = \frac{P_2}{P_{max}} = 1 - |\rho(j\omega)|^2 \tag{2.6}$$

Utilizing two port network theory, the reflection coefficient can be written as,

$$\rho(s) = \frac{z(s) - 1}{z(s) + 1} = \frac{n(s) - d(s)}{n(s) + d(s)} = \frac{F(s)}{E(s)} \tag{2.7}$$

Here, $z(s)$ represents normalized impedance of the two port network with respect to source port resistance R_1 as shown in figure 2.1. Impedance $z(s)$ is a positive real function which can be represented as the ratio of the two polynomials $n(s)$ and $d(s)$

$$z(s) = \frac{n(s)}{d(s)} \tag{2.8}$$

Writing the reflection and transmission coefficients in terms of characteristic polynomials,

$$\rho(s) = \frac{F(s)}{E(s)} \tag{2.9}$$

and

$$t(s) = \frac{P(s)}{E(s)} \tag{2.10}$$

The transmission function and the characteristic function can be written in terms of characteristic polynomials as,

$$|K(s)|^2_{s=j\omega} = \frac{|\rho(j\omega)|^2}{|t(j\omega)|^2} = \frac{P_r}{P_t} \tag{2.11}$$

where P_r and P_t represent the reflected power and transmitted power respectively.

$$H(s) = \frac{E(s)}{P(s)} \tag{2.12}$$

and

$$K(s) = \frac{F(s)}{P(s)} \tag{2.13}$$

The reflection coefficient $\rho(s)$ and transmission coefficient $t(s)$ are synonymous with S_{11} and S_{21}. The scattering parameters for the filter network of figure 2.2 can be written in the matrix form as:

$$\begin{bmatrix} S_{11} & S_{12} \\ S_{21} & S_{22} \end{bmatrix} = \frac{1}{E(s)} \begin{bmatrix} \dfrac{F_s}{\epsilon_R} & \dfrac{P_s}{\epsilon} \\ \dfrac{P_s}{\epsilon} & \dfrac{(-1)^{(nfz+1)}F_s^*}{\epsilon_R} \end{bmatrix}$$

The properties of characteristic polynomials for lowpass prototype filter networks can be described as under:

1. $F(s)$ is the numerator polynomial of S_{11} and is of degree n which is the degree of the filter network under consideration. The roots of $F(s)$ lie along the imaginary axis as conjugate pairs. It can have multiple roots only at the origin. The roots of $F(s)$ represent frequencies at which no power is reflected and is termed as reflection zeros.

2. $P(s)$ is the numerator polynomial of S_{12} and S_{21}. Its roots lie on the imaginary axis in conjugate pairs. Such roots represent frequencies where no power is transmitted. These frequencies are termed as transmission zeros or attenuation poles.

3. $E(s)$ is a Hurwitz polynomial as all its roots lie in the left half of the s-plane.

In the above description ϵ and ϵ_R are real constants normalizing $P(s)$ and $F(s)$ polynomials to make their highest power coefficients unity. The characteristic function $K_n(\omega)$ is classified majorly into Maximally flat or Butterworth response, Chebyshev response and Elliptic function response [45]. Each characteristic function has its unique properties and is chosen depending upon the intended application of the filter. For the purpose of this dissertation, Chebyshev response is chosen as it has sharp transition between passband to stopband which suits the bandpass filter designs of this work. Following subsection describes the Chebyshev function response.
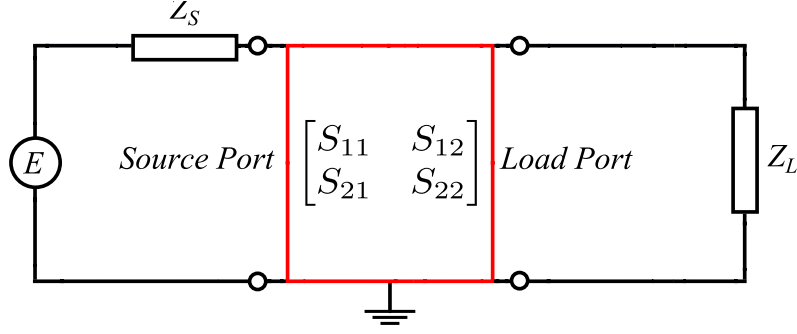
Figure 2.2: Two port network

2.1.2 Chebyshev response

Chebyshev response achieves steeper roll off characteristics as compared to the maximally flat response by allowing ripple in the frequency response. The Chebyshev filter response is defined by n^{th} degree polynomial $T_n(x)$ having following properties [46],

1. T_n is even(odd) if n is even(odd).

2. T_n has zeros in the interval $-1 < x < 1$.

3. T_n oscillates between values ± 1 in the interval $-1 \leq x \leq 1$.

4. $T_n(1) = 1$.

The chebyshev polynomial is defined by,

$$T_n(x) = cos\left(n\,cos^{-1}x\right) \tag{2.14}$$

Chebyshev filters are derived from this polynomial. The equation is derived using the following recursive relationship:

$$T_{n+1}(x) = 2\,x\,T_n(x) - T_{n-1}(x) \tag{2.15}$$

Since $T_0(x) = 1$ and $T_1(x) = x$ we can generate chebyshev polynomial for any order n. For a general chebyshev all pole filter response, synthesis process is as follows,

$$|S_{21}(s)|^2 = \frac{1}{1 + \epsilon^2\,T_n^2(\omega)} \tag{2.16}$$

In order to evaluate poles,

$$1 + \epsilon^2\,T_n^2(\omega) = 0 \tag{2.17}$$

$$T_n^2(\omega) = \frac{-1}{\epsilon^2} \tag{2.18}$$

or,

$$cos^2\left[n\,cos^{-1}\left(\omega\right)\right] = \frac{-1}{\epsilon^2} \tag{2.19}$$

To solve above equation we introduce a new parameter η, where,

$$\eta = \sinh \left[\frac{1}{n} \sinh^{-1} \left(\frac{1}{\eta} \right) \right] \tag{2.20}$$

or,

$$\frac{1}{\epsilon} = \sinh \left[n \, \sinh^{-1} (\eta) \right] \tag{2.21}$$

from above two equation,

$$\cos^2 \left[n \, \cos^{-1}(\omega) \right] = - \sinh^2 \left[n \, \sinh^{-1}(\eta) \right] \tag{2.22}$$

using identity,

$$- \sinh^2 [A] = \sin^2 (jA) \tag{2.23}$$

$$\cos^2 \left[n \, \cos^{-1} (\omega) \right] = \sin^2 \left[j \, n \sinh^{-1} (\eta) \right] \tag{2.24}$$

also using identity,

$$j \sinh^{-1} [A] = \sin^{-1} (jA) \tag{2.25}$$

therefore above equation reduces to,

$$\cos^2 \left[n \, \cos^{-1} (\omega) \right] = \sin^2 \left[n \, \sin^{-1} (j\eta) \right] \tag{2.26}$$

taking square root of both sides,

$$\cos \left[n \, \cos^{-1} (\omega) \right] = \sin \left[n \, \sin^{-1} (j\eta) \right] = \cos \left[n \, \sin^{-1} (j\eta) + \frac{\pi}{2} \right] \tag{2.27}$$

or,

$$\cos^{-1} (\omega) = \sin^{-1} (j\eta) + \theta_r \tag{2.28}$$

where,

$$\theta_r = \frac{(2r - 1)\,\pi}{2n} \tag{2.29}$$

solving for left half poles,

$$s(r) = \eta \sin(\theta_r) + j \left(1 + \eta^2\right)^{\frac{1}{2}} \cos \theta_r \tag{2.30}$$

These poles lie on an ellipse. In terms of scattering parameters,

$$S_{12}(s) = \prod_{r=1}^{n} \frac{\left[\eta^2 + \sin^2 \left((r\pi)/n\right)\right]^{\frac{1}{2}}}{s + j \cos \left[\sin^{-1}(j\eta) + \theta_r\right]} \tag{2.31}$$

$$S_{11}(s) = \prod_{r=1}^{n} \frac{\left[s + j \cos(\theta_r)\right]}{s + j \cos \left[\sin^{-1}(j\eta) + \theta_r\right]} \tag{2.32}$$

Lowpass filter network can then be synthesized using the ladder network by writing $S_{11}(s)$ in terms of input impedance $Z_{11}(s)$.

2.1.3 Chebyshev response with transmission zeros

Certain applications like satellite communication require high selectivity in the stopband. For such a desired response, it is necessary to place transmission zeros in the filter stopband. Transmission zeros are frequency location points where the transmission coefficient tends to 0 ($S_{21} = 0$). These specified frequency points are called prescribed transmission zero locations. In order to describe the polynomial synthesis of a Chebyshev filter response with prescribed transmission zeros, it is necessary to determine the characteristic polynomials $P(s)$, $F(s)$ and $E(s)$. Expressing transmission and reflection scattering parameters in terms of characteristic polynomials by taking $s = j\omega$ [44],

$$S_{11}(\omega) = \frac{F(\omega)/\epsilon_R}{E(\omega)} \tag{2.33}$$

$$S_{21}(\omega) = \frac{P(\omega)/\epsilon}{E(\omega)} \tag{2.34}$$

Where,

$$\epsilon = \frac{1}{\sqrt{10^{RL/10} - 1}} \left| \frac{P(\omega)}{F(\omega)/\epsilon_R} \right|_{\omega = \pm 1} \tag{2.35}$$

Here ϵ and ϵ_R are normalizing constants. Constant R_L is prescribed return loss in dB at $\omega = \pm 1$ rad/s. The corresponding development of the characteristic polynomials are explained as under.

- Polynomial $P(\omega)$ is constructed using $P(\omega) = \prod_{n=1}^{n_{fz}} (\omega - \omega_n)$ and carries n_{fz} prescribed transmission zeros.

- Polynomial $F(\omega)$ coefficients are found using recursive technique. Writing characteristic function $C_N(\omega)$ for chebyshev function as,

$$C_N(\omega) = \cosh \left[\sum_{n=1}^{N} \cosh^{-1}(x_n(\omega)) \right] \tag{2.36}$$

In order for $C_N(\omega)$ to be a Chebyshev function, the function $x_n(\omega)$ requires:

1. At $\omega = \omega_n$ rad/s, where ω_n is either $\pm\infty$ or a finite frequency transmission zero, $x_n(\omega_n) = \pm\infty$

2. At $\omega = \pm 1$ rad/s, $x_n(\omega) = \pm 1$.

3. While $-1 \leq \omega \leq 1$, $-1 \leq x_n(\omega) \leq 1$.

Satisfying above three conditions, $x_n(\omega)$ can be represented by the following formula,

$$x_n(\omega) = \frac{\omega - 1/\omega_n}{1 - \omega/\omega_n} \tag{2.37}$$

Using trigonometric identity,

$$\cosh^{-1}(x_n(\omega)) = \ln \left(x_n(\omega) + \sqrt{\left((x_n(\omega))^2 - 1 \right)} \right) \tag{2.38}$$

Now, $C_N(\omega)$ can be written as,

$$C_N(\omega) = \cosh\left[\sum_{n=1}^{N} \ln(a_n + b_n)\right] \qquad (2.39)$$

Above equation can be simplified as,

$$C_N(\omega) = \frac{1}{2}\left[\frac{\prod_{n=1}^{N}(c_n + d_n) + \prod_{n=1}^{N}(c_n - d_n)}{\prod_{n=1}^{N}\left(1 - \frac{\omega}{\omega_n}\right)}\right] \qquad (2.40)$$

where,

$$c_n = \left(\omega - \frac{1}{\omega_n}\right) \qquad (2.41)$$

and

$$d_n = \left(\omega'\sqrt{1 - \frac{1}{\omega_n^2}}\right) \qquad (2.42)$$

$$\omega' = \sqrt{\omega^2 - 1} \qquad (2.43)$$

In order to build the coefficient of the numerator of $[C_N(\omega)]$, a recursive technique is utilized where the solution of the nth degree polynomial is built up from the results of the $(n-1)^{th}$ degree polynomial [47]. The numerator $[C_N(\omega)]$ can be further simplified as,

$$Num\,[C_N(\omega)] = \frac{1}{2}\left[G_N(\omega) + G'_N(\omega)\right] \qquad (2.44)$$

where,

$$G_N(\omega) = \prod_{n=1}^{N}(c_n + d_n) = \prod_{n=1}^{N}\left[\left(\omega - \frac{1}{\omega_n}\right) + \omega'\sqrt{\left(1 - \frac{1}{\omega_n^2}\right)}\right] \qquad (2.45)$$

and

$$G'_N(\omega) = \prod_{n=1}^{N}(c_n - d_n) = \prod_{n=1}^{N}\left[\left(\omega - \frac{1}{\omega_n}\right) - \omega'\sqrt{\left(1 - \frac{1}{\omega_n^2}\right)}\right] \qquad (2.46)$$

Polynomial $G_N(\omega)$ can be rearranged in terms of two polynomials $U_N(\omega)$ and $V_N(\omega)$. $V_N(\omega)$ contains polynomials in terms of ω where the coefficients of auxillary polynomial $V_N(\omega)$ are multiplied by variable ω'.

$$G_N(\omega) = U_N(\omega) + V_N(\omega) \qquad (2.47)$$

where,

$$U_N(\omega) = u_0 + u_1\,\omega + u_2\,\omega^2 + ... + u_N\,\omega^N \qquad (2.48)$$

and,

$$V_N(\omega) = \omega'\left(v_0 + v_1\,\omega + v_2\,\omega^2 + ... + v_N\,\omega^N\right) \qquad (2.49)$$

If the same process is repeated for $G'_N(\omega)$,

$$G'_N(\omega) = U'_N(\omega) + V'_N(\omega) \tag{2.50}$$

then,

$$U'_N(\omega) = U_N(\omega) \tag{2.51}$$

and,

$$V'_N(\omega) = -V_N(\omega) \tag{2.52}$$

therefore,

$$Num\left[C_N(\omega)\right] = \frac{1}{2}\left[G_N(\omega) + G'_N(\omega)\right] = \frac{1}{2}\left[\left[U_N(\omega) + U'_N(\omega)\right]\right] \tag{2.53}$$

$$+ \frac{1}{2}\left[\left[V_N(\omega) + V'_N(\omega)\right]\right] = U_N(\omega) = F(\omega)$$

With above step, construction of polynomial $F(\omega)$ is complete.

- Finally using the conservation of energy equation, polynomial $E(\omega)$ is calculated.

$$S_{11}(\omega)S_{11}(\omega)^* + S_{21}(\omega)S_{21}(\omega)^* = 1 \tag{2.54}$$

Using alternating pole method, above equation can be written in terms of polynomials as,

$$\epsilon^2 \epsilon_R^2 E(\omega)E(\omega)^* = \left[\epsilon_R P(\omega) - j\epsilon F(\omega)\right]\left[\epsilon_R P(\omega) - j\epsilon F(\omega)\right]^* \tag{2.55}$$

The above equation can be represented in terms of characteristic function of degree n as,

$$S_{21}(\omega)S_{21}(\omega)^* = \frac{P(\omega)P(\omega)^*}{\epsilon^2 E(\omega)E(\omega)^*} = \frac{1}{\left[1 - j\dfrac{\epsilon}{\epsilon_R}\, k\, C_N(\omega)\right]\left[1 + j\dfrac{\epsilon}{\epsilon_R}\, k\, C_N(\omega)^*\right]} \tag{2.56}$$

Summarizing the above theory, following steps are to be performed to derive the characteristic polynomials.

1. Polynomial $P(\omega)$ is obtained from $P(\omega) = \displaystyle\prod_{n=1}^{n_{fz}}(\omega - \omega_n)$ where n_{fz} are prescribed transmission zeros.

2. Constant ϵ is calculated using

$$\epsilon = \frac{1}{\sqrt{10^{RL/10} - 1}}\left|\frac{P(\omega)}{F(\omega)/\epsilon_R}\right|_{\omega = \pm 1} \tag{2.57}$$

where R_L is prescribed return loss in dB at $\omega = \pm 1$.

3. $F(\omega)$ is obtained using recursive method explained above. $Num\left[C_N(\omega)\right] = F(\omega) = U_N(\omega)$.

4. Using the alternating pole method equation and rooting one of the RHS terms, simplified equation is obtained as below, $E(\omega) = \dfrac{P(\omega)}{\epsilon} - j\dfrac{F(\omega)}{\epsilon_R}$. To obtain polynomial $E(\omega)$, calculated values of ϵ, $P(\omega)$ and $F(\omega)$ are substituted in the above equation.

5. Since $E(\omega)$ is strictly hurwitz, roots of right half plane are converted to left half plane.

2.2   Filter Scaling and Transformations

This section describes the lowpass prototype filter networks which can be derived from the filter transfer function described in the previous section. These networks are vital in the study of coupled resonator filters as they form the basis to generate networks for different filter responses. Filter network transformations are presented in subsequent sections.

2.2.1   Low pass filter prototypes

A lowpass prototype filter is in general defined as the lowpass filter whose element values are normalized to make the source resistance or conductance equal to one (denoted by $g_0 = g_n = 1$) and the cutoff angular frequency to be unity (denoted by $\omega'_1 = 1\,rad/s$). Two forms of the low pass filter prototypes for realizing all pole filter response are shown in figure 2.3. Both the forms give identical response and can be utilized to realize different transfer functions including Butterworth, Chebyshev, Gaussian response [48,49]. In figure 2.3, symbol n represents the order of the filter and also the number of reactive elements of the low pass filter network. The g values represent inductances in henries(H), capacitance in farads(F), resistance in ohms(Ω), conductance in mhos (Ω^{-1}). The low pass filter prototypes mentioned can be utilized to construct many practical filters by using frequency and element transformations. In the representation of the low pass filter networks:
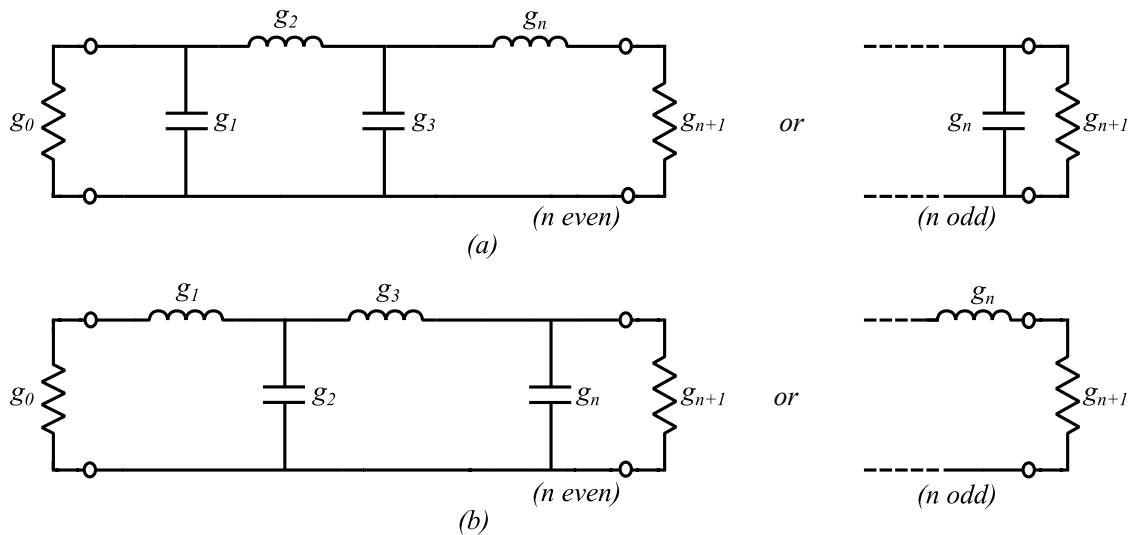
Figure 2.3: Low pass prototype networks

$$g_k = \begin{cases} \text{inductance of a series coil} \\ \text{capacitance of a shunt capacitor} \end{cases}$$

$$g_0 = \begin{cases} \text{generator resistance } R_0' \text{ if } g_1 = C_1', R_0' \text{ normalized to 1} \\ \text{generator conductance } G_0' \text{ if } g_1 = L_1', G_0' \text{ normalized to 1} \end{cases}$$

$$g_{n+1} = \begin{cases} \text{load resistance } R_{n+1}' \text{ if } g_n = C_n', R_{n+1}' \text{ normalized to 1} \\ \text{load conductance } G_{n+1}' \text{ if } g_n = L_n', G_{n+1}' \text{ normalized to 1} \end{cases}$$

2.2.2   Impedance scaling

Low-pass filter prototypes usually have a system impedance of $1\,\Omega$. To convert from a $1\,\Omega$ impedance level to an impedance level of $Z_0\,\Omega$ (usually $50\,\Omega$), impedances of the circuit elements in the filter are scaled by $Z_0\,\Omega$.

$$L \rightarrow Z_0 L \tag{2.58}$$

$$C \rightarrow \frac{C}{Z_0} \tag{2.59}$$

$$R \rightarrow Z_0 \tag{2.60}$$

$$G \rightarrow \frac{G}{Z_0} \tag{2.61}$$

2.2.3   Low-pass to Low-pass transformation

A low pass prototype has a band edge or cut off frequency $\omega_1' = 1$ rad/s. In order to convert ω_1' to an arbitrary frequency ω_c, while applying impedance scaling, the following transformation are applied,

$$\omega_1' \rightarrow \frac{\omega_1'}{\omega_c} \tag{2.62}$$

$$L \rightarrow \frac{Z_0 L}{\omega_c} \tag{2.63}$$

$$C \rightarrow \frac{C}{Z_0 \omega_c} \tag{2.64}$$

Here, inductive/capacitive element g in the low pass prototype are represented by L and C.

2.2.4   Low-pass to High-pass transformation

To convert low pass prototype with frequency $\omega_1' = 1$ to an arbitrary high pass frequency ω_c with impedance scaling following transformation are applied,

$$\omega_1' \rightarrow \frac{-\omega_c}{\omega_1'} \tag{2.65}$$

$$L \rightarrow \frac{Z_0}{\omega_c C} \tag{2.66}$$

$$C \rightarrow \frac{1}{Z_0 \omega_c L} \tag{2.67}$$

The inductive(L)/capacitive(C) element g in the low pass prototype will be inversely transformed to capacitive/inductive element in the high pass filter.

2.2.5   Low-pass to Bandpass transformation

For a bandpass transformation from a low pass prototype, inductive/capacitive element g in the low pass prototype will transform to a series/parallel LC resonant circuit in the bandpass filter. The band edges at $\omega = \pm 1$ rad/s of the low pass prototype must be mapped into the band edges of the bandpass filter at ω_1 and ω_2. The transmission zero at infinity in the lowpass prototype must now occur at both $\omega = 0$ rad/s and $\omega = \infty$ rad/s.

$$\frac{\omega'}{\omega_1'} = \frac{1}{\Delta} \left(\frac{\omega}{\omega_0} - \frac{\omega_0}{\omega} \right) \tag{2.68}$$

$$\Delta = \frac{\omega_2 - \omega_1}{\omega_0} \tag{2.69}$$

$$\omega_0 = \sqrt{\omega_2 \omega_1} \tag{2.70}$$

The elements for the series LC resonator in the bandpass filter with impedance scaling are given by,

$$L_s \rightarrow \frac{L Z_0}{\omega_0 \Delta} \tag{2.71}$$

$$C_s \rightarrow \frac{\Delta}{\omega_0 L Z_0} \tag{2.72}$$

Here, L represents the inductance value in the low pass prototype network. The elements for the shunt LC resonator in the bandpass filter with impedance scaling are given by,

$$L_p \rightarrow \frac{Z_0 \Delta}{\omega_0 C} \tag{2.73}$$

$$C_p \rightarrow \frac{C}{\omega_0 \Delta Z_0} \tag{2.74}$$

Here, C represents the capacitance of the capacitor in low pass prototype network.

2.2.6   Low-pass to Bandstop transformation

The frequency transformation from lowpass prototype to bandstop is achieved by the following transformation,

$$\frac{1}{\omega'} \to \frac{-1}{\Delta\omega'_1}\left(\frac{\omega}{\omega_0} - \frac{\omega_0}{\omega}\right) \tag{2.75}$$

This type of transformation is opposite to the bandpass transformation. For a bandstop transformation, an inductive/capacitive element g in the low pass prototype will transform to a parallel/series LC resonant circuit.

$$L_p \to \frac{L\Delta Z_0}{\omega_0} \tag{2.76}$$

$$C_p \to \frac{1}{\Delta L \omega_0 Z_0} \tag{2.77}$$

Here, L represents the inductance value in the low pass prototype network.

$$L_s \to \frac{Z_0}{\omega_0 C \Delta} \tag{2.78}$$

$$C_s \to \frac{C\Delta}{\omega_0 Z_0} \tag{2.79}$$

Here, C represents the capacitance of the capacitor in the low pass prototype network.

2.3   Coupled Resonator Filters Using Immittance Inverters

2.3.1   Immittance inverters

As compared to the prototype networks of figure 2.3, filter networks with the same single type of network elements are easily realizable. It is desirable to convert the prototypes of figure 2.3, which uses both inductances and capacitances, to equivalent forms which use only inductances or only capacitances. This can be done with the help of immittance inverters. The simplified network using inverters can be utilized to derive design equations for bandpass and bandstop filters.

  An idealized impedance inverter is a two port network which has a property that if it is terminated in an impedance Z_b on one end, the impedance Z_a seen looking in at the other end is $Z_a = \dfrac{K^2_{j,j+1}}{Z_b}$ as shown in figure 2.4(a). The transmission matrix of an impedance inverter is given by,

$$\begin{bmatrix} A & B \\ C & D \end{bmatrix} = \begin{bmatrix} 0 & \mp jK \\ \pm\dfrac{1}{jK} & 0 \end{bmatrix} \tag{2.80}$$

An idealized admittance inverter is a two port network which has a property that if it is terminated in an admittance Y_b on one end, the admittance Y_a seen looking in at the
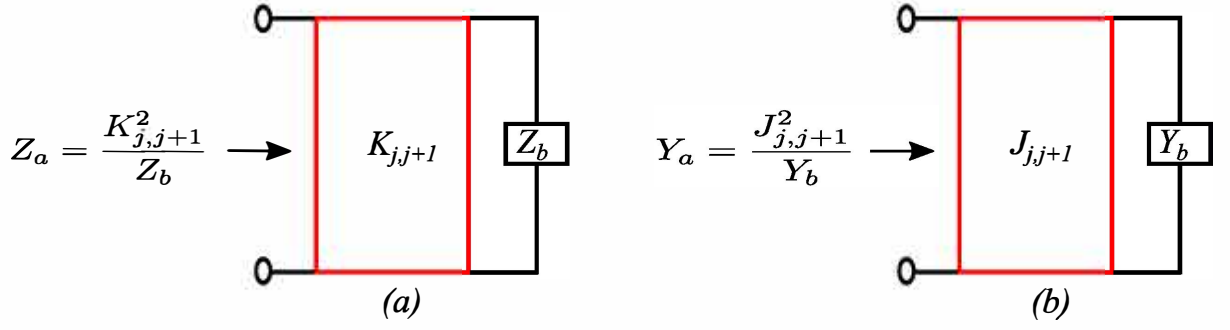
Figure 2.4: (a) Impedance inverter (b) Admittance inverter
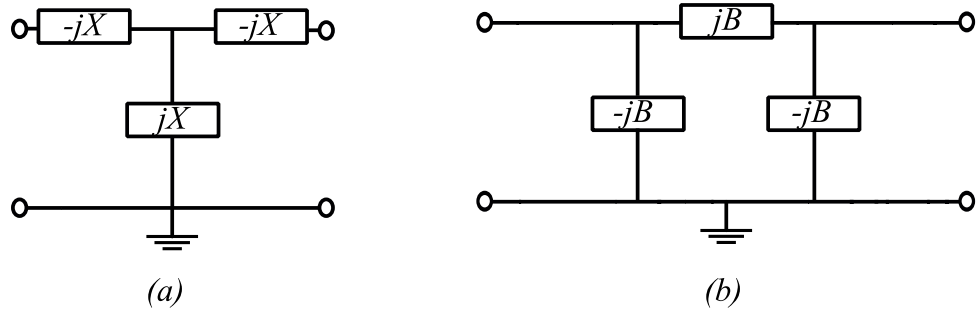
Figure 2.5: (a) Impedance inverter using T network (b) Admittance inverter using pi-network

other end is, $Y_a = \dfrac{J_{j,j+1}^2}{Y_b}$ as shown in figure 2.4(b). The transmission matrix of admittance inverter is given by,

$$\begin{bmatrix} A & B \\ C & D \end{bmatrix} = \begin{bmatrix} 0 & \pm\dfrac{1}{jJ} \\ \mp jJ & 0 \end{bmatrix} \tag{2.81}$$

These inverters can be constructed by T and Pi network configurations respectively using ideal frequency independent reactive elements. The impedance matrix of T network of figure 2.5(a) is given by,

$$\begin{bmatrix} Z_{11} & Z_{12} \\ Z_{21} & Z_{22} \end{bmatrix} = \begin{bmatrix} 0 & jX \\ jX & 0 \end{bmatrix} \tag{2.82}$$

Here, impedance inverter constant is given by,

$$K = |X| \tag{2.83}$$

The admittance matrix of pi network of figure 2.5(b) is given by,

$$\begin{bmatrix} Y_{11} & Y_{12} \\ Y_{21} & Y_{22} \end{bmatrix} = \begin{bmatrix} 0 & -jB \\ -jB & 0 \end{bmatrix} \tag{2.84}$$
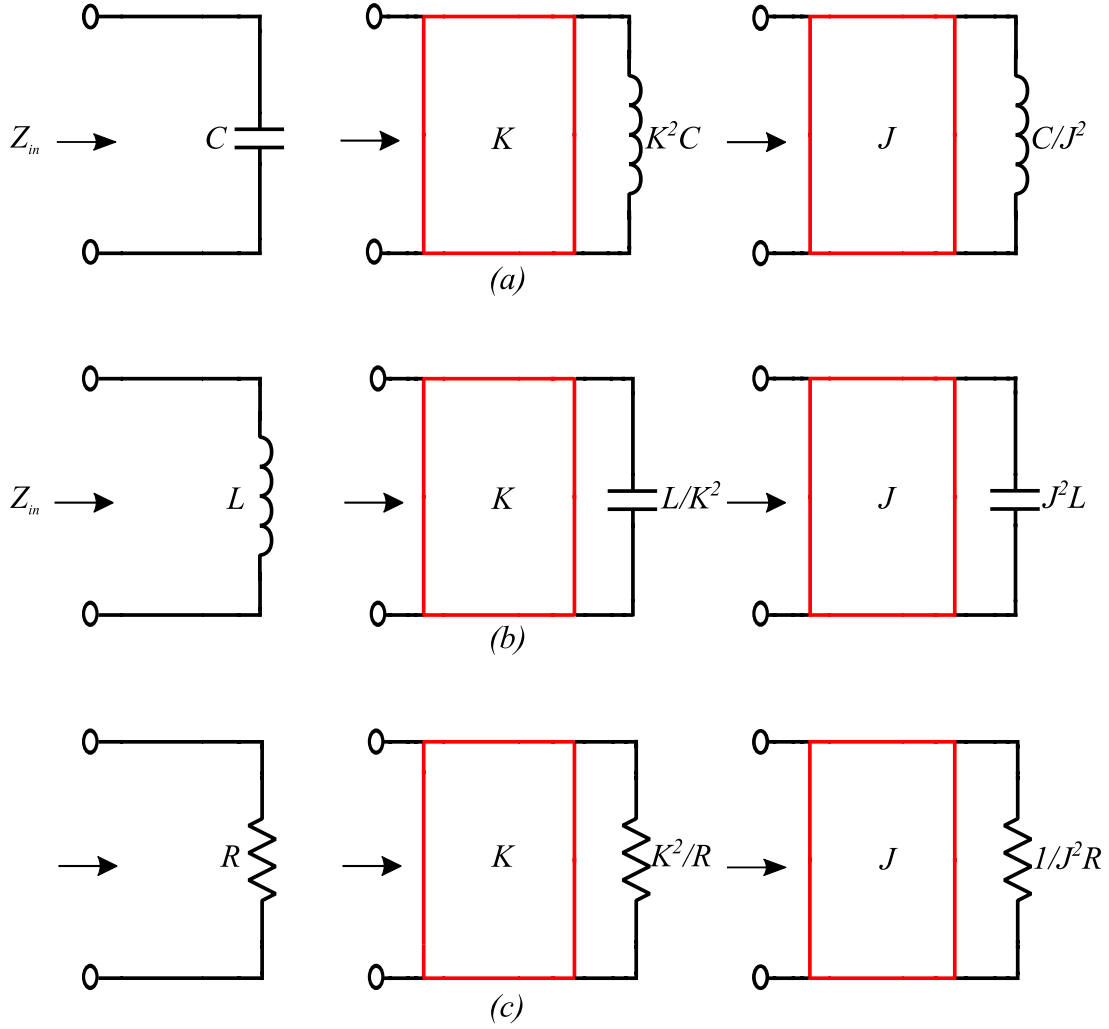
Figure 2.6: (a) Capacitive element (b) Inductive element (C) Resistive element

Here, admittance inverter constant is given by,

$$J = |B| \tag{2.85}$$

A series inductance with an impedance inverter on each side looks like a shunt capacitance from its exterior terminals. A shunt capacitance with an admittance inverter on both sides looks like a series inductance from its external terminals. Inverters can be used to transform elements or parts of circuits, as long as the input impedance remains equal. Basic transformations with the use of inverters is shown in figure 2.6.

2.3.2   Low pass prototype using immittance inverters

Using the impedance/admittance transforming property of inverters shown in figure 2.4, the prototype circuits of figure 2.3 can be converted to either of the equivalent forms of figure 2.9 which have identical transmission characteristics to the prototypes of figure 2.3. The impedance seen from any point in the circuits of figure 2.3 can be related to the corresponding impedance seen from the circuits in figure 2.9 [50]. For example, the impedance seen from L_{aj} in figure 2.9(a) is the same as seen from g_1 in figure 2.3(b).
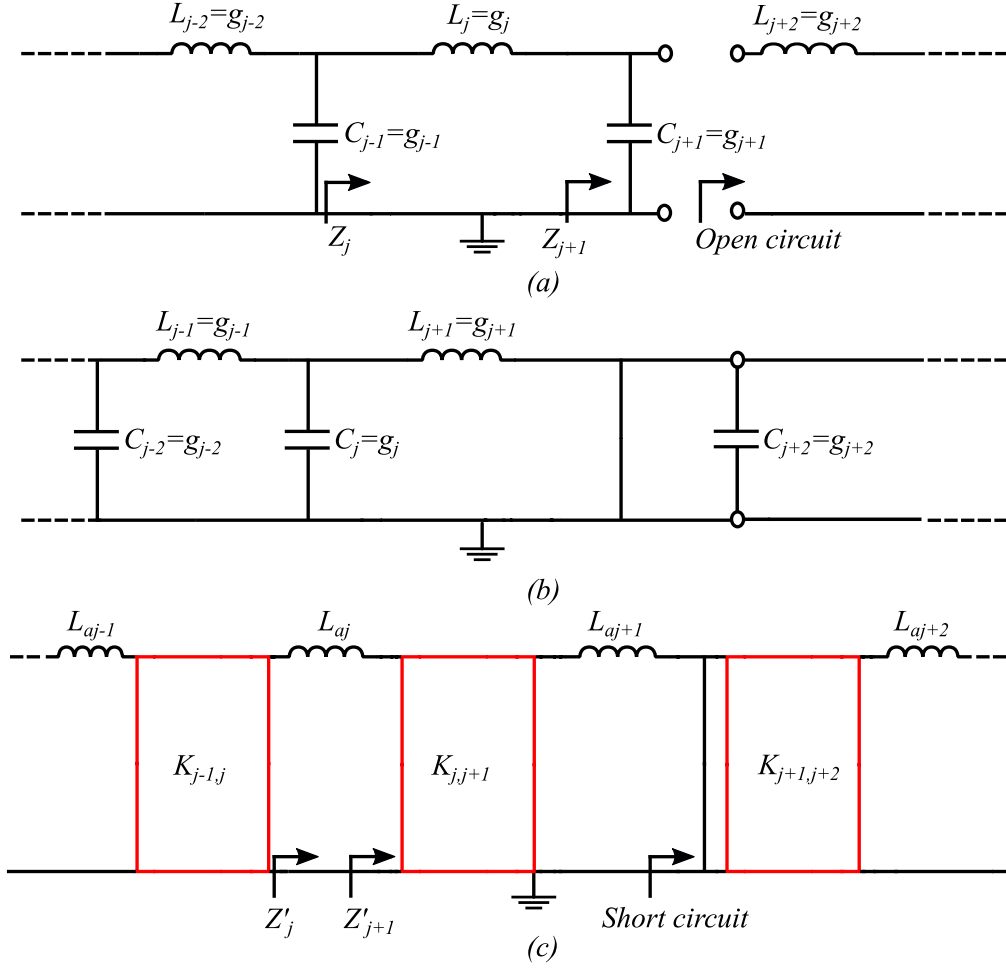
Figure 2.7: (a) Ladder network open circuited (b) Dual ladder network short circuited (c) Equivalent network with impedance inverters
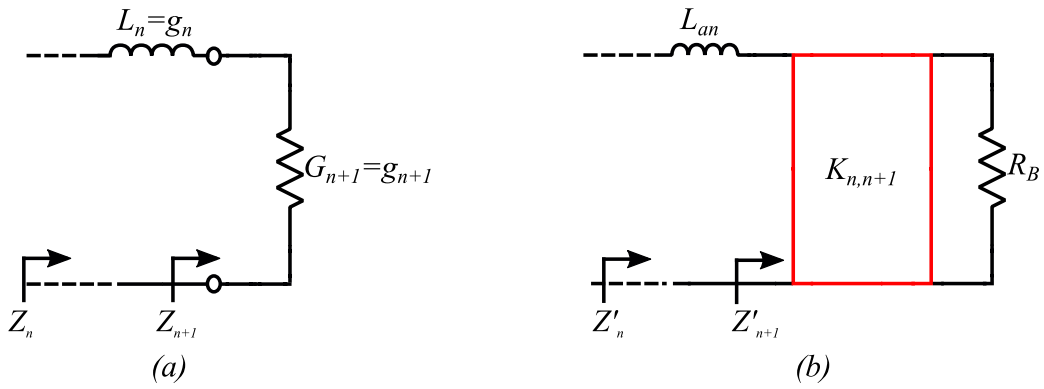
Figure 2.8: (a) Ladder network end elements (b) Equivalent network with impedance inverters

Figure 2.7(a) shows a portion of the low pass prototype circuit that has been open circuited just beyond capacitor C_{j+1}. The dual of the circuit is shown in figure 2.7(b), where the open circuit of figure 2.7(a) becomes short circuit. The equivalent circuit with

series inductor and K inverters is shown in figure 2.7(c). For the circuit of figure 2.7(a),

$$Z_j = j\omega L_j + \frac{1}{j\omega C_{j+1}}$$

For the circuit of figure 2.7(c),

$$Z'_j = j\omega L_{aj} + \frac{K^2_{j,j+1}}{j\omega L_{aj+1}}$$

Now, Z'_j must be identical to Z_j except for an impedance scale change of $\frac{L_{aj}}{L_j}$.

$$Z'_j = \frac{L_{aj}}{L_j} Z_j = j\omega L_{aj} + \frac{L_{aj}}{L_j} \frac{1}{j\omega C_{j+1}}$$

Equating the second terms of Z'_j,

$$K_{j,j+1} = \sqrt{\frac{L_{aj} L_{aj+1}}{L_j C_{j+1}}} \tag{2.86}$$

Substituting, $L_j = g_j$ and $C_{j+1} = g_{j+1}$,

$$K_{j,j+1} = \sqrt{\frac{L_{aj} L_{aj+1}}{g_j g_{j+1}}} \tag{2.87}$$

The K values for all the inverters can be calculated in the same way by moving the positions of the open circuit and short circuit points. For the end inverters, figure 2.8(a) shows the last two elements of the prototype circuit of figure 2.3(a) and figure 2.8(b) shows its corresponding form with a K inverter. For figure 2.8(a),

$$Z_n = j\omega L_n + \frac{1}{G_{n+1}}$$

while for figure 2.8(b),

$$Z'_n = j\omega L_{an} + \frac{K^2_{n,n+1}}{R_B}$$

Now, Z'_n must be identical to Z_n except for an impedance scale change of $\frac{L_{an}}{L_n}$.

$$Z'_n = \frac{L_{an}}{L_n} Z_n = j\omega L_{an} + \frac{L_{an}}{L_n} \frac{1}{G_{n+1}}$$

Equating the second terms of Z'_n,

$$K_{n,n+1} = \sqrt{\frac{L_{an} R_B}{L_n G_{n+1}}} \tag{2.88}$$

substituting $L_n = g_n$ and $G_{n+1} = g_{n+1}$,

$$K_{n,n+1} = \sqrt{\frac{L_{an} R_B}{g_n g_{n+1}}} \tag{2.89}$$

The equations for the admittance inverters $J_{j,j+1}$ can be derived in a similar manner.

$$K_{01} = \sqrt{\frac{R_A L_{aj}}{g_0 g_1}} \quad K_{j,j+1} = \sqrt{\frac{L_{aj} L_{aj+1}}{g_j g_{j+1}}} \quad K_{n,n+1} = \sqrt{\frac{R_B L_{ajn}}{g_n g_{n+1}}}$$

(a)

$$J_{01} = \sqrt{\frac{G_A C_{aj}}{g_0 g_1}} \quad J_{j,j+1} = \sqrt{\frac{C_{aj} C_{aj+1}}{g_j g_{j+1}}} \quad J_{n,n+1} = \sqrt{\frac{G_B C_{ajn}}{g_n g_{n+1}}}$$

(b)
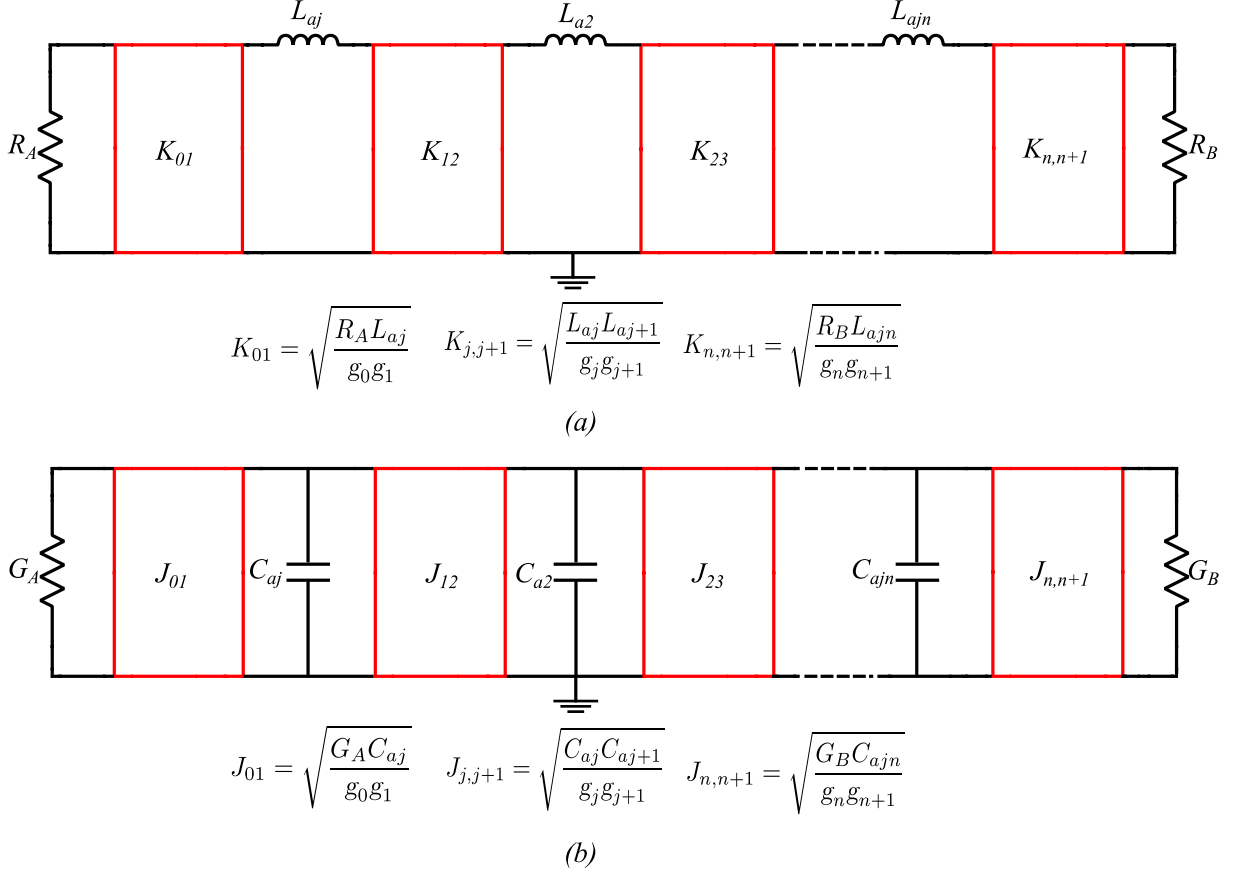
Figure 2.9: Low pass prototype with immittance inverters

2.3.3   Band pass filters using immittance inverters

Writing the band pass filter transformation equations from section 2.2.5 [50],

$$\frac{\omega'}{\omega_1'} = \frac{1}{\Delta}\left(\frac{\omega}{\omega_0} - \frac{\omega_0}{\omega}\right)$$

$$\Delta = \frac{\omega_2 - \omega_1}{\omega_0}$$

$$\omega_0 = \sqrt{\omega_2 \omega_1}$$

Here, ω_1' is the angular cut off frequency of the low pass prototype. Parameter ω' is an arbitrary angular frequency point while ω_0 corresponds to the centre frequency of the pass band. Parameter Δ corresponds to the fractional bandwidth. Writing reactance slope parameter x_j of series resonator corresponding to low pass prototype element $L_{aj} = g_j$.

$$x_j = \omega_0 L_s = \frac{1}{\omega_0 C_s} = \frac{\omega_1' g_j}{\Delta} = \frac{\omega_1' L_{aj}}{\Delta} \tag{2.90}$$

where,

$$L_{aj} = \frac{L_s \omega_0 \Delta}{\omega_1'} = \frac{x_j \Delta}{\omega_1'} \tag{2.91}$$

Also,

$$x_{j+1} = \omega_0 L_s^{'} = \frac{1}{\omega_0 C_s^{'}} = \frac{\omega_1^{'} g_{j+1}}{\Delta} = \frac{\omega_1^{'} L_{aj+1}}{\Delta} \qquad (2.92)$$

is the reactance slope parameter of the series resonator corresponding to the low pass prototype element $L_{aj+1} = g_{j+1}$ where,

$$L_{aj+1} = \frac{L_s^{'} \omega_0 \Delta}{\omega_1^{'}} = \frac{x_{j+1} \Delta}{\omega_1^{'}} \qquad (2.93)$$

For a low pass prototype,

$$K_{j,j+1} = \sqrt{\frac{L_{aj} L_{aj+1}}{g_j g_{j+1}}}$$

Substituting the the value of L_{aj} and L_{aj+1} for bandpass transformation we get,

$$K_{j,j+1} = \frac{\Delta}{\omega_1^{'}} \sqrt{\frac{x_j x_{j+1}}{g_j g_{j+1}}} \qquad (2.94)$$

Similarly, the end inverters in low pass prototype is given by,

$$K_{n,n+1} = \sqrt{\frac{L_{ajn} R_B}{g_n g_{n+1}}}$$

Converting, L_{ajn} to band pass case,

$$L_{aj} = L_{ajn} = \frac{L_s \omega_0 \Delta}{\omega_1^{'}} = \frac{x_n \Delta}{\omega_1^{'}}$$

Also,

$$L_{aj+1} = L_{ajn+1} = \frac{L_s^{'} \omega_0 \Delta}{\omega_1^{'}} = \frac{x_{n+1} \Delta}{\omega_1^{'}}$$

Substituting the value of L_{ajn} and L_{ajn+1} in the above equation,

$$K_{n,n+1} = \sqrt{\frac{R_B x_n \Delta}{\omega_1^{'} g_n g_{n+1}}} \qquad (2.95)$$

Figure 2.10 represents Bandpass filters using immittance inverters.

2.4   Immittance Inverter Models

This section provides a comprehensive listing of immittance inverter models used in coupled resonator filters. With the use of inverters, filter networks can be represented in a realizable form [51]. Immittance inverters are basically immittance transformers. Firstly, impedance inverters are listed followed by admittance inverters.

$$K_{01} = \sqrt{\frac{R_A x_1 \Delta}{g_0 g_1 \omega_1'}} \qquad K_{j,j+1} = \frac{\Delta}{\omega_1'} \sqrt{\frac{x_j x_{j+1}}{g_j g_{j+1}}} \qquad K_{n,n+1} = \sqrt{\frac{R_B x_n \Delta}{g_n g_{n+1} \omega_1'}}$$

(a)

$$J_{01} = \sqrt{\frac{G_A \beta_1 \Delta}{g_0 g_1 \omega_1'}} \qquad J_{j,j+1} = \frac{\Delta}{\omega_1'} \sqrt{\frac{\beta_j \beta_{j+1}}{g_j g_{j+1}}} \qquad J_{n,n+1} = \sqrt{\frac{G_B \beta_n \Delta}{g_n g_{n+1} \omega_1'}}$$

(b)
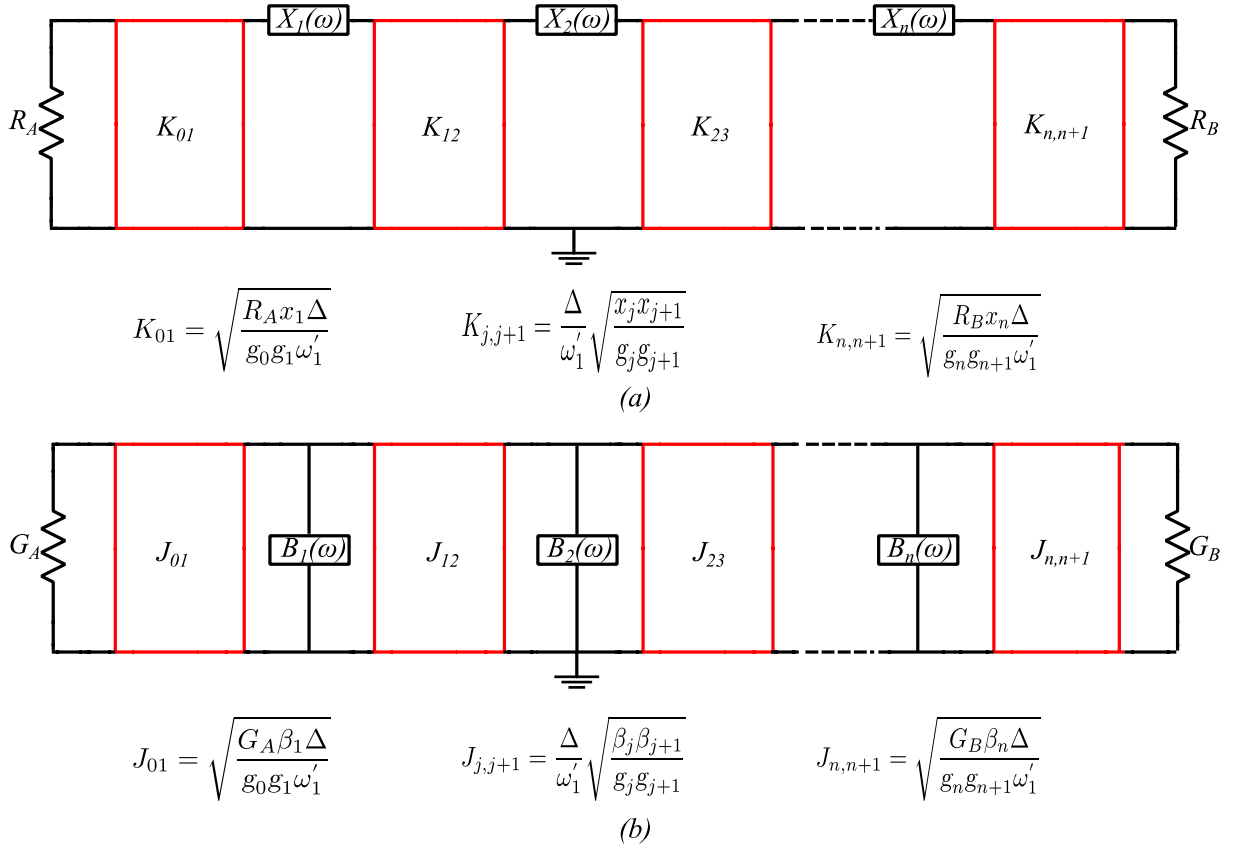
Figure 2.10: Bandpass filter using immittance inverter

2.4.1   Impedance inverter models

In order to evaluate inverter network parameters, it is necessary to establish a relation between impedance inverter constants K and inverter network parameters. Value of impedance inverter constant K can be derived from the specified coupling coefficient value k and the resonator slope parameter depending upon the choice of resonator. In the network representations shown below, the negative values of the inverter circuit elements are assumed to be absorbed in the adjacent resonators and parameter ω_0 specifies the centre frequency of operation of the filter . For figure 2.11(a), inverter constant is given by [50],

$$K = \omega_0 L$$

For figure 2.11(b), inverter constant is given by,

$$K = \frac{1}{\omega_0 C}$$

For figure 2.11(c) and figure 2.11(d), inverter constants are given by,

$$K = Z_0 \tan \left| \frac{\phi}{2} \right| \text{ ohms}$$

where,

$$\phi = -\tan^{-1} \frac{2X}{Z_0} \text{ radians}$$
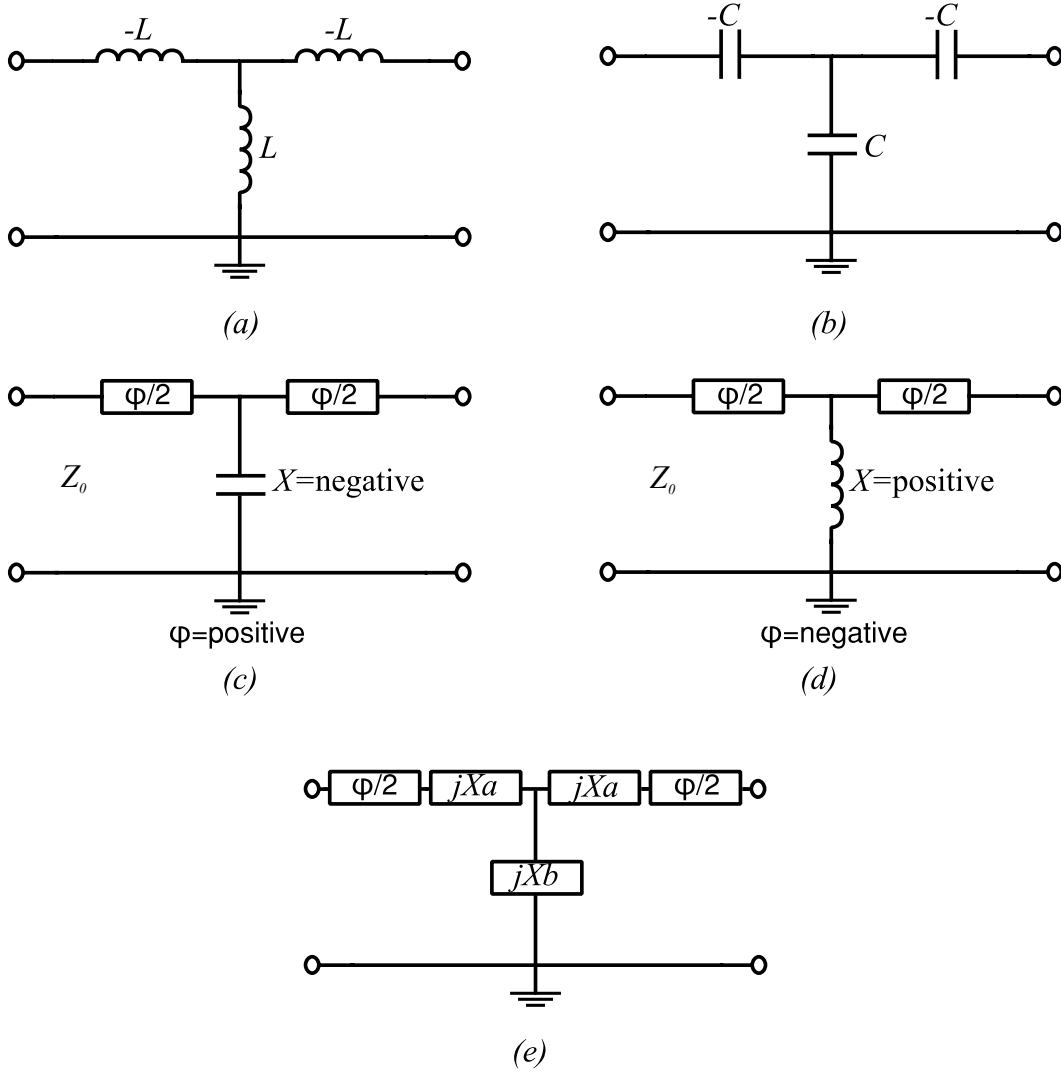
Figure 2.11: Impedance inverter

and,

$$\left| \frac{X}{Z_0} \right| = \frac{\dfrac{K}{Z_0}}{1 - \left(\dfrac{K}{Z_0} \right)^2}$$

For figure 2.11(e) inverter constant is given by,

$$K = Z_0 \left| \tan \left(\frac{\phi}{2} + \tan^{-1} \frac{X_a}{Z_0} \right) \right| \text{ ohms}$$

$$\phi = - \tan^{-1} \left(\frac{2X_b}{Z_0} + \frac{X_a}{Z_0} \right) - \tan^{-1} \frac{X_a}{Z_0} \text{ radians}$$

2.4.2 Admittance inverter models

In this section, admittance inverter models are listed to establish a relation between the admittance inverter constant J and admittance inverter network parameters. Value of
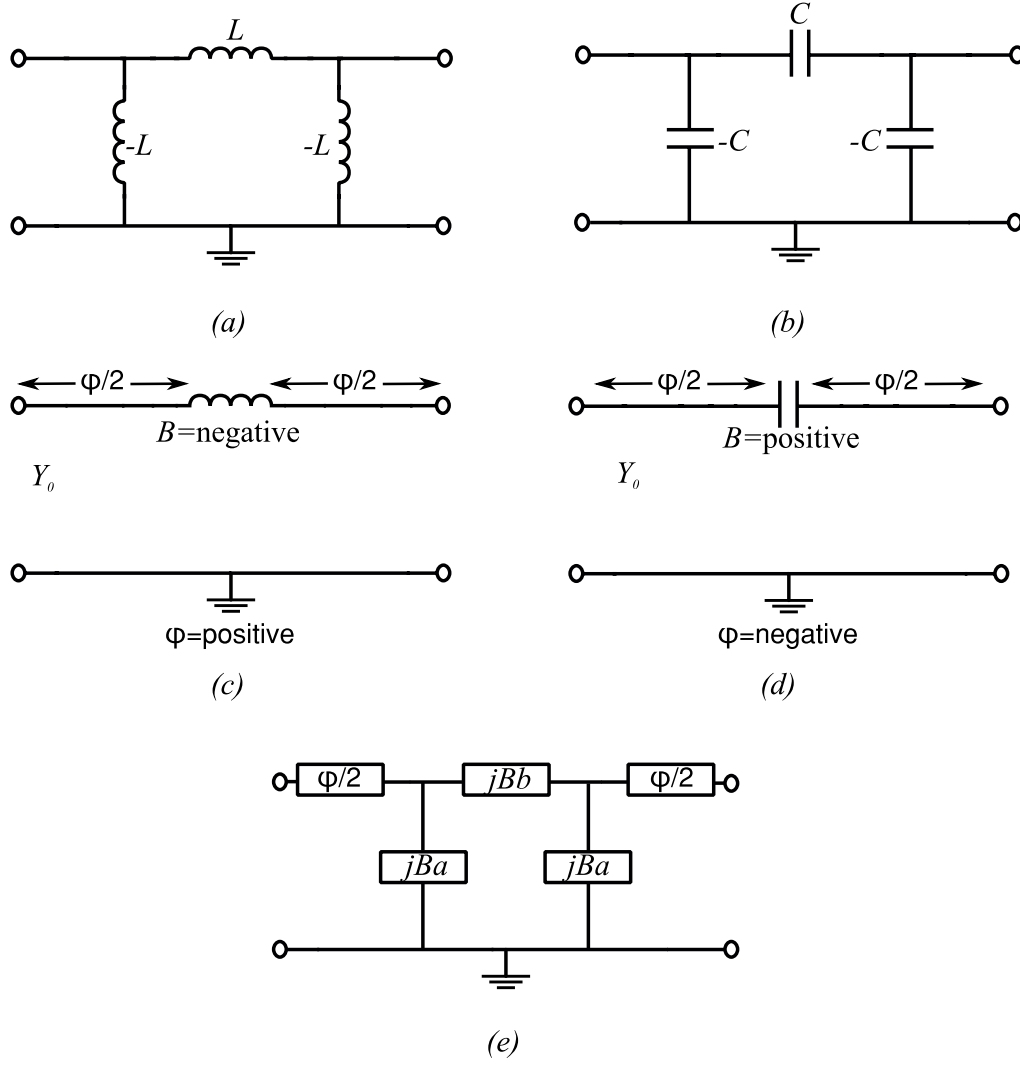
Figure 2.12: Admittance inverter

admittance inverter constant J can be derived from the specified coupling coefficient value k and resonator slope parameter. In the network representations shown below, the negative values of inverter circuit elements are assumed to be absorbed in the adjacent resonators and parameter ω_0 specifies the centre frequency of operation of the filter . For figure 2.12(a), admittance inverter constant is given by [50],

$$J = \frac{1}{\omega_0 L}$$

For figure 2.12(b), admittance inverter constant is given by,

$$J = \omega_0 C$$

For figure 2.12(c) and 2.12(d), admittance inverter constant is given by

$$J = Y_0 \tan \left| \frac{\phi}{2} \right| \text{ mhos}$$

where,

$$\phi = - \tan^{-1} \frac{2B}{Y_0} \text{ radians}$$

and,

$$\left| \frac{B}{Y_0} \right| = \frac{\dfrac{J}{Y_0}}{1 - \left(\dfrac{J}{Y_0} \right)^2}$$

For figure 2.12(e), admittance inverter constants is given by,

$$J = Y_0 \left| \tan \left(\frac{\phi}{2} + \tan^{-1} \frac{B_a}{Y_0} \right) \right| \text{ mhos}$$

where,

$$\phi = -\tan^{-1} \left(\frac{2B_b}{Y_0} + \frac{B_a}{Y_0} \right) - \tan^{-1} \frac{B_a}{Y_0} \text{ radians}$$

## 2.5 Tuning Elements

External tuning elements when attached to a passive microwave circuit enhances the functionality of the passive circuit by making it reusable over different frequencies. In this section, commonly used tuning elements specifically in planar microwave circuits are discussed as it correlates with the work presented in this thesis in the subsequent chapters. The choice of the tuning element depends upon aspects like design of the corresponding circuit in which the tuning element is to be utilized, requirement of discrete or continuous tuning, desired performance specification range, tolerances etc.

2.5.1 Semiconductor varactor diodes

A varactor diode is a p-n junction diode whose capacitance is varied by varying the reverse voltage. The term varactor originated from 'variable capacitor'. When a reverse bias voltage is applied, the electrons from the n-region and the holes from the p-region move away from the junction. As a result, the width of the depletion region increases and the capacitance decreases. If the applied reverse bias voltage is very low, the width of the depletion region decreases and the capacitance will be very large. The property of the capacitance change with respect to bias voltage is utilized to achieve a change in the frequency and/or the phase of an electrical circuit. Varactor diodes are classified into two types based on the varactor diode junction properties. These are termed as abrupt varactor diodes and hyperabrupt varactor diodes. Hyperabrupt junction diodes are more expensive as compared to abrupt junction diodes and provide better performance. Hyperabrupt junction diodes provide a narrow band linear frequency variation and gives a much greater capacitance change for a given voltage change. Typical materials used for their fabrication is Silicon and Gallium arsenide. A simple model of a packaged varactor diode is shown in figure 2.13. In figure 2.13, C_j is the variable junction capacitance of the diode die and R_s is the variable series resistance of the diode die. C_p is the fixed parasitic capacitance arising from the installation of the die in a package. Contributors to the parasitic capacitance are the package material, geometry and the bonding wires or ribbons. These factors also contribute to the parasitic inductance L_p. Semiconductor varactor
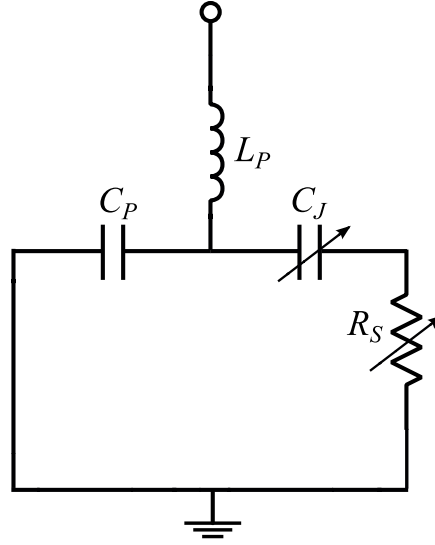
Figure 2.13: Varactor diode package

diodes are used both as a continuous tuning element and as a discrete tuning element in reconfigurable microwave circuits. Typical applications of varactor diodes include RF filters, voltage controlled oscillators (VCO), parametric amplifiers etc. [52], [53]. Typical manufacturers include Skyworks, MACOM, Infineon.

2.5.2   Ferroelectric material based varactor diodes

Dielectric materials have the property of dielectric polarization where positive charges are displaced in the direction of the field and negative charges shift in the opposite direction. This creates an internal electric field that reduces the overall field within the dielectric itself. The materials showing dielectric polarization have polarization induced P, almost exactly proportional to the applied external electric field E, so the polarization is a linear function. Ferroelectric materials exhibit spontaneous electric polarization that can be reversed by applying an electric field. The polarization is therefore dependent not only on the current electric field but also on its history, yielding a hysteresis loop. Typically, materials demonstrate ferroelectricity only below a certain phase transition temperature, called the Curie temperature (T_C). The nonlinear nature of ferroelectric materials can be used to make capacitors with tunable capacitance. Ferroelectric capacitors are being used to make ferroelectric RAM for computers and RFID cards.

One such material is Barium Strontium Titanate (BST) which has recently become more attractive for the development of electronically tunable microwave circuits because of their high tuning speed [54], [55]. In general, a BST varactor can be designed in the form of a metal-insulator-metal capacitor or as an interdigital capacitor (IDC). Typical IDC BST varactors are fabricated based on the structure in [56]. A 0.5 micro meter thick $Ba_{0.5}Sr_{0.5}TiO_{03}$ (BST) thin film is deposited onto a MgO substrate of a thickness of 0.5 mm. The fabricated BST material exhibits a relative permittivity varying from 700 to 1,200 with a change of electric field strength from 3.5 to 0 V/mm. Capacitive tunability

for the BST varactor is defined as :

$$Tunability = \frac{C_{max} - C_{min}}{C_{max}} \times 100$$

where C_{max} and C_{min} correspond to maximum and minimum capacitance respectively. A BST varactor typically consists of a cell of interdigital capacitors. In [56], an interdigital capacitor with six fingers as a basic cell for the BST varactors are developed. The IDC fingers have a gap of 10 micrometer between them. These fingers are 220 micrometer long and 10 micrometer wide. This basic BST varactor cell has a capacitive tunability of about 28.6% for the given range of the DC bias voltages. A two pole tunable Bandstop filter using developed BST varactors is reported.

2.5.3   MEMS

Microelectromechanical systems perform electrical and mechancial functions with components of the size of micrometers. MEMS in microwave circuits have been primarily used as metal contact switches with operation from DC to 100 GHz, as analog varactors with tuning range varying from 1.5:1 to 8:1 from frequency range varying from 500 MHz to greater than 100 GHz and as capacitive switches. They exhibit advantages of low loss, high linearity, high Q and high power handling. MEMS products can be broadly classified into three different categories:

a. MEMS sensors: These are being mainly used in sensing applications namely acoustic wave, biomedical, chemical, inertia, optical, pressure, radiation, thermal, etc.

b. MEMS actuators: Used in electrical and optical relays, switches and varactors, grippers, tweezers and tongs, linear and rotary motors, etc.

c. MEMS Device components: used as mini robots, micro surgical equipments, etc.

MEMS actuators utilize mechanical movement using electrostatic, magnetostatic, piezo-electric, or thermal force [57]. The electrostatic actuation method is the most widely used technique in the RF community. The conventional RF-MEMS varactor is essentially a parallel plate capacitor whose capacitance is determined by the spacing between a fixed bottom plate and a movable suspended top plate. Electrostatic actuation occurs when an electrostatic force is created by applying a DC voltage between the capacitor plates, thereby displacing the movable plate towards the fixed plate. A typical example of MEMS used as a switch element is proposed in [58] where a bandpass filter with a switchable inductor at the centre of the filter is presented. MEMS switches force two different operations of the filter at 10 GHz and 30 GHz.

2.5.4   P-I-N Diodes

The *p-i-n* diode consists of two narrow, but highly doped, semiconductor regions separated by a thicker, lightly-doped material called the intrinsic region. One of the heavily doped

regions is a p-type material and the other is n-type. The same semiconductor material, usually Silicon, is used for all three areas. Silicon is used most often for its power-handling capability and because it provides a highly resistive intrinsic *(i)* region. The *p-i-n* diode acts as an ordinary diode at frequencies up to about 100 MHz, but above this frequency the operational characteristics change. The large intrinsic region increases the transit time of electrons crossing the region. Above 100 MHz, electrons begin to accumulate in the intrinsic region. The carrier storage in the intrinsic region causes the diode to stop acting as a rectifier and begin acting as a variable resistance.

When the bias on a *p-i-n* diode is varied, its microwave resistance changes from a typical value of 6 kilo-ohms under negative bias to about 5 ohms when the bias is positive. Due to this property, *p-i-n* diodes are frequently used to produce reconfigurable discrete states on a filter response and are very attractive for low cost implementations. Two switchable bandstop filters are designed in [59]. These filters can switch between the two center frequency states, each having a defined fractional bandwidth.

Besides the above mentioned components, FET and ferromagnetic materials like Yttrium Iron Garnet (YIG) are also used to implement tunable components. For the purpose of this dissertation, varactor diodes are chosen as external tuning components as they offer considerable advantages of low noise characteristics and are readily available and economical. Varactor diodes come in smaller sizes and are lightweight and can be easily integrated to the planar filter circuits presented in this dissertation as discussed in the subsequent chapters.

2.6 Non-Resonant Nodes

Non-Resonant Nodes have primarily been used in filter networks to realize finite frequency transmission zeros. As mentioned in sections 2.1.2 and 2.1.3, by relating the scattering parameters S_{21}, S_{11} to characteristic polynomials $F(s)$, $P(s)$ and $E(s)$, Chebyshev transfer function can be classified into either an all-pole response or a response with prescribed transmission zeros. For an all-pole response, all the transmission zeros are located at infinity. At $s = j\infty$, $S_{21} = 0$ and this phenomenon is known as transmission zero at infinity. An all-pole response can be easily synthesized using ladder network synthesis. For Chebyshev transfer functions having prescribed transmission zeros, the transmission zeros locations can be pre-specified for the filter response. The synthesis of the transfer function for such a response is presented in section 2.1.3. The Chebyshev transfer functions with prescribed transmission zeros can be realized either using cross coupled networks, extracted pole networks or through modular components like singlets, doublets etc.

The cross-coupled filter topology consists of mainline couplings and cross couplings within the same filter network. The term mainline couplings refers to the inter-resonator couplings between two in-line (adjacent) resonators. The term cross couplings refers to the couplings between non adjacent resonators. A number of synthesis techniques have been proposed to realize such a network [46], [44,60,61]. In [46], a cross coupled network is synthesized using a generalized Chebyshev transfer function with prescribed transmission zeros as presented in section 2.1.3. Firstly, scattering parameters are represented in terms

of even and odd mode admittances which correspond to the input admittances when an open or short circuiting plane is inserted along the line of symmetry. This is followed by representing scattering parameters in terms of characteristic function as presented in section 2.1.1. The two representations of scattering parameters are then utilized to obtain a relation between characteristic function and even/odd mode admittances. A Hurwitz polynomial is then created and an even mode admittance polynomial is derived from it utilizing the fact that left half plane zeros belong to the even mode admittance Y_e. Finally, Y_e is represented as a ratio of odd polynomial to even polynomial and network elements are extracted. A fourth order cross coupled ladder network with two transmission zeros at infinity and two at finite positions are synthesized using the proposed technique. In [61], using a similar technique as in [46], a low pass prototype suited for implementation in TEM mode filters is presented. The low pass prototype produces an even multiple of transmission zeros at a finite point on the $j\omega$ axis and three transmission zeros at infinity. A low pass prototype implementation in suspended substrate stripline (SSS) topology at 4 GHz with order $N = 11$, return loss $RL = 26$ dB, having a minimum stopband insertion loss $IL = 40$ dB, based on a generalized chebyshev function is presented. In [44], cross coupled filter networks are represented for an asymmetric filter response using frequency invariant reactances (FIR) in the filter networks. Transmission matrices are derived and cross couplings are implemented by using parallel coupled inverters which are inverters between non adjacent resonators.

The cross coupled network has a drawback that when the transmission zeros are close to a passband edge, the values of the required couplings may be physically unrealisable. Moreover, if cross couplings are used, the designer does not have specific control over the position of the zeros which makes the structure sensitive and difficult to adjust. To overcome the shortcomings of cross coupled network, the Extracted Pole technique was introduced where the term 'Non-Resonant Nodes' originated. The Extracted Pole technique starts with the specification of a Chebyshev transfer function with prescribed transmission zeros. The specified transfer function is then utilized to synthesize transmission zeros generating elements (stubs) connected in series or parallel of a ladder network. It was first introduced for a symmetric response in [62] and later extended to include asymmetric responses as presented in [44]. In [62], different extraction cycles are performed to synthesize extracted pole network. Firstly, unity impedance phase shifters from either end of the network are extracted. This is followed by extraction of single shunt resonators from either end to extract a complimentary pair of j-axis transmission zeros from each side of the passband. This process is repeated until all the finite j-axis transmission zeros have been extracted and the remaining network can be realized by cross-coupled network. A sixth order elliptic function prototype with four j-axis transmission zeros is synthesized. A 6th order waveguide filter is designed at 19.6 GHz using the proposed technique. In [44], similar technique is repeated for a case of asymmetric response filters with frequency invariant reactances (FIR) and a 4th order filter with two transmission zeros is synthesized and designed in waveguide technology as shown in fig. 2.14 and fig. 2.15.

In [63–66] in-line filter prototypes with non-resonant node (NRN) producing one or two transmission zeros are extracted at the input end and/or at the output end of the
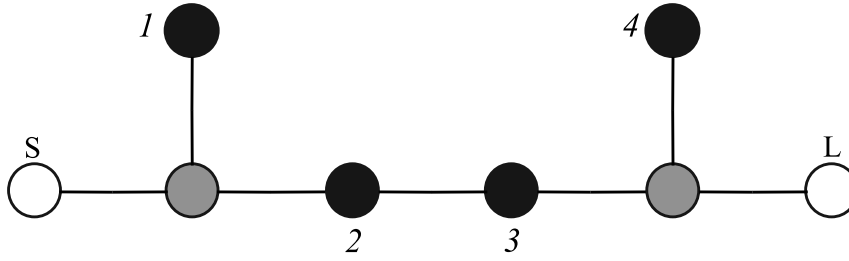
Figure 2.14: Fourth order filter network with two transmission zeros using extracted pole
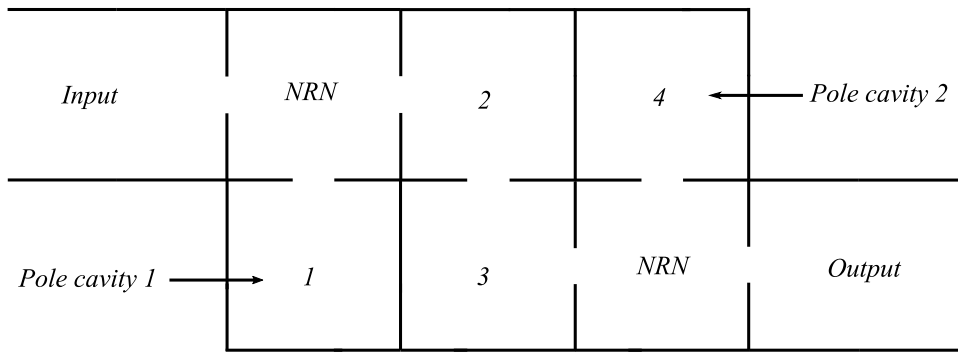
Figure 2.15: Waveguide realization of the filter with NRN

filter network. In [63], [64], [65] the filter topology consists of resonators coupled through inverters, with input and/or output taken at the second and/or last but one resonator. The first and last resonators together with their adjacent inverters form the non-resonant node (NRN). These NRN act as bandstop resonators (similar as in case of extracted pole method) and up to two transmission zeros can be introduced in the filter response. In [64], it is shown that as the source is coupled to the first two resonators, a triplet is formed at the source end and a similar triplet is formed at the load end consisting of the last two resonators and the load. A synthesis technique to extract triplets at the source or load ends is presented. In [65] circuit transformations are applied to convert synthesized triplets to an in-line topology in order to realize the filters in combline or interdigital topology.

Non-resonant nodes play a significant role in filters designed with a modular approach. In a modular approach, building blocks capable of generating and controlling one or two transmission zeros are cascaded. These building blocks comprise of cascaded singlets, cascaded doublets, cascaded triplets and cascaded quadruplets. A singlet, doublet, and a triplet configuration can generate one transmission zero on the complex s-plane. A quadruplet can generate a pair of transmission zeros, which are either on the imaginary axis or on the real axis of the s-plane. Each building block is separated by a non-resonant node (NRN) synthesized in between the different building blocks. The insertion of a NRN between the different building blocks allows the individual elements to be designed sepa-

rately and connected together with minor dimensional adjustments. With this approach, a filter of order N can generate up to N transmission zeros directly. In [67], a singlet building block is presented which can generate single transmission zero. The singlet network consists of a single resonator coupled to source and load end where source and load are in turn coupled to each other. A non-resonant node model is presented which consists of cascaded singlets separated by a non-resonant node. Such a cascaded modular structure gives independent tuning of transmission zeros and a second order filter network with two transmission zeros is presented.

2.7   Conclusion

This chapter reviews the basic fundamentals of coupled resonator filters. Filter transfer function and characteristic function definitions are reviewed. Detailed discussion on the use of Chebyshev response in filter networks is discussed. Classical lowpass prototype network and its corresponding transformations are presented. Theory of immittance inverters is reviewed. Design equations for coupled resonator filters with immittance inverters for low-pass and bandpass case are presented. Commonly used immittance inverter models are listed. A section on tunable elements used in modern day tunable filters is reviewed. Finally, theory of non-resonant node is discussed with relevant citations of literature. Chapter 3 presents the theory of novel non-resonant node inverters. Design procedures for implementing non-resonant node inverters in microstrip and substrate integrated waveguide technologies is presented with illustration using design examples.

Chapter 3

NRN Inverters (NIs)

As discussed in the introduction chapter, reconfigurable front end systems require tunable filters to tune these systems to multiple frequency bands. While tuning the operating centre frequency of these wireless systems using tunable filters, the desired bandwidth gets altered. The primary reason for the bandwidth change is the use of fixed frequency inverters between resonators. Inverters are the primary elements in filters and are the deciding factors for the bandwidth and external quality factor for the filter. A number of inverters are listed in the previous chapter, however, most of them are capable of working only at a single frequency, which is the centre frequency of operation of the filter. There is a need to investigate new inverter topologies capable of controlling the coupling between resonators and maintaining a constant bandwidth across the entire frequency tuning range. This chapter describes a new class of inverters called 'non-resonant node inverters' which are capable of controlling the bandwidth.

3.1 NI Circuit Model and Design Equations: Microstrip Implementation

3.1.1 Non-resonant node inverters

The technique of extracting non-resonant nodes (NRNs) in the filter networks have been limited to the use of generating transmission zeros. Most of the network synthesis techniques developed are more suitable for implementation in waveguide technology. The NRNs synthesized in the Extracted Pole Technique as discussed in section 2.6, are usually placed either in between the source node and the first resonator or the load node and the last resonator of a fixed frequency response filter. Limited work on extracting NRNs in planar technology have been demonstrated. As discussed in section 1.1, coupling reducer elements in the form of detuned resonators presented in [25], are placed in between adjacent resonators to vary the bandwidth. However, no attempt is made to formalize or generalize the concept beyond the application to combline filters. In addition, the dimensional parameters of the coupling reducer elements are obtained through optimization only, and a synthesis procedure to obtain the dimensional information is not presented. The idea for the present work originates with the investigation of extracting NRNs in between adjacent resonators in the form of tunable inverters, in order to control the inter-
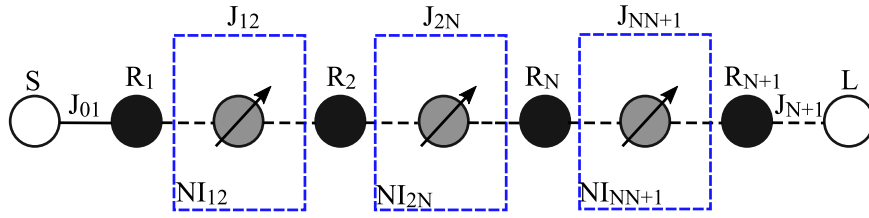
NI: Reconfigurable Non Resonant Node Inverter

R : Resonater

J : Admittance Inverter

S : Source

L : Load

Figure 3.1: Filter topology using reconfigurable NI

resonator couplings in a tunable filter. A new class of inverters named non-resonant node inverters (NIs) is proposed which is capable of maintaining constant absolute bandwidth as the centre frequency of the filter is tuned. To simplify the mathematical analysis and the filter prototype designs, an all pole Chebyshev filter transfer function is chosen and the proposed NI is implemented in planar filters based on microstrip and substrate integrated waveguide (SIW) technologies.

3.1.2 Development of NI model

Figure 3.1 describes a tunable filter topology with fixed frequency pi-inverters and proposed tunable non-resonant node based inverters (NIs). The white circles denote the source and load ports while the black circles denote tunable resonators of the filter. Considering the case of capacitive coupling, blue square dashed boxes denote conventional fixed frequency pi-inverters, designed to operate at the nominal centre frequency of a tunable filter. As the resonators are tuned to different centre frequencies, the configuration of the pi-inverter does not change, resulting in changed bandwidth. This condition can be avoided by using the proposed NIs depicted by grey circles with arrows. These inverters are capable of tuning the coupling coefficient between the resonators and hence can be utilized to maintain a constant absolute bandwidth across the entire centre frequency tuning range of the filter. Therefore, the limitations of conventional pi-inverters of operating at a single centre frequency can be avoided with the use of non-resonant node inverters.

Figure 3.2(a) represents the filter network consisting of adjacent resonators and a tunable NI is placed in between them. Figure 3.2(b) represents the complete circuit model of NI suitable for microstrip implementation. As depicted in figure 3.2(b), the NI circuit model comprises of two susceptive pi-networks represented by dashed lines with susceptances jB' and a section of open-circuited transmission line T_{LB} with electrical length θ' and characteristic impedance Z'_0. The transmission line T_{LB} is embedded between the two susceptive pi-networks and has a resonant frequency far out of the band of operation of the filter. Variable susceptances jB'_{var} are connected to the ends of the node line T_{LB}

and correspond to the varactor diodes to be attached in the final filter prototypes. These varactor diodes are utilized to adjust the effective electrical length θ' of the transmission line T_{LB} and maintain a constant bandwidth response at different centre frequencies of the filter prototype.

In order to derive the design equations for NIs, a circuit substitution is performed as shown in figure 3.2(c). It is known that an open ended transmission line with variable susceptances connected to its ends results in its effective electrical length changed with the line appearing longer [68,69]. Utilizing this fact, the inner pi-network of figure 3.2(c) (comprising of transmission line T_{LB} and difference of variable susceptance jB'_{var} and susceptance jB') can be equated to the transmission line T_{LC}. Transmission line T_{LC} is a general open-ended transmission line of effective electrical length θ and characteristic impedance Z_0. The electrical length θ of the transmission line T_{LC} represents the sum of the electrical length θ' of the transmission line T_{LB} and the electrical length corresponding to the difference of susceptances jB'_{var}-jB'. A relationship between the two networks of figure 3.2(c) can be established by equating their transmission matrices respectively. The equivalent transmission line T_{LC} of figure 3.2(c) is substituted in figure 3.2(a) in place of the inner pi-network (comprising of T_{LB} and jB'_{var}-jB') and hence the network of figure 3.2(a) is reduced to figure 3.2(d). The network of figure 3.2(d) results in an equivalent inverter at f_0.

The purpose of reducing the network of figure 3.2(a) into figure 3.2(d) is that the network of figure 3.2(d) can be easily equated to a conventional pi-inverter. Since the two networks are in the same form, their transmission matrices can be easily equated. By equating the transmission matrices, design equations can be formulated. The design equations would compute the output parameters of an equivalent NI from the input parameters of a conventional pi-admittance inverter designed for the desired filter specification.

3.1.3 Design equations for NI parameters

In order to derive the design equations for a NI and formulate the coupling coefficient in terms of the NI parameters, the following steps are performed.

1. An equivalence is established between the pi-network (comprising of transmission line T_{LB}, susceptance $jB'_{var} - jB'$) and transmission line T_{LC} as shown in figure 3.2(c) by equating their transmission matrices respectively.
The transmission matrix of the pi-network is given as,

$$A_{T_{LB}} = \cos\theta' - B_{var}Z_0'\sin\theta'$$
$$B_{T_{LB}} = jZ_0'\sin\theta'$$
$$C_{T_{LB}} = 2jB_{var}\cos\theta' + jY_0'\sin\theta' - jB_{var}^2Z_0'\sin\theta'$$
$$D_{T_{LB}} = \cos\theta' - B_{var}Z_0'\sin\theta'$$
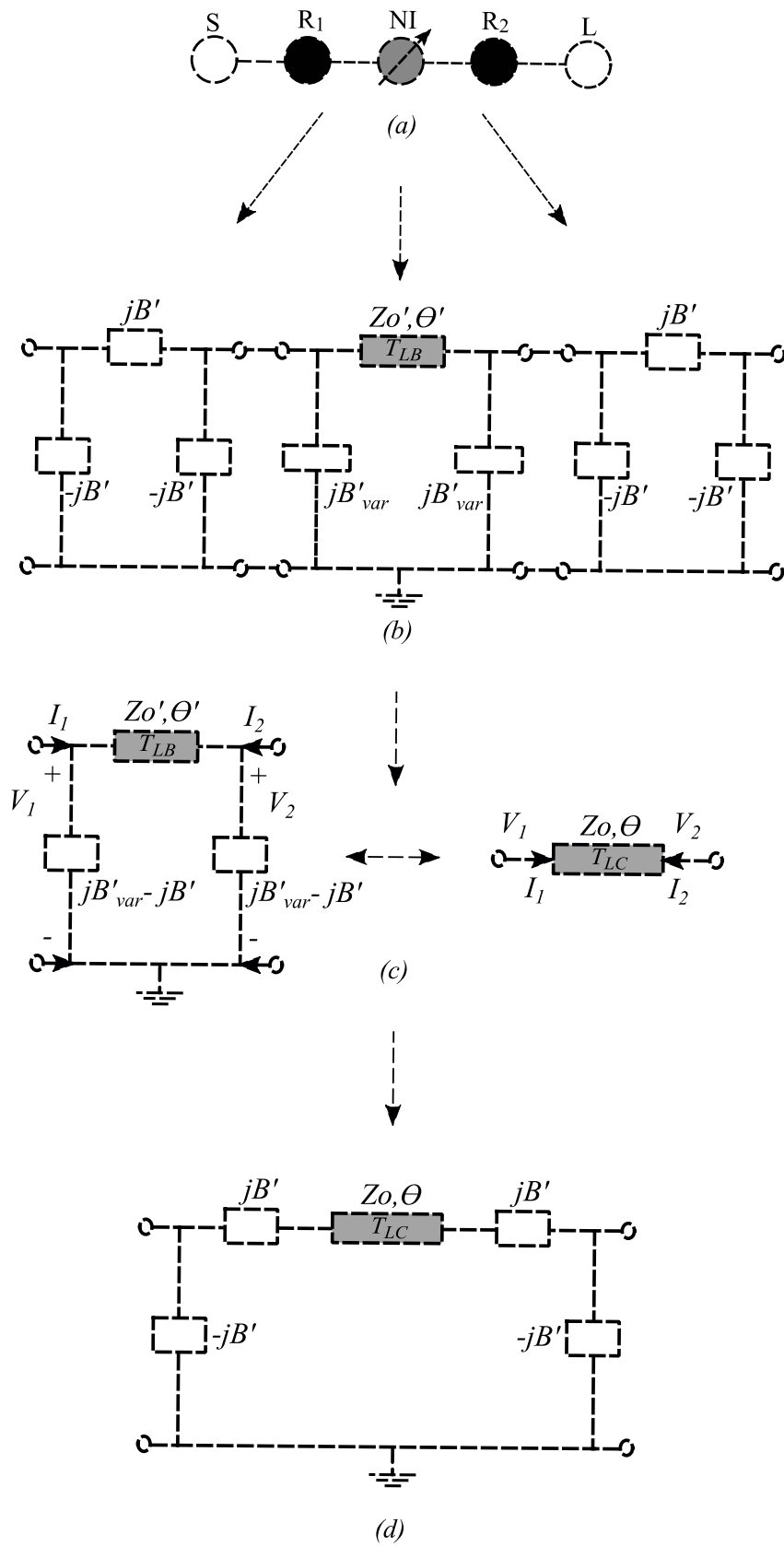
here,

$$jB_{var} = jB'_{var} - jB'$$

Figure 3.2: Development of NI circuit model

and

$$B_{var} = \omega_0 C_{var}$$

The parameter ω_0 correspond to the resonant frequency and C_{var} corresponds to the variable capacitance offered by the varactor diodes. Parameter θ', Z_0' correspond to the electrical length and characteristic impedance of the transmission line T_{LB}.

The transmission matrix of the transmission line T_{LC} is simply given by,

$$A_{T_{LC}} = \cos\theta$$
$$B_{T_{LC}} = jZ_0 \sin\theta$$
$$C_{T_{LC}} = jY_0 \sin\theta$$
$$D_{T_{LC}} = \cos\theta$$

Parameter θ, Z_0 correspond to the electrical length and characteristic impedance of the transmission line T_{LC}.

Equating coefficients $A_{T_{LB}}$ to $A_{T_{LC}}$ and $D_{T_{LB}}$ to $D_{T_{LC}}$,

$$\cos\theta = \cos\theta' - B_{var}Z_0'\sin\theta' \tag{3.1}$$

Equating coefficients $B_{T_{LB}}$ to $B_{T_{LC}}$,

$$jZ_0\sin\theta = jZ_0'\sin\theta'$$

or,

$$Y_0'\sin\theta = Y_0\sin\theta' \tag{3.2}$$

Equating coefficients $C_{T_{LB}}$ to $C_{T_{LC}}$,

$$Y_0\sin\theta = 2B_{var}\cos\theta' + Y_0'\sin\theta' - B_{var}^2 Z_0'\sin\theta' \tag{3.3}$$

Out of the three equations 3.1-3.3 established, equation 3.3 consists of all the parameters of the equivalance depicted in figure 3.2(c) and can be utilized to derive an expression for pi-network parameters (θ',Y_0',B_{var}) in terms of T_{LC} parameters (θ, Y_0). Equation 3.3 is rewritten in a simplified form by substituting for $\cos\theta'$ from equation 3.1 into equation 3.3,

$$Y_0 Y_0'\sin\theta = 2B_{var}Y_0'\left[\cos\theta + \frac{B_{var}\sin\theta'}{Y_0'}\right] + Y_0'^2\sin\theta' - B_{var}^2\sin\theta'$$

or,

$$Y_0 Y_0'\sin\theta = 2B_{var}Y_0'\cos\theta + B_{var}^2\sin\theta' + Y_0'^2\sin\theta' \tag{3.4}$$

writing in terms of $\sin\theta'$,

$$\sin\theta' = \frac{Y_0 Y_0'\sin\theta - 2B_{var}Y_0'\cos\theta}{B_{var}^2 + Y_0^{2'}} \tag{3.5}$$

Equation 3.5 is useful to derive the length θ' from the synthesized value of NI parameter θ for the chosen values of parameters Y_0',Y_0 and B_{var} as discussed in the implementation example in section 3.4. It is to be pointed out that alternate formulations to establish a relation between pi-network parameters and the transmission line T_{LC} parameters are also possible using equations 3.1 to 3.3.

2. In order to formulate the design equations, the transmission matrix of the reduced NI model of figure 3.2(d) is equated to the transmission matrix of a conventional pi-inverter.

The transmission matrix of NI is given by cascading the individual transmission matrices of the shunt and series arm,

$$\begin{bmatrix} A & B \\ C & D \end{bmatrix}_{NI} = \begin{bmatrix} A & B \\ C & D \end{bmatrix}_{shunt} \begin{bmatrix} A & B \\ C & D \end{bmatrix}_{series} \begin{bmatrix} A & B \\ C & D \end{bmatrix}_{shunt} \tag{3.6}$$

The transmission matrix of the shunt arm is given by matrix,

$$\begin{bmatrix} A & B \\ C & D \end{bmatrix}_{shunt} = \begin{bmatrix} 1 & 0 \\ -jB' & 1 \end{bmatrix} \tag{3.7}$$

The transmission matrix of the series arm is given by,

$$\begin{bmatrix} A & B \\ C & D \end{bmatrix}_{series} = \begin{bmatrix} 1 & \dfrac{1}{jB'} \\ 0 & 1 \end{bmatrix} \begin{bmatrix} \cos\theta & \dfrac{j\sin\theta}{Y_0} \\ jY_0\sin\theta & \cos\theta \end{bmatrix} \begin{bmatrix} 1 & \dfrac{1}{jB'} \\ 0 & 1 \end{bmatrix} \tag{3.8}$$

Thus,

$$A_{Series} = \cos\theta + \frac{\sin\theta Y_0}{B'}$$
$$B_{Series} = \frac{2\cos\theta}{jB'} + \frac{Y_0\sin\theta}{jB'^2} + \frac{j\sin\theta}{Y_0}$$
$$C_{Series} = jY_0\sin\theta$$
$$D_{Series} = \cos\theta + \frac{\sin\theta Y_0}{B'}$$

After substituting the corresponding transmission matrices of equation 3.7 and 3.8 in equation 3.6, the overall T-matrix of the NI is given by,

$$A_{NI} = -\cos\theta + \frac{\sin\theta B'}{Y_0}$$
$$B_{NI} = \frac{2\cos\theta}{jB'} + \frac{Y_0\sin\theta}{jB'^2} + \frac{j\sin\theta}{Y_0}$$
$$C_{NI} = \frac{-jB'^2\sin\theta}{Y_0}$$
$$D_{NI} = -\cos\theta + \frac{B'\sin\theta}{Y_0}$$

By equating the transmission matrix of NI to the transmission matrix of a pi-inverter, corresponding design equations can be formulated.

$$\begin{bmatrix} A & B \\ C & D \end{bmatrix}_{NI} = \begin{bmatrix} 0 & \dfrac{1}{jJ} \\ -jJ & 0 \end{bmatrix}_{pi}$$

In the above equation, J refers to the inverter constant of a pi-inveter and is given by,

$$J = |B| \tag{3.9}$$

where B represents the susceptance of a pi-inverter.

Equating coefficients A and D of both inverters,

$$\frac{Y_0}{B'} = \tan\theta \tag{3.10}$$

equating coefficients of element C of both inverters,

$$J = |B| = \frac{B'^2 \sin\theta}{Y_0} \tag{3.11}$$

using equation 3.10, equation 3.11 can be written as,

$$J = |B| = \frac{B'^2 \sin\theta}{Y_0} = \frac{B'^2 \sin\theta}{B' \tan\theta} = B' \cos\theta$$

equating coefficients of element B of both inverters,

$$\frac{1}{J} = \frac{1}{|B|} = \left[\frac{2\cos\theta}{B'} + \frac{Y_0 \sin\theta}{B'^2} - \frac{\sin\theta}{Y_0} \right]$$

taking $\sin\theta$ common,

$$\frac{1}{J} = \frac{1}{|B|} = [\sin\theta] \left[\frac{2\cot\theta}{B'} + \frac{Y_0}{B'^2} - \frac{1}{Y_0} \right]$$

substituting for $\cot\theta$ from equation 3.10 and $\sin\theta$ from equation 3.11, above equation reduces to,

$$\frac{1}{J} = \frac{1}{|B|} = \frac{BY_0}{B'^2} \left[\frac{1}{Y_0} + \frac{Y_0}{B'^2} \right]$$

Solving above equation for B,

$$J = |B| = \pm \frac{B'^2}{\sqrt{B'^2 + Y_0^2}} \tag{3.12}$$

or,

$$J = |B| = \pm \frac{B'}{\sqrt{1 + \frac{Y_0^2}{B'^2}}} \tag{3.13}$$

Finally rewriting equation 3.10, 3.11 and 3.13 as final design equations,

$$\frac{Y_0}{B'} = \tan\theta \tag{3.14}$$

$$J = |B| = \frac{B'^2 \sin\theta}{Y_0} = \frac{B'^2 \sin\theta}{B' \tan\theta} = B' \cos\theta \tag{3.15}$$

or,

$$J = \pm \frac{B'}{\sqrt{1 + \frac{Y_0^2}{B'^2}}} \tag{3.16}$$

Design equation 3.14 gives an inverse relation between B' and θ. Equation 3.15 and 3.16, establish a relation between pi-inverter constant and NI inverter parameters.

3.1.4   Coupling coefficient in terms of NI parameters

The coupling coefficient between resonators k for a conventional pi-inverter is a function of the susceptance B which is normally determined by a physical distance between the resonators and can not be modified once fixed [46,51].

$$k = f(B) \tag{3.17}$$

given as,

$$k = B/\beta \tag{3.18}$$

where,

$$J = |B| \tag{3.19}$$

is the inverter constant and β is the resonator slope parameter if identical resonators are used. The coupling coefficient k can be derived in terms of NI parameters θ, B' and Y_0 of figure 3.2(d). To derive the expression for k, the tunable filter is considered to be configured at its initial starting centre frequency f_0 by adjusting the capacitance C_{var} offered by varactor diodes attached to the resonators to their minimum capacitance value. Rewriting equation 3.15, using 3.18 and 3.19,

$$k = \frac{B'^2 \sin \theta}{Y_0 \beta} \tag{3.20}$$

The equation above represents k in terms of parameters B', θ, Y_0 as shown in figure 3.2(d). For a general pi-inverter, the coupling coefficient $k \propto \dfrac{1}{\beta}$, where β is the susceptance slope parameter of the resonators. For tunable filters, as the centre frequency is changed, the susceptance slope parameter β changes and hence the coupling coefficient changes. As shown in equation 3.20, for non-resonant node inverter (NI) based filters, the coupling coefficient $k \propto (B', \theta)$, while $k \propto \dfrac{1}{\beta Y_0}$. As the centre frequency of the filter is tuned, the length θ of the NI can be adjusted by variable capacitances in order to compensate for the change in the susceptance slope parameter and maintain a constant coupling coefficient throughout the centre frequency tuning range.

For the case of planar filters considered in this dissertation, the length θ of the NI as shown in figure 3.2(d), is implemented using the pi-network of figure 3.2(c). It is useful to formulate the coupling coefficient in terms of the NI implementing parameters θ', Y_0' and B_{var} as shown in figure 3.2(c). By substituting the value of $\sin \theta$ from equation 3.3 into equation 3.20,

$$k = \left[\frac{B'^2}{\beta Y_0} \right] \left[\frac{2 B_{var} Y_0' \cos \theta' + Y_0'^2 \sin \theta' - B_{var}^2 \sin \theta'}{Y_0 Y_0'} \right]$$

or,

$$k = \left[\frac{B'^2}{\beta Y_0} \right] \left[\frac{2 B_{var} Y_0' \cos \theta' + \sin \theta' (Y_0'^2 - B_{var}^2)}{Y_0 Y_0'} \right] \tag{3.21}$$

Further, substituting $\cos\theta'$ from equation 3.1 in equation 3.21,

$$k = \left[\frac{B'^2}{\beta Y_0}\right]\left[\frac{2B_{var}Y_0'\left[\cos\theta + \dfrac{B_{var}\sin\theta'}{Y_0'}\right] + Y_0'^2\sin\theta' - B_{var}^2\sin\theta'}{Y_0Y_0'}\right]$$

or,

$$k = \frac{B'^2(2B_{var}\cos\theta Y_0' + B_{var}^2\sin\theta' + Y_0'^2\sin\theta')}{Y_0'Y_0^2\beta} \tag{3.22}$$

In order to utilize the above equations 3.21 and 3.22, firstly, NI parameters B' and θ are calculated using design equations for a chosen value of Y_0 as shown in figure 3.2(d). Calculated parameters B' and θ depend upon the specified value of coupling coefficient k, at the starting centre frequency f_0 of the tunable filter as depicted by the design equations.

Further, by choosing the value of parameter Y_0' and specifying the value of the resonator slope parameter β, above equations 3.21 and 3.22 can be used to plot a graph between the coupling coefficient k and the initial variable susceptance B_{var} offered by practical varactor diodes for different values of electrical length θ'. Such a graph would help the designer by providing multiple sets of implementing parameters θ' and B_{var}, for a desired value of coupling coefficient k, at the specified centre frequency f_0. This graph is plotted at the specified value of the starting centre frequency of the filter, f_0, which is given by the chosen resonators with the susceptance slope parameter β.

However, equation 3.21 has a limiting condition because of the term $Y_0'^2 - B_{var}^2$ in the numerator. Susceptance parameter B_{var} is implemented using variable capacitor C_{var} and is given by,

$$B_{var} = \omega_0 C_{var}$$

For a chosen value of θ', if the initial capacitance offered by the varactor diodes C_{var} is chosen such that B_{var} is greater than Y_0', the numerator term $Y_0'^2 - B_{var}^2$ becomes negative and the overall coupling coefficient k is predicted lower than its original value. This non linearity is more evident as the angles of θ' become larger.

In order to avoid above condition, equation 3.22 is formulated by substituting for $\cos\theta'$ from equation 3.1 in to equation 3.21. Equation 3.22 is written in terms of mixed NI parameters, $\theta, B', Y_0, Y_0', \theta'$ and B_{var} represented by figure 3.2(c) and 3.2(d) and is valid for all the practical values of initial capacitance C_{var} offered by the varactor diodes. Equation 3.22 utilizes the value of minimum variable capacitance C_{var} offered by the varactor diodes as specified in their data sheets, to determine an optimum value of electrical length θ' of the NI required to realize a desired coupling coefficient k at the desired starting centre frequency f_0.

To summarize, three formulations for k are presented in this section to represent the non-resonant node inverters (NIs). Equation 3.20, representing k in terms of (B', θ, Y_0) where the effect of C_{var} is embedded in line length θ and is well suited for lumped element circuit simulation. Equation 3.21, representing k in terms of $(\theta', B', Y_0, Y_0', B_{var})$ valid for $B_{var} < Y_0'$. Equation 3.22, representing k in terms of $(\theta, \theta', B', Y_0, Y_0', B_{var})$ is suited for

distributed circuit implementation and considers all practical values of initial capacitance C_{var} offered by the varactor diodes as per their data sheet. The utility of equation 3.22 is demonstrated with the help of a practical design example in section 3.4.

An electromagnetic simulation based study is performed to further investigate the idea of utilizing non-resonant nodes for tunable bandwidth filters. A simulation based dimensional analysis of non-resonant nodes is performed in the following section. The theoretical model is then compared and validated against EM simulation results.

3.2 Dimensional Analysis for Case I ($C_{var} = 0$): Microstrip Implementation
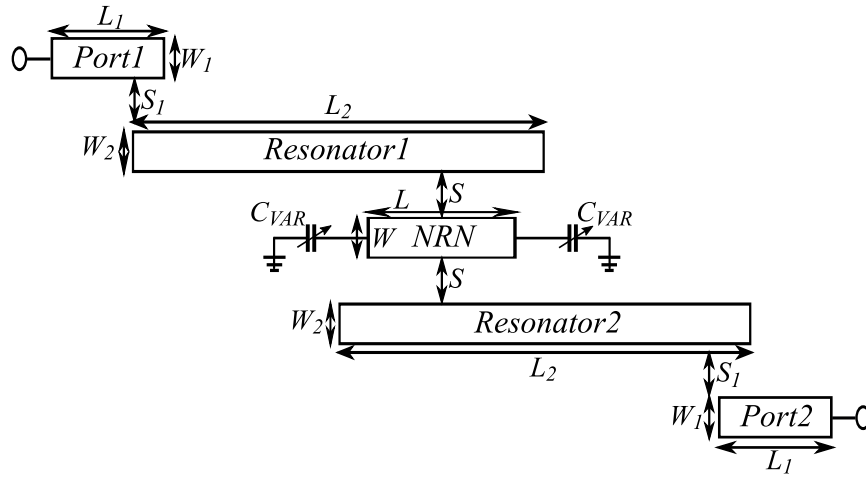

Figure 3.3: Dimensional analysis setup

The theory developed in the previous section presents a mathematical model and design equations for the formulation of non-resonant node inverters for a desired coupling coefficient at the desired starting centre frequency of the filter. This section demonstrates a more detailed analysis of NI parameters for a practical implementation setup with the help of EM simulations and comparisons with the circuit models are performed.

For a practical implementation of NI, a planar microstrip structure is chosen. The NI model is realized in a parallel half-wave coupled microstrip structure as shown in figure 3.3. In figure 3.3, the longer microstrip lines L_2 represent the two half-wavelength microstrip resonators and the shorter line L in between the resonators together with susceptive gaps S represent the NI. In order to get maximum variation in the coupling between the resonators, the NI is placed at a point of maximum coupling between the resonators which occurs when the two half-wavelength resonators overlap by a distance of quarter-wavelength. Hence, the second resonator is kept at an offset by quarter-wavelength from the first resonator and NI is placed in between them. Rogers RO 4003C substrate with dielectric constant of 3.38 and height of 0.508 mm is chosen for the study. Lines $L1$ represent the feed lines corresponding to 50 ohm termination. The dimensions of the setup of figure 3.3 are $L2 = 17$ mm, $W2 = W = W1 = 1.175$ mm, $L = 3.5$ mm and $L1 = 10.6$ mm. The resonators have a resonant frequency of 5 GHz and impedance of 50

ohms. Two cases are taken for this study to understand the effect of NI parameters on the coupling coefficient between the resonators.

For the first case, variable capacitance C_{var} attached to the ends of the NI transmission line L are set to an open state $C_{var} = 0$. This condition resembles the reduced NI model of figure 3.2(d), where the effect of variable capacitance C_{var} is embedded in the length parameter θ of NI. The NI parameters of the reduced network model of figure 3.2(d) correspond to the physical dimensional parameters of NI as shown in figure 3.3. Parameter θ of figure 3.2(d) corresponds to the physical length L of NI as shown in figure 3.3. Parameter impedance Z_0 correspond to the physical width W of the NI. Susceptance jB' correspond to the susceptive gap S between the resonator and NI. A study of the effect of variation of dimensions on the coupling coefficient k between resonators and its corresponding effect on the center frequency f_0 of the resonators is performed using CST EM simulator. For the case of $C_{var} = 0$, a parametric sweep using the Eigenmode solver is performed. The EM simulated results are then compared with the mathematical model parameters.
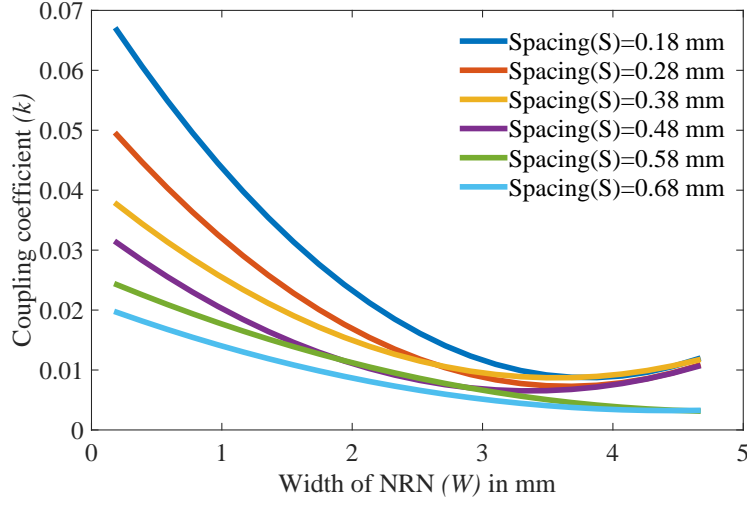
3.2.1 Effect of varying width (W)

Increasing the width W of NI correspond to increasing admittance Y_0 of the NI transmission line (decreasing impedance Z_0 of the NI transmission line). As the width W of NI is varied for different spacing values S between the resonators for a fixed length L of 3.5 mm, the coupling coefficient k tends to decrease as shown in the graph of figure 3.4(a). The coupling coefficient varies between 0.01 to 0.07 as the width varies between 1 to 5 mm (corresponding to Y_0 ranging from 0.01 to 0.05 mhos). The spacing between the resonators and NI transmission line is varied from 0.18 mm to 0.68 mm with an interval of 0.1 mm.

For comparison with the circuit model of NI, Equation 3.20 represents the case of $C_{var} = 0$ and shows that the coupling coefficient is inversely proportional to the admittance. Increased admittance (corresponding to decreased impedance) results in decreased coupling between resonators because of the shielding of the electric fields. For the above set up in figure 3.3, utilizing the fact that the resonator susceptance slope for half-wavelength open circuited resonators is given by,

$$\beta = (\pi/2)Y_{0res} = 0.0314 \tag{3.23}$$

where, admittance $Y_{0res} = 0.02$ mho corresponds to the 50 ohm half-wavelength resonator, model equation 3.20 is used to plot admittance Y_0 of the NI transmission line against the coupling coefficient k for different susceptance values B'. The length L of NI is fixed at 3.5 mm, which corresponds to an electrical length $\theta = 35°$ or 0.61 radians at 5 GHz. Coupling coefficient varies between 0.01 to 0.085 as admittance varies between 0.01 to 0.04 mhos.

As shown in the graph of figure 3.4(b), the model equation 3.20 correlates well with the practical setup and follows a similar trend to the EM simulation results. The width of the NI transmission line plays a role in maintaining the required value of coupling coefficient for a given filter specification.

(a) EM simulations
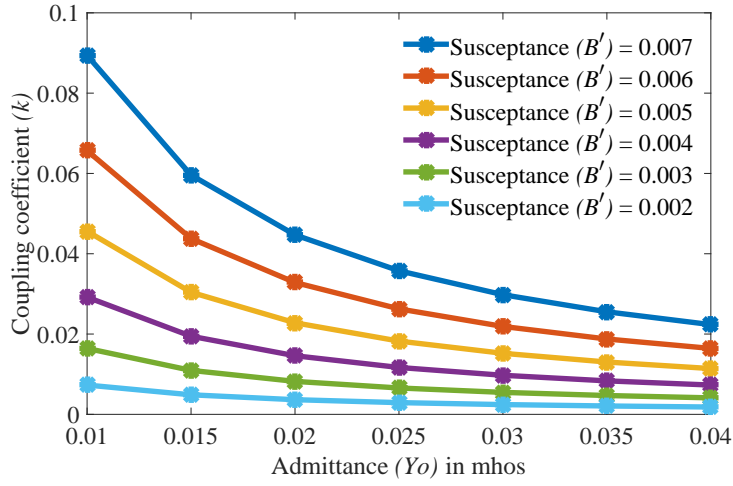

(b) Circuit model

Figure 3.4: Effect of varying width W

3.2.2 Effect of varying length (L)

The effect of varying the length L of a NI transmission line is studied for variation in coupling coefficient k between resonators for different spacing values S and fixed width W. A parameter sweep is performed by varying the length L of the NI for different spacing values S with the width W of the NI kept constant at 1.175 mm which corresponds to an admittance $Y_0 = 0.02$ mhos (representing 50 ohm impedance). The length L of the NI is increased from 2 mm to 9.5 mm with a step size of 1.5 mm. The spacing S between resonators and the NI transmission line is varied from 0.18 mm to 0.68 mm with an interval of 0.1 mm. For a specific spacing value S with the width W constant, an increase in the length L of the NI correspond to an increase in the coupling coefficient. The coupling coefficient k varies between 0.01 to 0.05 as the length of the NI varies from 2 mm to 9.5 mm as shown in figure 3.5(a). The variation of physical length L from 2 mm to 9.5 mm correspond to a range of $\pi/8$ to $\pi/2$ in radians for an electrical length θ of NI at 5 GHz.

The setup of figure 3.3 with $C_{var} = 0$, represents the circuit of figure 3.2(d) where

(a) EM simulations

(b) Circuit model
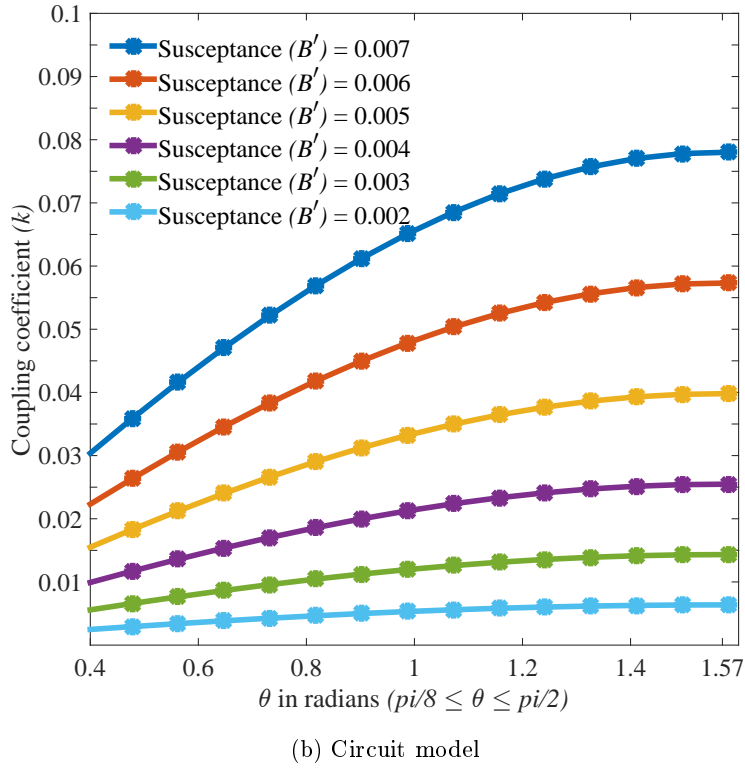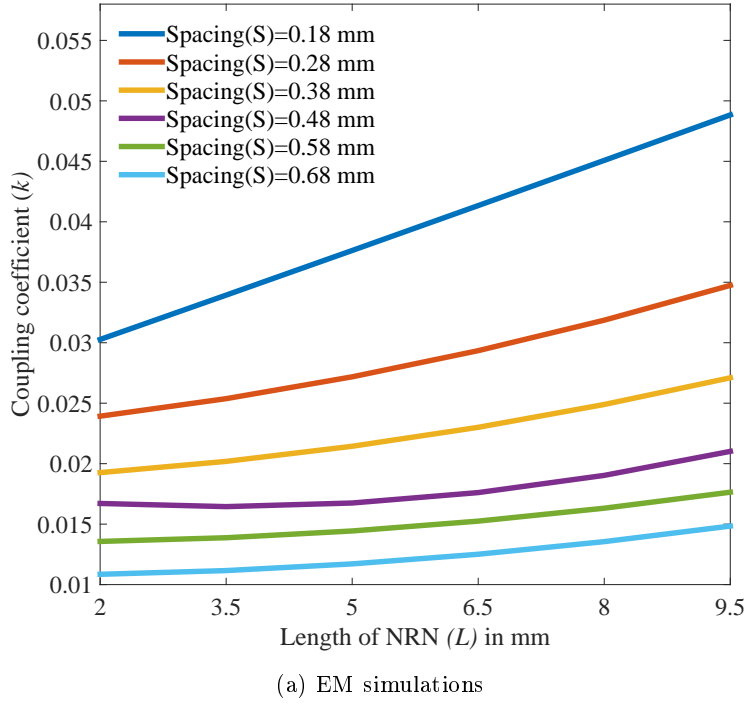
Figure 3.5: Effect of varying length L

dimension L of figure 3.3 corresponds to the length θ and spacing S correspond to the parameter B' of figure 3.2(d). By using the resonator slope parameter given by equation 3.23 and keeping the width W of NI fixed at 1.175 mm which translates to Y_0=0.02 mhos at 5 GHz (corresponding to 50 ohm lines), equation 3.20 is utilized to plot the coupling coefficient between the half-wavelength resonators against the electrical length θ of the NI, for different susceptance B' values.
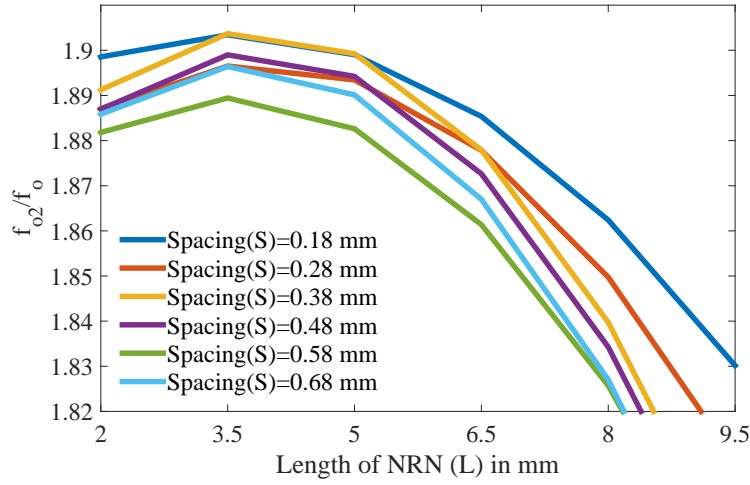
Figure 3.6: fo2/fo vs length

As shown in the graph of figure 3.5(b), as the electrical length θ of NI vary from $\pi/8$ to $\pi/2$ radians, the coupling coefficient k varies from 0.01 to 0.1. The model equation 3.20 fits well with the practical setup. There is a non-linearity arising at the higher angles (close to $\pi/2$) because of the dominance of the sine function in equation 3.20 at higher angles. The presented graphs show that with a small variation in the length of NI, significant change in the coupling coefficient k can be achieved. This property can be utilized to maintain the constant coupling coefficient across the entire centre frequency tuning range of a tunable filter.

Denoting the actual resonant frequency of the NI by f_{02} and the centre frequency of the resonators by f_0, factor f_{02}/f_0 is calculated to study the effect of the length of NI on the second resonance. As the length L of NI increases, its resonant frequency decreases and becomes closer to the resonant frequency of the two resonators which is around 5 GHz. As shown in the graph of fig. 3.6, as the length of NI increases, its resonant frequency becomes closer to the resonant frequency of the resonators and the factor f_{02}/f_0 becomes closer to 1. For the purpose of maintaining a constant coupling coefficient across the entire centre frequency tuning range of the filter, the resonance frequency of NI should be kept far away from the filter passband so that it does not effect the filter response. The second resonance gets attenuated with the use of varactor diodes as shown in the next section.

3.3 Dimensional Analysis for Case II ($C_{var} \neq 0$): Microstrip Implementation

3.3.1 Effect of varying variable capacitor (C_{var})

In this section, variable capacitance C_{var} is attached to the NI transmission line L as shown in figure 3.3. Parameter C_{var} corresponds to the variable capacitance offered by the varactor diodes. The NI transmission line L with the variable capacitance C_{var} attached to its ends, together with the susceptive gaps S forms the non-resonant node based inverter (NI). For this case, the practical setup of figure 3.3 correspond to the NI model of figure

3.2(b). NI parameters of the circuit model of figure 3.2(b) correspond to the physical dimension parameters of NI as shown in figure 3.3. Parameter θ' corresponds to the physical length L of NI while admittance Y_0' correspond to the physical width W of the NI. Susceptance jB' correspond to the susceptive gap S between the resonator and the NI. As shown in figure 3.3, NI is placed in between the two half-wavelength resonators which are placed at an offset of a quarter-wavelength and are lightly coupled to the feed lines L_1.

Compared to the previous section where the physical length L of the NI transmission line was varied and coupling coefficient k was observed, here, the length of the NI transmission line is varied by means of variable capacitances C_{var} attached to its ends. The effect of the coupling coefficient between the resonators as a result of varying C_{var} is studied for the practical setup of figure 3.3 and is compared with the circuit model. Keeping the width W of the NI fixed at 1.175 mm (corresponding to 50 ohm line), the spacing between resonators and the NI transmission line is varied from 0.18 mm to 0.68 mm with an interval of 0.1 mm. As the variable capacitance C_{var} is increased from 0 to 0.6 pF, coupling coefficient k tends to increase from 0.01 to 0.06 as shown in figure 3.7(a).

The electrical length θ' of the NI transmission line in figure 3.2(b) corresponds to dimension $L = 3.5$ mm of figure 3.3 which translates to $\theta' = 35°$ or 0.61 radians at 5 GHz. With $\theta' = 35°$, taking admittances $Y_0 = 0.02$ mhos (corresponding to 50 ohm) and $Y_0' = 0.02$ (corresponding to 50 ohm) with susceptance slope parameter β given by equation 3.23, equation 3.21 is utilized to plot the coupling coefficient k against variable capacitance C_{var} for different susceptance values B' as shown in figure 3.7(b). As the variable capacitance C_{var} is varied between 0 to 0.6 pF, the coupling coefficient k varies between 0.01 to 0.12. Equation 3.21 is utilized for the experimental setup of figure 3.3 consisting of microstrip resonators at 5 GHz. This experiment establishes the fact that by attaching variable capacitances to the NI transmission line, an effect of increase in length is observed and hence coupling coefficient tends to increase. Therefore, non-resonant node based inverters (NIs) with variable capacitances attached to its ends can be utilized to develop constant bandwidth filters. The NIs can also be utilized to develop variable bandwidth filters at a fixed centre frequency f_0.

The NI circuit produces an out of band resonance peak denoted by f_{02}. In order to analyze the effect of the second resonance on the filter response, factor f_{02}/f_0 is calculated for the capacitance range of 0 to 0.6 pF as shown in figure 3.8. As the capacitance is increased, the second resonance offered by NI circuit comes closer to the first resonance given by the resonators.

Variation in the coupling coefficient for the setup of figure 3.3 is further investigated by observing the variation in even and odd mode frequencies in between the resonators. For this study, the scattering parameters for the set up of figure 3.3 are investigated using frequency domain slover of CST. Figure 3.9(a) shows the graph between S_{21} and frequency and depicts the change in the coupling when capacitors connected at the ends of the NI are varied from 0 pF to 0.8 pF. The out of band spikes in figure 3.9(a) correspond to the resonant frequency of the NI circuit.

In order to test the impact of the out of band spike in a practical filter network setup,
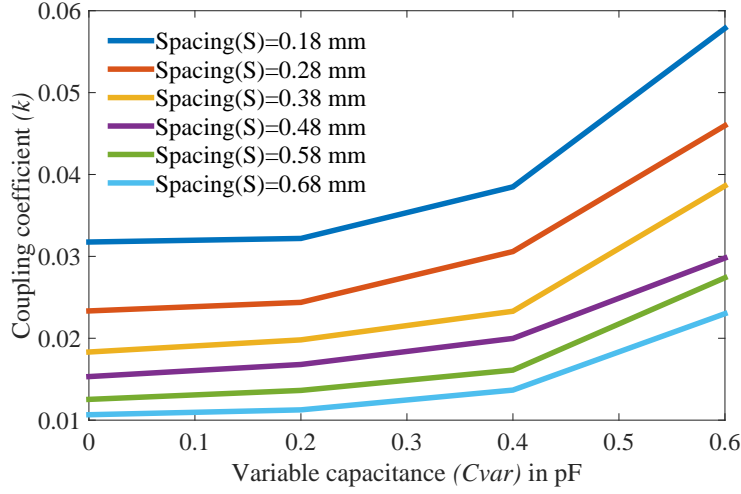
(a) EM simulations
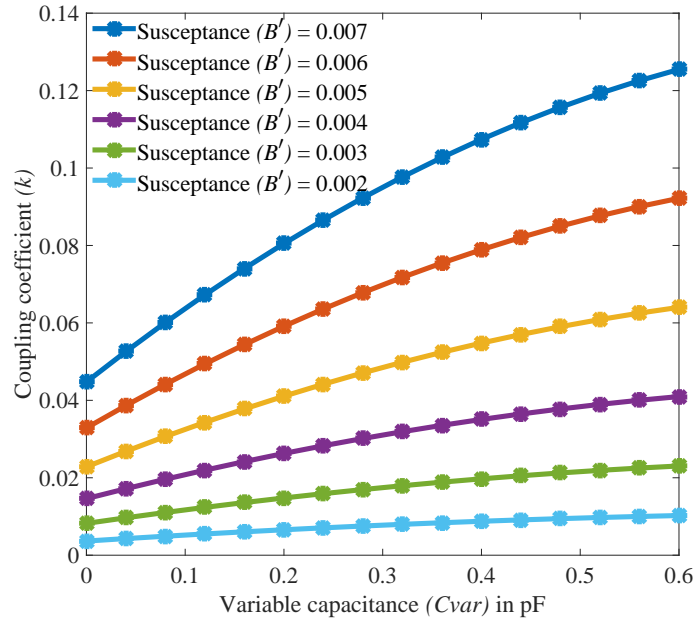
(b) Circuit model

Figure 3.7: Variable capacitance vs coupling coefficient

spice model of MA46H120 varactor diodes (from MACOM) operating between 0-12 V is added to the ends of NI transmission line in place of capacitors. The circuit is then simulated in ADS and simulation response is as shown in figure 3.9(b). By adding spice models, significant reduction in the out of band spike is achieved. This happens because losses due to quality factor of varactor diodes and substrate losses attenuate and displace the out of band spikes.

From the discussions presented in this section, it is established that with smaller capacitance change, significant coupling variation can be achieved keeping the second resonance of the NI well out of band and the structure is suitable to be implemented in filters with tunable centre frequency and constant bandwidth (CBW). The technique can be applied in filters with fixed centre frequency and tunable bandwidth. In addition, NI inverters can also be utilized in filters with constant fractional bandwidth (CFB) over centre frequency tuning range.
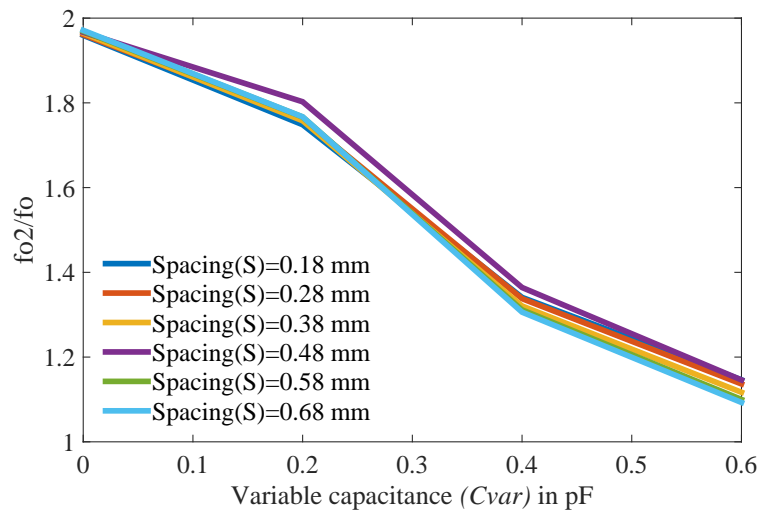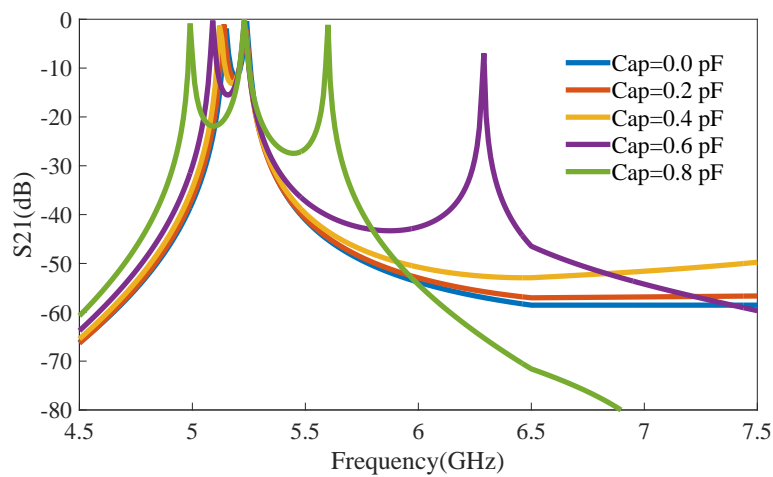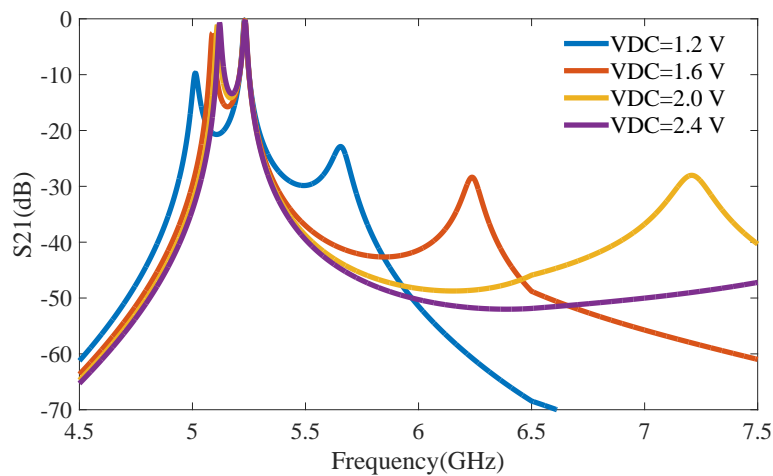
Figure 3.8: fo2/fo for different capacitance values

(a) Capacitor as tuning element

(b) Varactor diode as tuning element

Figure 3.9: Capacitor and varactor diode as tuning elements S_{21} (dB) vs frequency (GHz)

3.4   Design Steps and Numerical Example: Microstrip Implementation

In the previous two sections, a circuit model for the NI and a detailed dimensional analysis for the NI parameters is presented. This section builds on the theory developed in the previous sections and provides design steps to implement NIs in microstrip filters. A design example is then presented following the design steps.

3.4.1   Design steps for NI

The design steps for filters based on NI are as follows:

1. General design equations presented in [50] are utilized to calculate coupling coefficients k and external quality factor Q for an Nth order filter.

2. Inverter constant $J = |B|$ for an admittance pi-inverter is calculated first to utilize general design equations 3.14 - 3.16. Susceptance parameter B depends upon the resonator slope parameter β and coupling coefficient k. Using coupling coefficients calculated in step 1 and susceptance slope parameter β, inverter constant $|B| = J$ for general admittance pi-inverters is calculated using equation 3.18.

3. To use the design equations 3.14 - 3.16 for NI model, either one of the three parameters need to be fixed in order to synthesize the other two parameters. Admittance parameter Y_0=0.02 mhos (corresponding to 50 ohm line) is chosen as fixed parameter. With the calculated B from step 2. using design equation 3.16, B' is calculated.

4. Using either of the design equation 3.14 or 3.15, electrical length parameter θ shown in figure 3.2(d) is synthesized. Equation 3.20 can be used to generate a lumped element equivalent circuit of NI at this stage.

5. The synthesized electrical length θ represents sum of node length θ' and length corresponding to variable capacitance offered by varactor diodes, depicted by susceptance $B_{var} = B'_{var} - B'$ as shown in figure 3.2(c). For the resultant length θ derived in step 4 and fixing parameter $Y'_0 = 0.02$ mhos (corresponding to 50 ohm), electrical length θ' can be synthesized for the value of initial variable capacitance C_{var} offered by varactor diodes. Higher initial variable capacitance would result in smaller θ'. Equation 3.5 can be used directly to synthesize a set of θ' and C_{var}. Equation 3.22 can be used to plot design graph in terms of parameters θ' and B_{var} for the desired filter specifications. With this step, design of an equivalent NI inverter for a desired initial response of the filter is complete at the starting centre frequency f_0 of the filter.

6. Finally, for the complete design of tunable filters with NI, generalized group delay tuning method specified in [70] can be used to fine tune the filter using simulations.

3.4.2   Numerical Example: parameter calculations

A reconfigurable second order filter with tunable centre frequency and bandwidth is designed using the proposed non-resonant node inverter (NI). Microstrip parallel coupled line filter topology is chosen for the implementation of the filter. The design example begins with the specifications required for the filter followed by synthesizing design parameters for NI using design equations. With the calculated NI parameters, reconfigurable second order filter is implemented in microstrip technology with a parallel coupled line filter topology and simulation results are presented.

Specifications for second order filter are as follows:

Fractional Bandwidth $\Delta = 5\%$

Order $N = 2$

Centre frequency $f_0 = 6.2$ GHz

Passband Ripple= 0.1 dB Chebyshev

Following the design steps:

1. The coupling coefficient k and external quality factor Q of the filter are calculated as follows:

$$k_{12} = \frac{\Delta}{\sqrt{g_1 g_2}} = 0.069045$$

$$Q_S = \frac{g_0 g_1}{\Delta} = 16.862$$

$$Q_L = \frac{g_n g_{n+1}}{\Delta} = 16.862$$

2. In order to calculate inverter constants, slope parameter for chosen resonators are calculated first. Considering the case of open circuited microstrip transmission line resonators with characteristic impedance $Z_{0Res} = 50$ ohm$(Y_{0Res} = 0.02$ mhos$)$

$$\beta = \frac{Y_{0Res}\pi}{2} = 0.0314$$

The inverter constant J_{12} for a conventional pi-admittance inverter is calculated as,

$$J_{12} = k_{12} \times \beta = 0.069045 \times 0.0314 = 0.0021680$$

or,

$$|J_{12}| = |B| = 0.0021680 \tag{3.24}$$

The calculated inverter constant B will be utilized to calculate NI parameters.

3. A relation between the susceptance of the pi-inverter represented by B, NI suscep-
tance parameter B' and admittance Y_0 is established in design equation 3.16. Rewriting
equation 3.16:

$$J = \pm \frac{B'}{\sqrt{1 + \dfrac{Y_0^2}{B'^2}}}$$

Utilizing the fact that $J = |B|$ for the original inverter and taking the positive value of
the right hand side and writing above equation in terms of susceptances,

$$B = \frac{B'}{\sqrt{1 + \dfrac{Y_0^2}{B'^2}}} \tag{3.25}$$

where the symbols are defined as:

$$J = |B| = \text{Susceptance of the original pi inverter}$$

$$B' = \text{Susceptance of Non-Resonant Node inverter (NI)}$$

$$Y_0 = \frac{1}{Z_0} = \text{Admittance of the node transmission line}$$

To utilize the above equation value of Y_0 needs to be chosen. In order to match the filter
impedance scaling of $Z_0 = 50$ ohms, we choose Y_0 as

$$Y_0 = \frac{1}{Z_0} = \frac{1}{50} = 0.02 \tag{3.26}$$

Substituting equations 3.24 and 3.26 in equation 3.25,

$$0.0021680 = \pm \frac{B'}{\sqrt{1 + \dfrac{0.02^2}{B'^2}}}$$

squaring both sides of the above equation,

$$0.0021680^2 = \frac{B'^2}{1 + \dfrac{0.02^2}{B'^2}} \tag{3.27}$$

The above equation can be further written as,

$$B'^4 - (0.0021680)^2 B'^2 - (0.02)^2 (0.0021680)^2 = 0$$

or,

$$B'^4 - 4.70 \times 10^{-6} B'^2 - 1.880 \times 10^{-9} = 0$$

By solving the above equation, four roots for B' are obtained:

$$B' = 0.0068$$

$$B' = -0.0068$$

$$B' = 0.0064j$$

$$B' = -0.0064j$$

Out of the four values for B', value $B' = 0.0068$ is realizable for the filter design.

4. To calculate the value of θ, equation 3.14 is utilized as,

$$\frac{Y_0}{B'} = \tan \theta$$

or,

$$\theta = \arctan \frac{Y_0}{B'} = \arctan \frac{0.02}{0.0068} = \arctan 2.9411$$

giving,

$$\theta = 71.22°$$

5. As mentioned earlier, the node-line length θ in figure 3.2(d) is the sum of NI length θ' and the line length corresponding to the capacitance offered by the varactor diodes represented by B_{var} as shown in figure 3.2(c). Either of equation 3.5 or 3.22 can be utilized to calculate the NI design parameters θ' and B_{var}. For this example, utility of both the equations are shown. Firstly, equation 3.22 is utilized. Rewriting equation 3.22,

$$k = \frac{B'^2(2B_{var}\cos\theta Y_0' + B_{var}^2 \sin\theta' + Y_0'^2 \sin\theta')}{Y_0'Y_0^2\beta} \tag{3.28}$$

By specifying the calculated values of B', θ and chosen values of Y_0, Y_0', a design chart is generated between coupling coefficient k and initial variable capacitance $C_{var} = B_{var}/\omega_0$ for different node-line lengths θ' as shown in figure 3.10. For the required coupling coefficient value of $k = 0.069045$, design parameter values of θ' and B_{var} are chosen from the design chart. In order to implement the variable capacitance, MACOM MA46H120 varactor diodes from MACOM technology with initial capacitance of 0.14 pF are chosen. For the specified $k = 0.069045$ and $C_{var} = 0.14$ pF, value $\theta' = 40°$ is chosen from the graph.

If we utilize equation 3.5 to calculate the value of θ' by specifying the values of θ, chosen B_{var} and Y_0, Y_0',

$$\sin\theta' = \frac{Y_0 Y_0' \sin\theta - 2B_{var}Y_0' \cos\theta}{B_{var}^2 + Y_0'^2} \tag{3.29}$$

Synthesized value is $\theta' = 38°$ which is close to the value predicted from the graph of equation 3.22. To, summarize, for the chosen NI parameter of $Y_0 = 0.02$ mhos, $Y_0' = 0.02$ mhos, $C_{var} = 0.14$ pF and calculated NI parameters $B' = 0.0068$ and $\theta = 71.22°$, both the design equations nearly give the same value of $\theta' = 40°$ for chosen $C_{var} = 0.14$ pF.
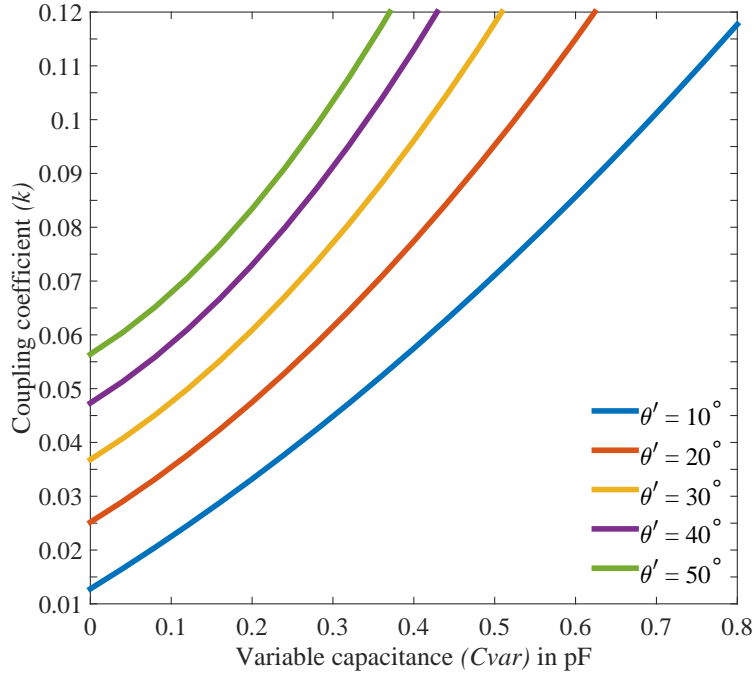
Figure 3.10: Coupling coefficient (k) vs Variable capacitance (C_{var}) for different electrical length θ'

3.4.3 Numerical Example: implementation

The non-resonant node inverter (NI) designed is suitable for implementation in capacitively coupled filters. Microstrip parallel coupled line filter topology is chosen for the implementation. Parallel coupled line filter has two half-wavelength resonators kept at an offset of a quarter-wavelength from each other resulting in strong capacitive coupling and is well suited for the implementation of the designed NI. The use of half-wavelength resonators provide an advantage of larger center frequency tuning range as compared to the popularly used quarter-wavelength resonators. In addition, the parallel coupled line filter topology can be utilized for biasing the varactor diodes using spatial biasing which has a reduced biasing circuitry as discussed in chapter 4.

The filter is designed in CST Microwave Studio and the layout of the filter is shown figure 3.11. Rogers RO 4003C substrate with dielectric constant of 3.38 and height of 0.508 mm is chosen for the design. The filter is placed in a metallic box of height 4.5 mm. Fig 3.11(a) shows the top view of the filter marked with dimensional parameters while figure 3.11(b) shows the bottom view of the filter. As shown in figure 3.11(a), the non-resonant node inverter is placed in between two half-wavelength resonators at the point of maximum coupling in order to get maximum variation in the bandwidth. Two varactor diodes are attached at the ends of the non-resonant node inverter to vary the bandwidth. Two varactor diodes are attached at the ends of the resonators in order to tune the center frequency of the filter. Varactor diodes $D_1 - D_4$ are used for frequency tuning while varactor diodes $D_5 - D_6$ are used for bandwidth tuning as shown in figure 3.11.

The electromagnetic model of the filter is simulated using frequency domain solver of the CST Microwave Studio. The initial set of NI parameters calculated using circuit model are utilized and parametric simulations are performed to finalize the filter dimensions for
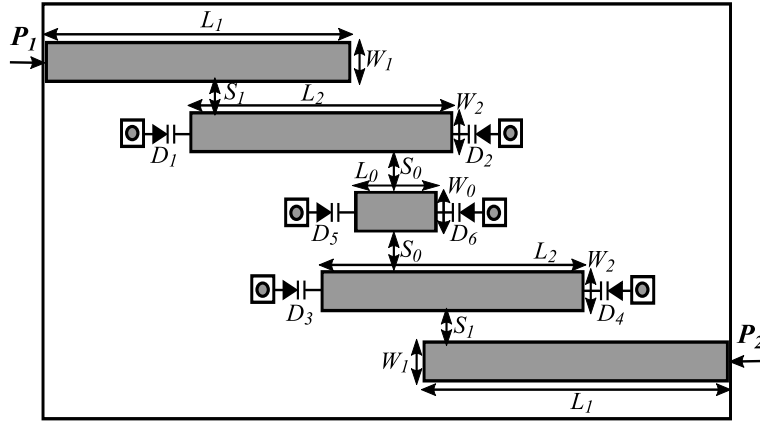
(a) Top view
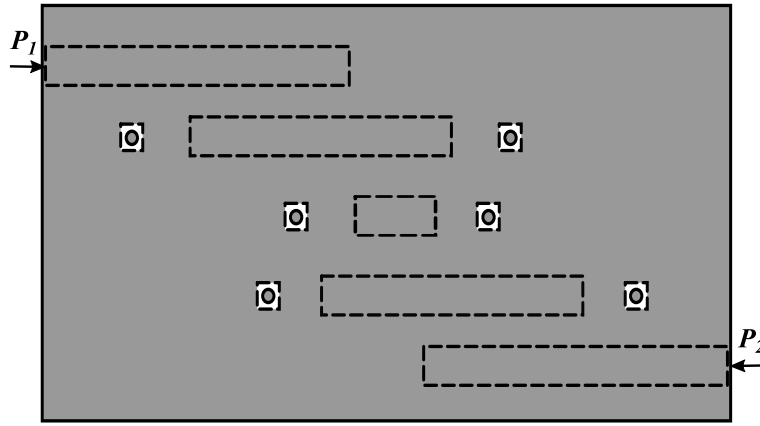
(b) Bottom view

Figure 3.11: CST layout for the designed reconfigurable second order filter in microstrip

Parameter Name	Parameter Value
L_1	23 mm
W_1	1.1561 mm
S_1	0.18 mm
L_0	3.4 mm
W_0	1.1561 mm
S_0	0.18 mm
L_2	14.262 mm
W_2	1.1561 mm

Table 3.1: Parameter values for the CST layout of the microstrip example

the desired specifications. Table 3.1 presents the dimensions of the designed filter. The S-parameters are further exported to Agilent ADS in touchstone format to add spice parameters for the MACOM MA46H120 varactor diodes. To demonstrate the bandwidth variation using NI, centre frequency of the filter is set to its starting value of 6.2 GHz by providing maximum reverse bias voltage to the varactor diodes attached to the resonators which corresponds to minimum capacitance offered by the varactor diodes. The reverse bias voltage of the varactor diodes attached to the NI is then varied to vary the bandwidth.
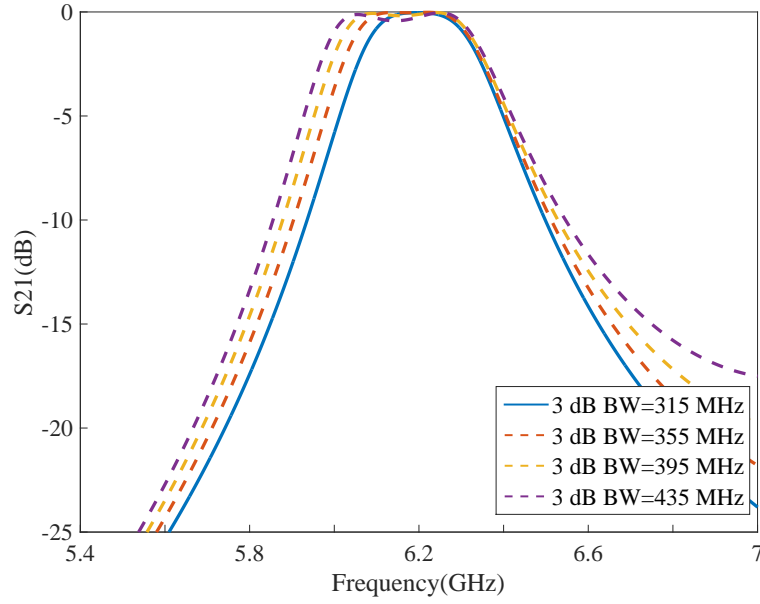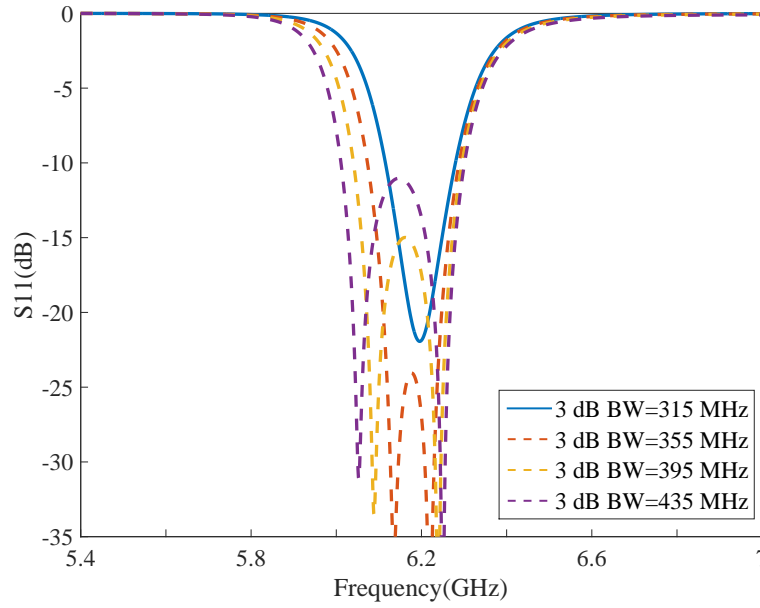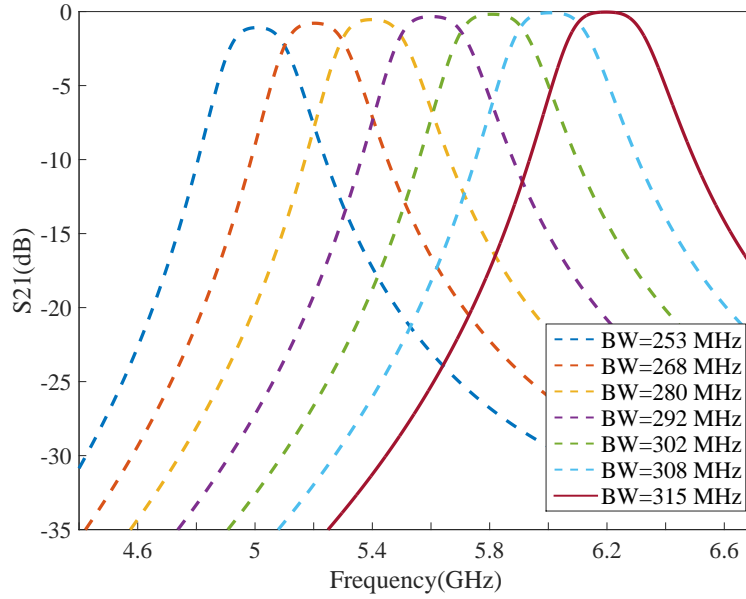
(a) S_{21} (dB) vs frequency (GHz)

(b) S_{11} (dB) vs frequency (GHz)

Figure 3.12: Bandwidth variation at fixed centre frequency $f_0 = 6.2$ GHz

Figure 3.12(a) presents the insertion loss as the bandwidth is varied while figure 3.12(b) presents the corresponding return loss. An increase of 38% is observed with a negligible variation in the centre frequency from 6.2 GHz to 6.16 GHz. The minimum variation in centre frequency with significant change in bandwidth gives the NI based bandwidth tuning mechanism a significant performance advantage over other bandwidth tuning techniques.

Two sets of simulations are then performed in Agilent ADS as shown in figure 3.13 and figure 3.14 in order to demonstrate the utility of the NI inverters in constant absolute bandwidth filters. In the first set, the filter response is initially maintained at the starting centre frequency of 6.2 GHz with all the varactor diodes attached to the NI and to the

resonators set to their minimum capacitance range. This is followed by changing only the centre frequency of the filter using the varactor diodes attached to the resonators and the varactor diodes on the NI are kept at their minimum capacitance range by supplying maximum reverse bias voltage.
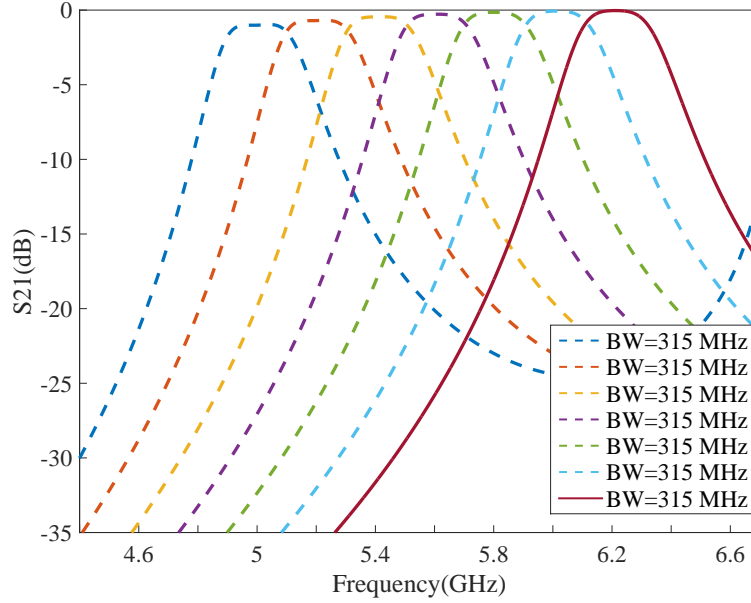

(a) S_{21} (dB) vs frequency (GHz)
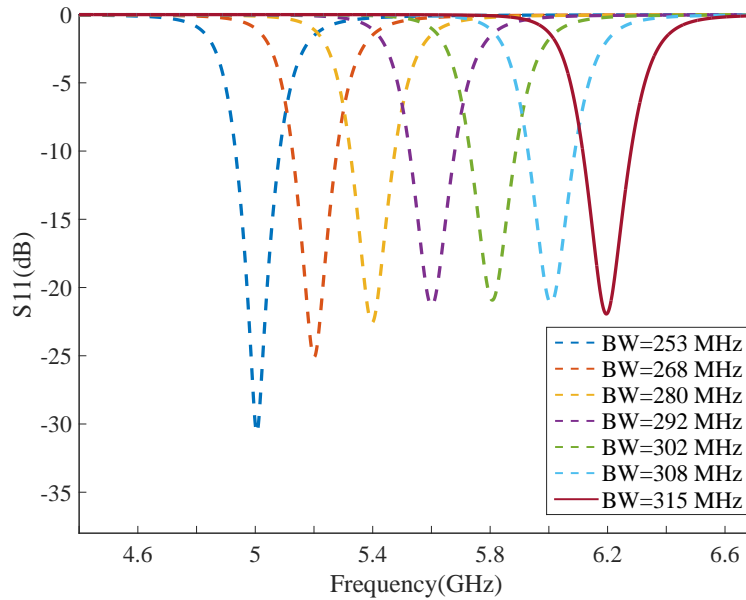
(b) S_{11} (dB) vs frequency (GHz)

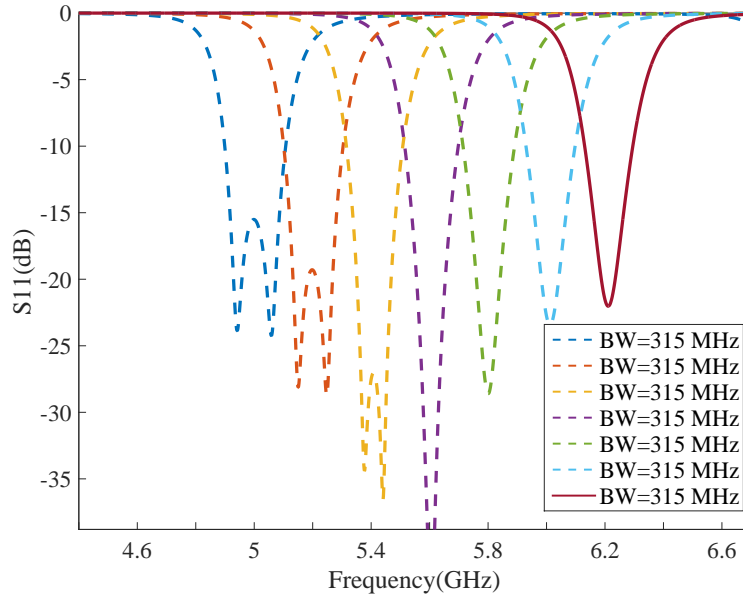Figure 3.13: Scattering parameter without use of NI (a) Insertion loss (b) Return loss

As shown in figure 3.13, as the centre frequency of the filter is swept from 6.2 GHz to 5 GHz at an interval of 100 MHz, there is a significant decrease in the bandwidth of about 19% with insertion loss increasing towards the lower end of the tuning range.

In the second set of simulations, both the centre frequency and bandwidth are tuned to maintain a constant absolute bandwidth response. The centre frequency is again tuned

from 6.2 GHz to 5 GHz at an interval of 100 MHz by varying the reverse bias voltage on the resonators while bandwidth is adjusted by varying the reverse bias voltage on the varactor diodes attached to the NI.

(a) S_{21} (dB) vs frequency (GHz)

(b) S_{11} (dB) vs frequency (GHz)

Figure 3.14: Scattering parameter with use of NI (a) Insertion loss (b) Return loss

As presented in figure 3.14, constant absolute bandwidth of 315 MHz is maintained using the NI across the entire centre frequency tuning range of 1.2 GHz. The example validates the synthesis method proposed and demonstrates the utility of the NI.

## 3.5 Dimensional Analysis for Case I ($C_{var} = 0$): SIW Implementation

The proposed idea of using non-resonant node based inverters can be utilized to design tunable filters in different technologies. This section demonstrates the use of non-resonant node inverters in designing filters with adjustable bandwidth at a specified centre frequency in substrate integrated waveguide technology (SIW). A detailed dimensional analysis for SIW based NI is presented in this section for a case where the effect of variable capacitance attached to non-resonant node inverters is neglected.

A substrate integrated waveguide (SIW) is a waveguide implementation in planar dielectric substrates and closely mimics actual waveguide behaviour. Substrate integrated waveguide (SIW) structure comprises of a high frequency dielectric substrate with rows of vias drilled between the two ground planes on either side of the substrate. SIW offers functionality of a waveguide with advantages of being cost-effective, lightweight and easy integration in planar structures [71–91].

In [92], SIW T-ridge pedestal resonators based on a combination of SIW technology with concepts of ridge waveguide are proposed. These resonators are made up of a rectangular or cross-shaped flat conductors on a single or a set of vias, positioned centrally inside each SIW cavity forming a T-ridge. The proposed T-ridge structure offers increased separation between the cut-off frequencies of the first two fundamental modes as in case of a conventional ridge waveguide. These resonators can be utilized to design filters with wide stopbands.

This dissertation utilizes the T-ridge SIW structure to design a SIW based non-resonant node inverter (SIW-NI) which is capable of varying the bandwidth of the filter at a specified centre frequency. As the use of T-ridge pedestal resonator reduces the dimensions of the filter structure, the SIW-NI based variable bandwidth filters designed in this thesis utilize the T-ridge pedestal topology to implement resonators also. The dimensional analysis is performed using an electromagnetic simulator to study the effect of varying the dimensions of the SIW-based NI on the coupling coefficient between the resonators and its corresponding effect on the centre frequency of the resonators. The setup is as shown in figure 3.15. Two T-ridge pedestal SIW resonators R_{SIW} having a resonant frequency of 5.1 GHz are taken for the study. A smaller dimension T-ridge pedestal SIW resonator N_{SIW} is placed in between the two resonators as shown in fig. 3.15(b). The N_{SIW} is specifically placed at the iris between the two resonators R_{SIW} which is the point of maximum coupling between them. The dimensions of smaller SIW resonator N_{SIW} is chosen such that it resonates at a frequency that is much higher than the resonant frequency of the resonators R_{SIW}. The out of band resonator N_{SIW} together with susceptive gaps S forms the SIW based non-resonant node inverter (SIW-NI). Rogers RO 4003 C substrate with dielectric constant of 3.38 and height of 0.508 mm is chosen for the study. Two cases are taken for dimensional analysis. For the first case, a variable capacitor is attached to the via D of N_{SIW} and is set to an open state, $C_{var} = 0$ pF, as shown in figure 3.16. For the second case, the effect of C_{var} is included as shown in figure 3.20.
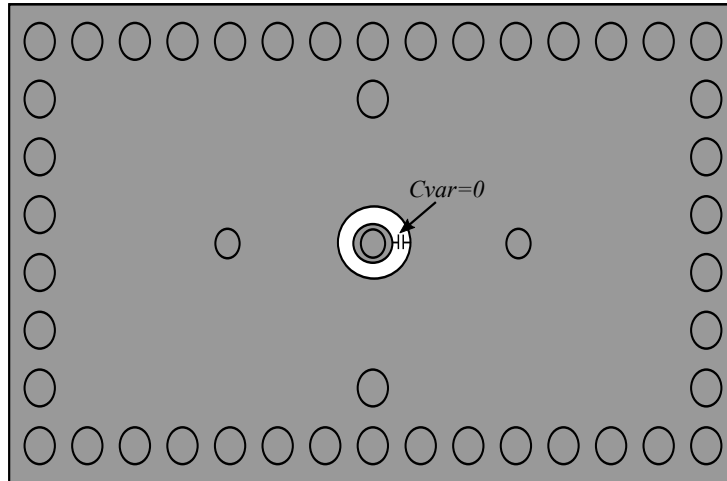
For the first case, dimensions of the setup of figure 3.15 are a= 22.99 mm, b= 11.99
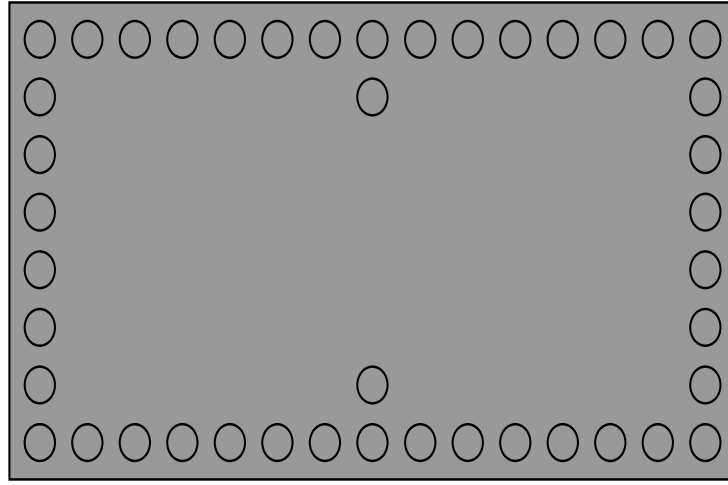
(a) Top view
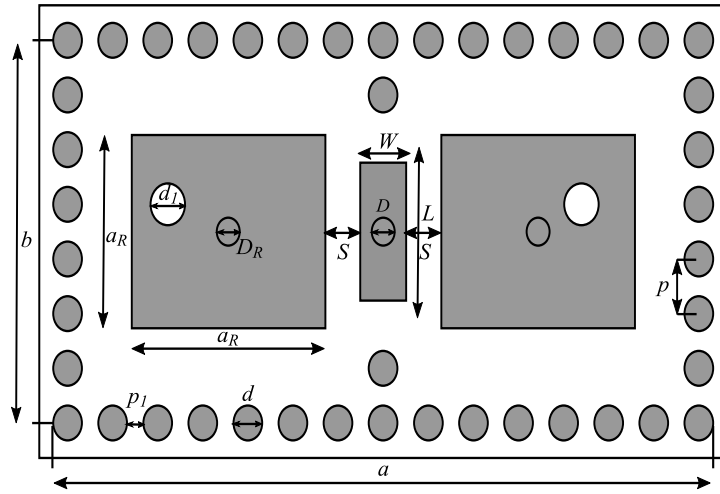
(b) Middle layer

Figure 3.15: CST layout for dimensional analysis without variable capacitance ($Cvar$)

Figure 3.16: CST layout for the dimensional analysis without variable capacitance ($Cvar$)-Bottom view

mm, a_R=5.5 mm, D_R=0.8 mm, d_1=1 mm, d=1 mm, p_1=0.57 mm, p=1.57 mm, W=1.6 mm, L=1.6 mm, D=0.8 mm and S=0.48 mm. CST Eigenmode solver is used to perform

the dimensional analysis.

3.5.1 Effect of varying width (W)

To study the effect of varying the width W, the length L of N_{SIW} is kept fixed at 1.6 mm and the width W of N_{SIW} is varied from 1.6 mm to 4.8 mm with a step size of 0.8 mm. The spacing S between N_{SIW} and resonators is varied from 0.48 mm to 0.98 mm with an interval of 0.1 mm. As the width of N_{SIW} is increased for a fixed length of 1.6 mm, the coupling coefficient tends to decrease for an increase in the spacing value S as shown by the graph of fig. 3.17. The reason for the decrease in the value of k is because as the width is increased, the separation between resonators increases resulting in the shielding of fields.
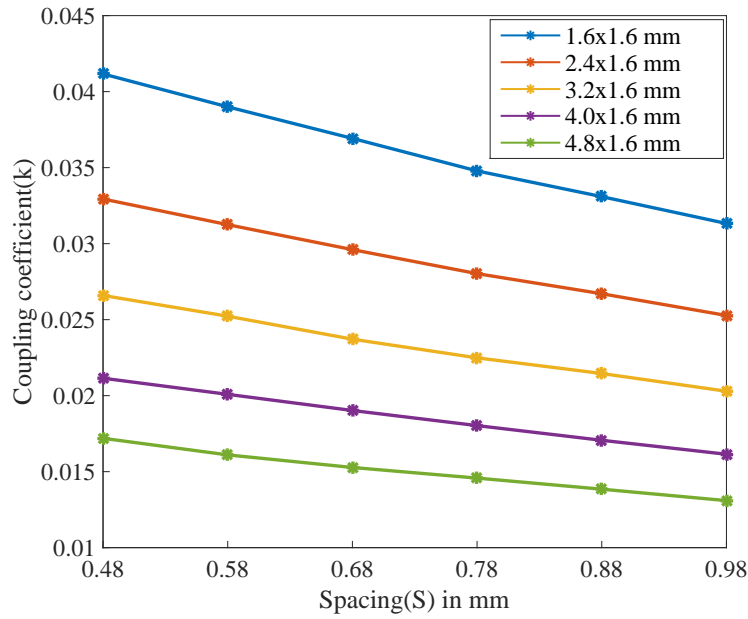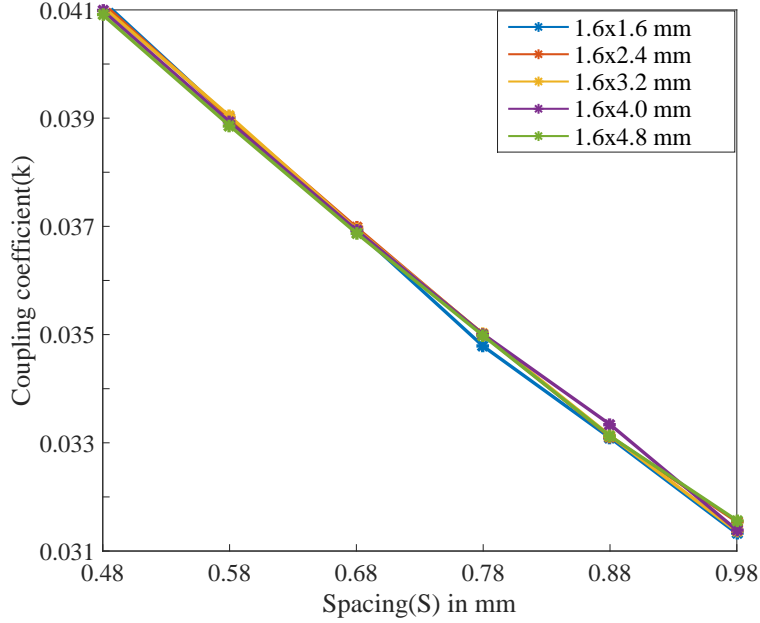

Figure 3.17: Coupling coefficient (k) vs spacing (S) for different patch width (W)

3.5.2 Effect of varying length (L)

For this case, the width W of N_{SIW} is kept constant at 1.6 mm and the length L is varied from 1.6 mm to 4.8 mm with a step size of 0.8 mm. The spacing S between the resonators and N_{SIW} is varied from 0.48 mm to 0.98 mm with a step size of 0.1 mm. As the length of N_{SIW} is increased, keeping the width constant, the coupling coefficient k tends to decrease as the spacing S is increased as shown by graph of figure 3.18. In addition, there is no significant difference in the coupling coefficient k values for different lengths of N_{SIW} at a specific spacing value S and fixed width W. For a change in the parameter length, the separation between resonators (given by S) is not affected and hence the coupling coefficient value remains almost constant when the width is kept fixed.

Figure 3.18: Coupling coefficient (k) vs spacing (S) for different patch length (L)

## 3.6 Dimensional Analysis for Case II ($C_{var} \neq 0$): SIW Implementation

For the second case, a similar setup as used in the previous section comprising of two T-ridge pedestal SIW resonators R_{SIW}, both having resonant frequencies of 5.1 GHz are taken for the study. A smaller dimension T-ridge pedestal SIW resonator N_{SIW} is placed in between the two resonators at the iris junction separating them. As mentioned earlier, N_{SIW} is kept at the iris junction as it is the point of maximum coupling between the resonators and hence will result in maximum variation in the bandwidth. The resonators R_{SIW} are lightly coupled to the feed lines L_F. The setup is as shown in figure 3.19. A variable capacitance C_{var} is attached between the bottom ground plane and the via of the N_{SIW} as shown in figure 3.20.

It was established in the previous section that for fixed width W and fixed spacing S from the resonator, a change in the length L of the N_{SIW} does not change the coupling coefficient k significantly. Utilizing this fact, two N_{SIW} with same width W and different length parameter L are chosen for this study. The purpose of using two N_{SIW} is to analyse the effect of changing the dimensions of N_{SIW} on the capacitance range required for changing the inter-resonator coupling coefficient. The two N_{SIW} with dimensions 1.6x3.2 mm and 1.6x4.8 mm are kept at the iris junction at a fixed separation of S=0.68 mm from the resonators. The lines L_F represent the feed lines with feed pins of diameter D_F which couple inductively to the resonators. The dimensions of figure 3.19 (a) and (b) are a= 22.99 mm, b= 11.99 mm, a_R=5.5 mm,D_R=0.8 mm, d_1=1 mm, d=1 mm, p_1=0.57 mm, p=1.57 mm, W=1.6 mm, L=1.6 mm, D=0.8 mm, S=0.48 mm, L_F= 6.2 mm, W_F= 1.2 mm and D_F= 0.8 mm.
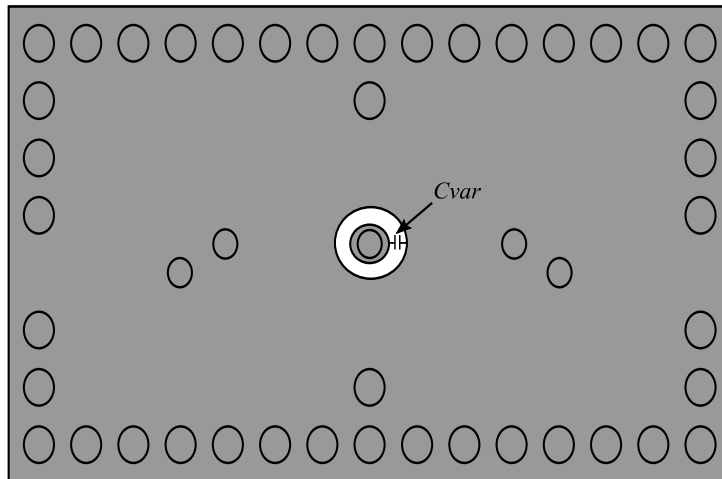
To analyse the two cases of N_{SIW} discussed in this work, firstly, scattering parameters S_{21} and S_{11} are obtained for a range of capacitance values using CST Frequency domain solver. The purpose of obtaining S_{21} and S_{11} parameters is to derive the odd (fodd)
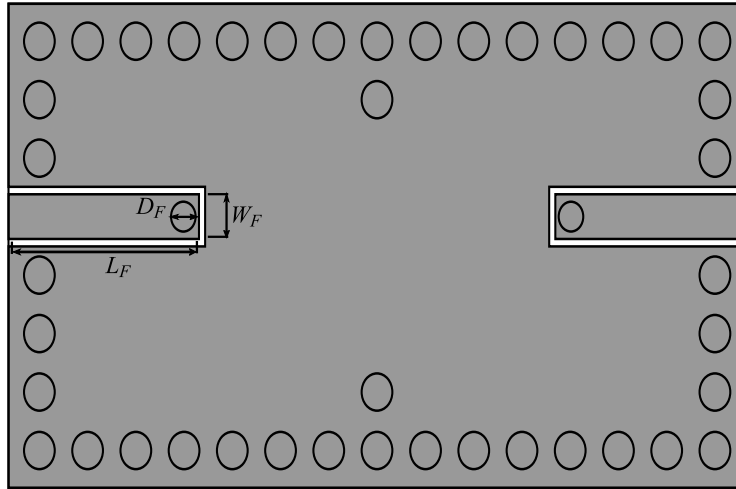
(a) Top view
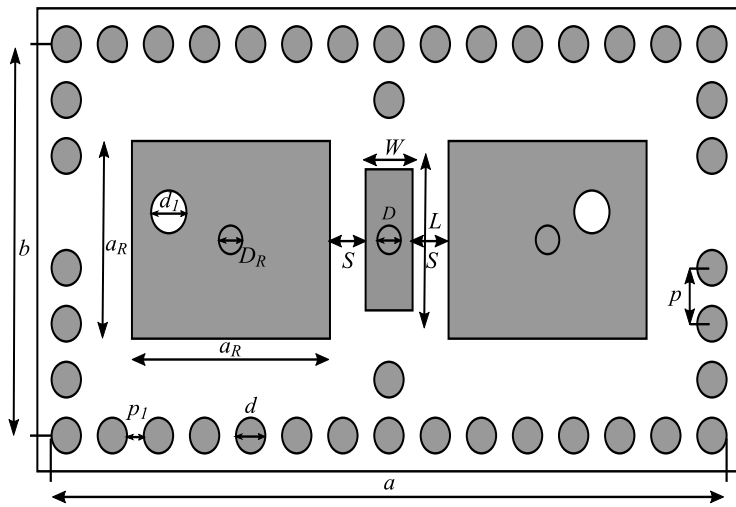
(b) Middle layer

Figure 3.19: CST layout for dimensional analysis with variable capacitance ($Cvar$)

Figure 3.20: CST layout for the dimensional analysis with variable capacitance ($Cvar$)-Bottom view

and even mode (feven) frequencies for a specified value of variable capacitance C_{var}. With the help of odd mode and even mode frequencies, coupling coefficient k can be derived for a range of capacitance values. Further, by studying the variation in even mode frequency, the capacitance range required to bring a specified variation in bandwidth can be estimated.

For the first case of N_{SIW} with dimensions 1.6x3.2 mm, keeping spacing S constant at 0.68 mm, as the variable capacitance C_{var} is varied from 0 pF to 10 pF, the coupling coefficient k increases from 0.031 to 0.047 as shown in figure 3.21. Figure 3.22 shows the scattering parameters S_{21} and S_{11} for the same case. A bandwidth increase of approximately 51% is observed as the variable capacitance C_{var} is increased from 0 pF to 10 pF. It can be observed from fig. 3.22 that an out of band resonance peak moves towards the passband. This out of band peak is due to the resonant frequency of N_{SIW}. As the variable capacitance C_{var} attached to N_{SIW} is increased, the out of band resonant frequency of N_{SIW} moves closer to the resonant frequency of the resonators. The out of band peak shows its presence because of the fact that an ideal capacitor is utilized to implement C_{var} to bring a change in the resonant frequency of N_{SIW}. The use of an ideal capacitor does not consider the losses due to the quality factor of practical varactor diodes. As described in the previous section 3.3.1, with the use of varactor diodes in practical applications, considerable reduction in the out of band peak can be observed.

For the second case of N_{SIW} with dimensions 1.6x4.8 mm, keeping spacing S constant at 0.68 mm, as the capacitance is varied from 0 pF to 2.3 pF, the coupling coefficient increases from 0.031 to 0.05 as shown in figure 3.23. Figure 3.24 describes the scattering parameters for the same case. A bandwidth increase of approximately 60% is observed as capacitance is increased from 0 pF to 2.3 pF. It can be observed from figure 3.24 that an out of band resonance peak moves towards the passband. As mentioned earlier, this out of band peak is due to the resonant frequency of N_{SIW} as variable capacitance C_{var} attached to the N_{SIW} is varied. As described in the previous section 3.3.1, with the use of varactor diodes in practical applications, considerable reduction in the out of band peak can be achieved.
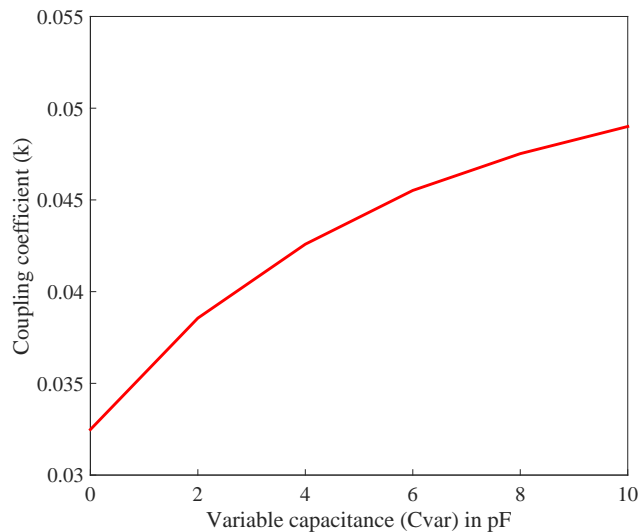

Figure 3.21: Coupling coefficient(k) vs variable capacitance ($Cvar$) for 1.6x3.2 mm NI

(a) Insertion loss (dB) vs frequency (GHz)

(b) Return loss (dB) vs frequency (GHz)

Figure 3.22: S-parameter simulation results vs variable capacitance for 1.6x3.2 mm NI
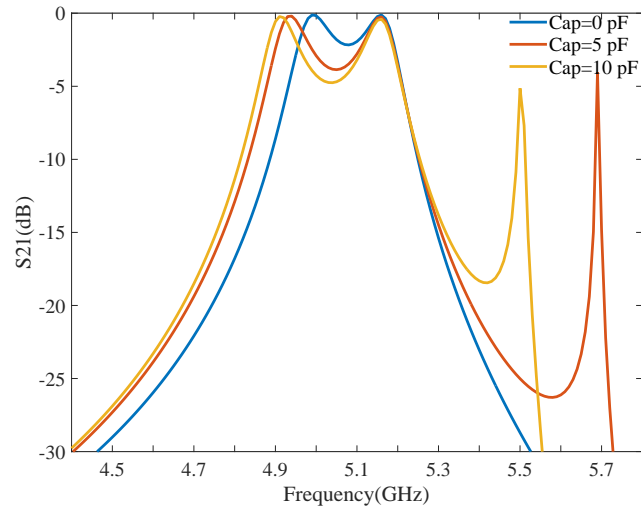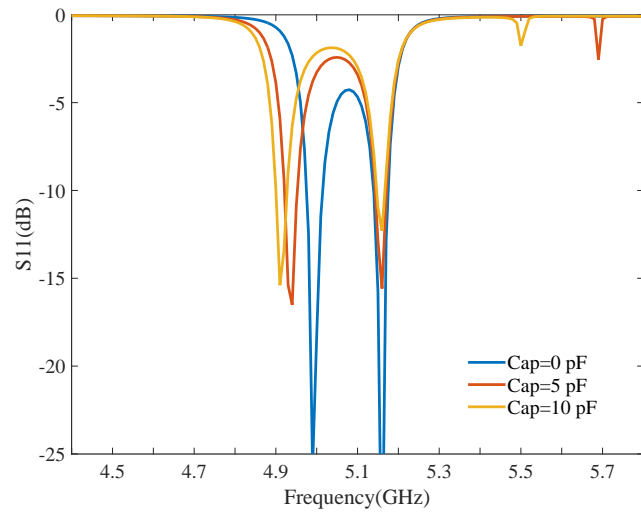

Figure 3.23: Coupling coefficient(k) vs variable capacitance ($Cvar$) for 1.6x4.8 mm NI
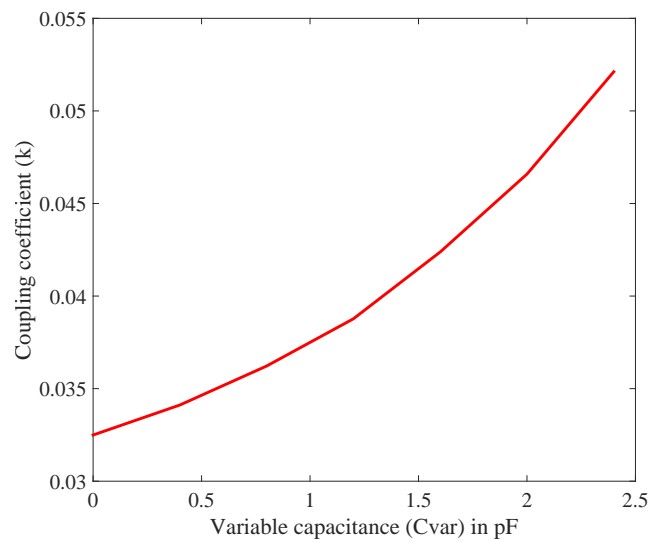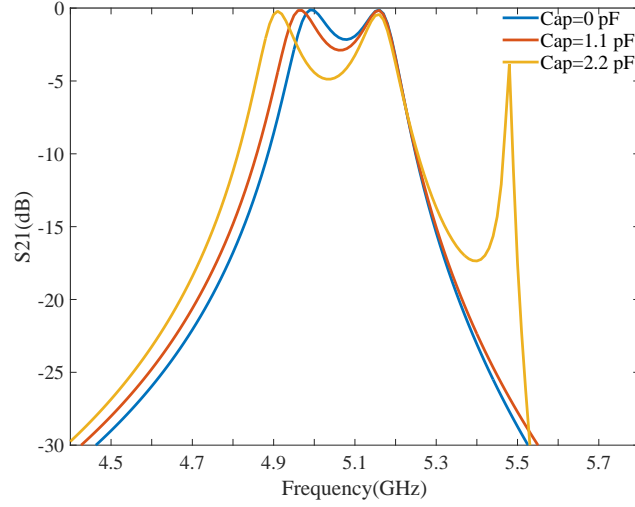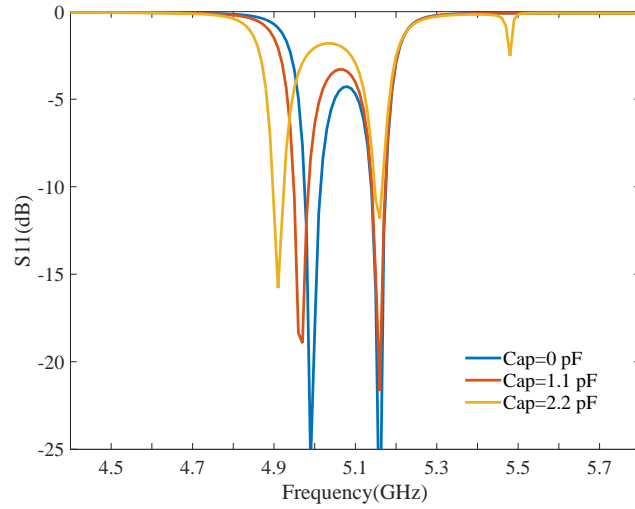
(a) Insertion loss (dB) vs frequency (GHz)

(b) Return loss (dB) vs frequency (GHz)

Figure 3.24: S-parameter simulation results vs variable capacitance for 1.6x4.8 mm NI

For comparison between the two cases, it is to be mentioned that the distance S of the N_{SIW} from the resonator is kept constant at 0.68 mm. The initial value of the variable capacitance C_{var} is taken to be 0 pF which is an open state for both the cases. As mentioned earlier, since the length parameter L does not change the coupling coefficient k significantly for a fixed width W and spacing S, the initial bandwidth at $C_{var}= 0$ pF is approximately 165 MHz for both the cases of dimensions of 1.6x3.2 mm and 1.6x4.8 mm. To attain a specific bandwidth variation, N_{SIW} with dimensions of 1.6x3.2 mm require more capacitance as compared to one with dimensions 1.6x4.8 mm. The overall bandwidth variation attained is larger in larger dimension N_{SIW} with dimensions 1.6x4.8 mm.

The dimensions of the N_{SIW} together with susceptive gaps S play a role in realizing a desired coupling coefficient k for the value of the variable capacitor C_{var} attached to the N_{SIW}. Depending upon the coupling coefficient value required, dimensions of N_{SIW} and gap size S can be synthesized for nominal variable capacitance C_{var} (offered by chosen varactor diodes) using an EM simulator. The presented dimensional analysis is utilized

to design a bandwidth tunable filter at a specified centre frequency as described in the next section.

3.7   Design Steps and Numerical Example: SIW Implementation

A detailed dimensional analysis of SIW based NI is presented in the previous section. This section utilizes the results of the previous sections and design steps for SIW based non-resonant node inverters (SIW-NI) are listed. The design steps are then subsequently followed to design a second order T-ridge pedestal resonator based SIW filter with bandwidth control.

3.7.1   Design steps for NI based in SIW

The following design steps can be summarized for tunable filters using SIW based non-resonant node inverter:

1. The coupling coefficient and external quality factor are calculated using general design equations presented in [50] for a Nth order filter.

2. Dimensional analysis is performed using an electromagnetic simulator as discussed in section 3.6 on dimensional analysis. For the desired coupling coefficient k, at the specified centre frequency of the filter f_0, patch width W, patch via D, patch length L and spacing S are fixed with respect to the nominal variable capacitance (C_{var}) offered by the chosen type of varactor diodes using an EM simulator.

3. Finally, for the complete design of tunable filters with NI inverters, generalized group delay tuning method specified in [70] can be utilized to fine tune the filter using simulations.

3.7.2   Numerical Example

Using the analysis presented in the previous section, a second order bandwidth tunable filter is designed. The specifications for the filter are as follows:
Fractional Bandwidth Δ=4%
Order $N = 2$
Passband Ripple = 0.1 dB chebyshev
Centre frequency $f_0 = 5.12$ GHz.

   The resonators are designed using T-ridge pedestal topology in SIW at the specified centre frequency. Following the proposed design procedure:

1. The coupling coefficient k and external quality factor Q values are calculated as $k = 0.05523$ and $Q = 21.075$.

2. MACOM MA46H120 varactor diodes are chosen for the implementation of the variable capacitor C_{var}. Rogers RO 4003C substrate with dielectric constant of 3.38

and height of 0.508 mm is chosen for the implementation of SIW based NI. For the desired value of k as in step 1, at the specified centre frequency f_0, considering the nominal capacitance value offered by MACOM varactor diodes, width W=1.6 mm, length L=4.8 mm, patch via D=0.8 mm and spacing S=1.225 mm are synthesized using an EM simulator.

3. Finally, for the complete design, generalized group delay tuning method specified in [70] is used to fine tune the filter using simulations.

Rogers RO 4003 C substrate with dielectric constant of 3.38 and height of 0.508 mm is chosen for the implementation of the second order filter. Figure 3.25(a) shows the top layer of the filter while figure 3.25(b) shows the middle layer. Figure 3.26 shows the bottom layer. The dimensions of the filter are presented in table 3.2. To perform simulations, the filter is designed with the centre frequency of 5.12 GHz with 4% fractional bandwidth corresponding to the nominal capacitance of 0.14 pF as offered by the MACOM varactor diode D_1. As mentioned in the design steps, in order to utilize the complete tuning range, the varactor diodes are set to their nominal capacitance value in the simulation analysis to maintain the required value of coupling coefficient. The varactor diode D_1 is simulated as a variable capacitance in simulations. Figure 3.27(a) shows the S_{21} response when the variable capacitance representing diode D_1 is varied from 0 pF to 1.8 pF. An overall bandwidth increase of 31% (62 MHz) from 200 MHz to 262 MHz is achieved. Figure 3.27(b) shows the corresponding S_{11} plot for the designed filter. The presented example establishes the fact that by using SIW based NI, bandwidth variable filters can be designed.

Parameter Name	Parameter Value
a	22.99 mm
b	11.99 mm
a_R	5.5 mm
D_R	0.8 mm
d_1	1 mm
d	1 mm
p_1	0.57 mm
p	1.57 mm
W	1.6 mm
L	1.6 mm
D	0.8 mm
S	0.48 mm
L_F	6.2 mm
W_F	1.2 mm
D_F	0.8 mm

Table 3.2: Parameter values for the CST layout of the SIW example
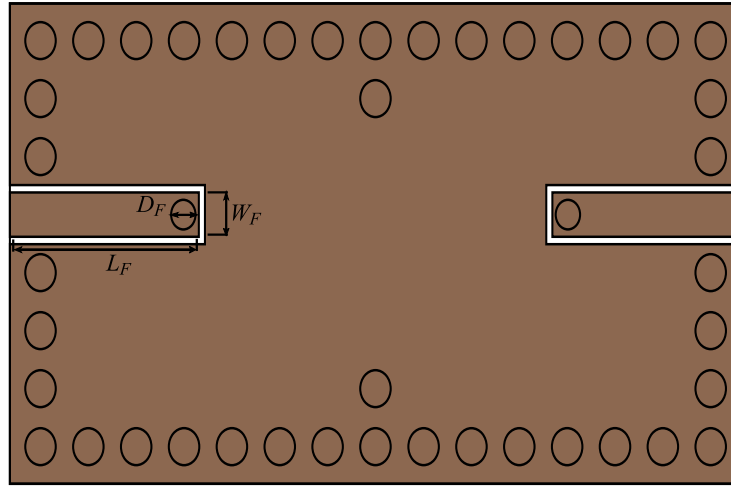
(a) Top view
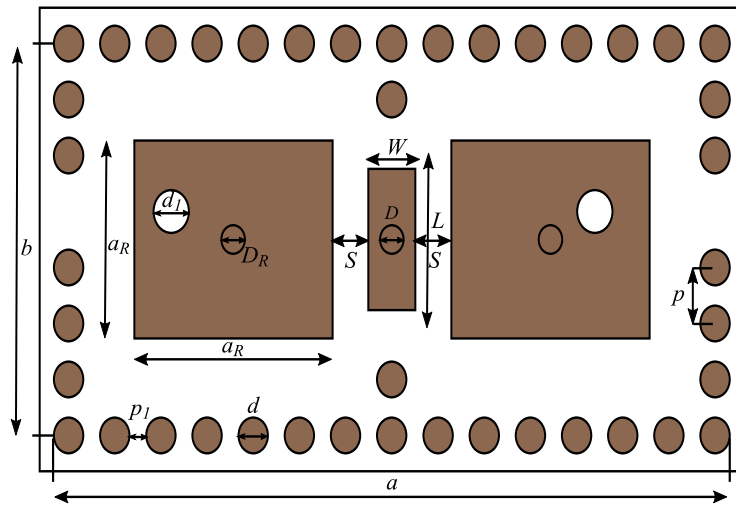
(b) Middle Layer

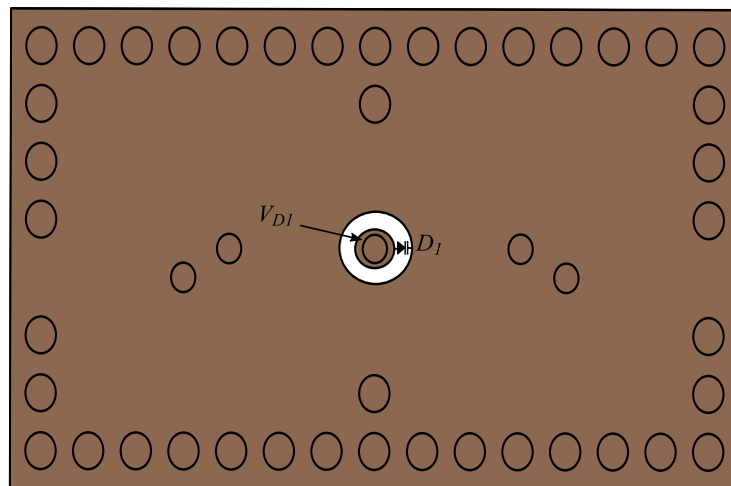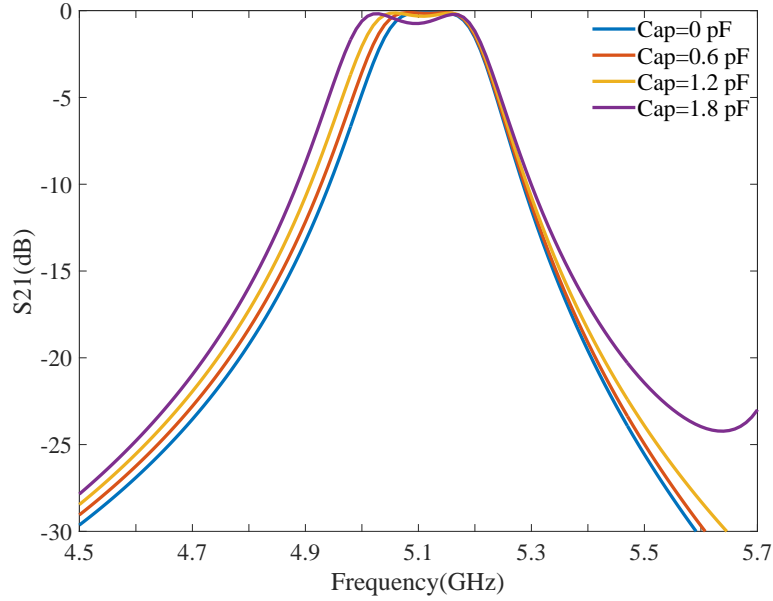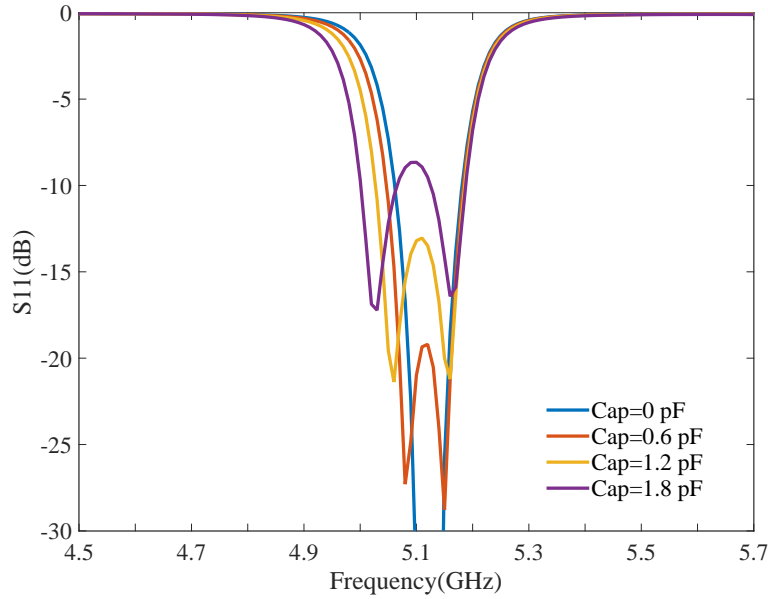Figure 3.25: CST layout for the second order filter in SIW using NI

Figure 3.26: CST layout for the second order filter in SIW using NI-Bottom view

(a) Insertion loss (dB) vs frequency (GHz)

(b) Return loss (dB) vs frequency (GHz)

Figure 3.27: Simulated results for the designed second order filter with bandwidth control

3.8   Conclusion

This chapter presents a design technique utilizing non-resonant node inverters (NI) to design filters with bandwidth control. The idea of using NI in coupled resonator filters are illustrated in microstrip and SIW technologies. A circuit model and a synthesis method is developed for microstrip filters based on NI. A detailed dimensional analysis of NI is presented and results are compared with the circuit model. A design procedure is proposed for tunable microstrip filters based on NI. The developed model and theory is validated by a design example of a reconfigurable second order microstrip filter based on NI. The proposed technique is further illustrated in SIW technology. Dimensional analysis of NI in T-ridge pedestal SIW resonator based topology is presented and a design procedure is

proposed. The proposed design procedure is validated with the help of a design example of a second order T-ridge SIW filter with bandwidth control. In chapter 4, the developed theory for microstrip filters is utilized to design filter prototypes and measured results are discussed.

Chapter 4

Filter Design and Measurements

This chapter presents the design and measurement results for second and third order filter prototypes implemented in microstrip technology using non-resonant node inverters (NI). The theoretical models and electromagnetic simulation experimental setup presented in the previous chapter are utilized extensively to construct filters with constant bandwidth. The chapter presents the construction steps followed by a discussion of the measurement results of the filter prototypes.

4.1 Second Order Filter Using NI

4.1.1 Second order filter design

Using the synthesis design steps presented in section 3.4.1, a second order filter with tunable centre frequency and constant bandwidth is designed. The specifications for the second order filter are a fractional BW of 4% on a chebyshev function with 0.1 dB ripple. The centre frequency of the filter is 4.7 GHz.

1. Using design step 1, values for the coupling coefficient and external quality factor are calculated as $k_{12} = 0.05523$ and $Q_e = 21.075$.

2. Using design step 2 and utilizing the susceptance slope parameter for a half-wavelength open circuited resonator as β=0.0314 mho, the inverter constant $B = 0.0017342$ is calculated.

3. Choosing admittance parameter Y_0=0.02 mhos (corresponding to 50 ohm), utilizing design equation 3.16, $B' = 0.0060$ is synthesized.

4. Using design equation 3.11, $\theta = 73.3°$ is calculated. An equivalent model of NI as shown in figure 3.2(d) with parameters (B', θ, Y_0) is derived with this step.

5. For practical implementation of the filter in microstrip technology, NI model of figure 3.2(b) with parameters $(B', \theta', Y_0', B_{var})$ is to be derived from figure 3.2(d) using equivalance of figure 3.2(c). As shown in figure 3.2(c), synthesized electrical length θ is the sum of node length θ' and initial variable susceptance $B_{var} = \omega_0 C_{var}$ offered by varactor diodes. Utilizing the values of the derived parameters in the

earlier steps and choosing $Y_0' = 0.02$ mhos, design parameters θ' and C_{var} required for different coupling coefficient k are plotted using equation 3.22. The graph of figure 4.1, gives values of θ' and initial capacitance C_{var} offered by the varactor diodes which can be utilized to implement the required $k_{12} = 0.05523$. MA46H120 varactor diodes($Ct \sim 0.14 - 1$ pF, Rs $= 0.8$ ohms) from MACOM technology are chosen to implement the variable capacitances (C_{var}) attached to the NI. For the initial capacitance of $C_{var} = 0.14$ pF, as offered by chosen MA46H120 varactor diodes, the calculated susceptance B' of 0.006 mho results in $\theta' = 55°$ in order to realize coupling coefficient $k_{12} = 0.05523$. The value of B' is optimized to 0.0068 mho and $\theta' = 35°$ is selected to implement the NI using figure 4.1. The optimized susceptance value of B' corresponds to the reduced gap between the resonator and the NI and hence results in shorter length of NI which further helps in reducing the board space. With this step, the design of an equivalent NI inverter to be implemented in a half-wavelength microstrip resonator based second order filter is complete.
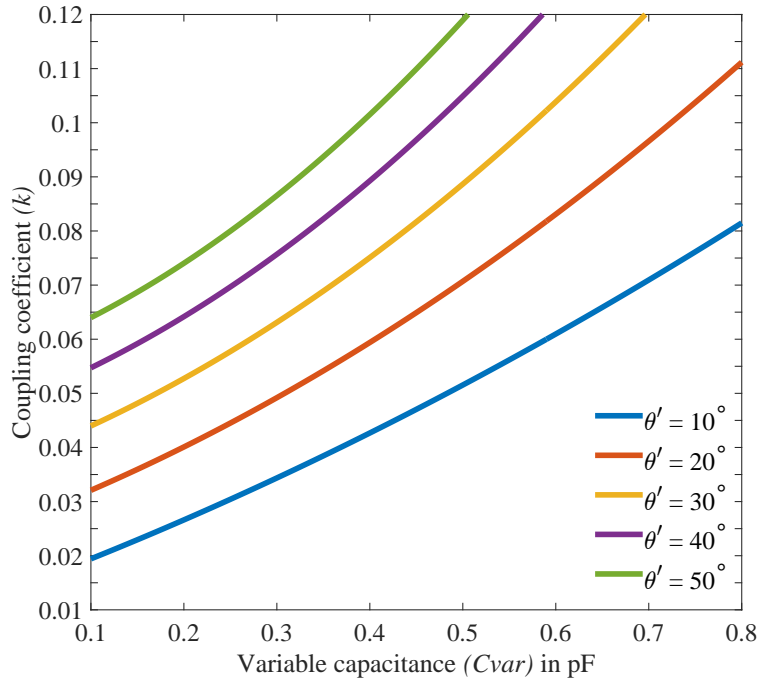

Figure 4.1: NI parameters for the second order filter ($B' = 0.0068$)

The layout of the filter is shown in figure 4.2. The filter is fabricated on Rogers RO 4003C substrate with relative dielectric constant $\varepsilon_r = 3.38$ and loss tangent $\tan\delta$ of 0.0027. The substrate thickness is 0.508 mm. In order to utilize the complete tuning range of the varactor diodes, all the varactors used in the filter designs, either on the resonators or on NI are set to their minimum initial capacitance value in the simulation analysis performed. The calculated parameter values using circuit model are utilized and extensive parameter sweeps are performed to calculate the filter dimensions for the desired filter response. The finalized filter design parameters are $L_1 = 24$ mm, $W_1 = 1.17537$ mm, $S_1 = 0.2$ mm, $L_2 = 16.86$ mm, $W_2 = 1.17537$ mm, $L_0 = 3.55$ mm, $W_0 = 1.17537$ mm and $S_0 = 0.48$

mm. The dimensions of the filter is 16x44 mm. The electromagnetic model of the filter is developed in CST while ADS is used to add the spice parameters of the varactor diodes to the exported EM model from CST, in order to consider all the parasitic effects and losses.

A spatial biasing mechanism, specifically suitable to bias the tuning elements in a circuit
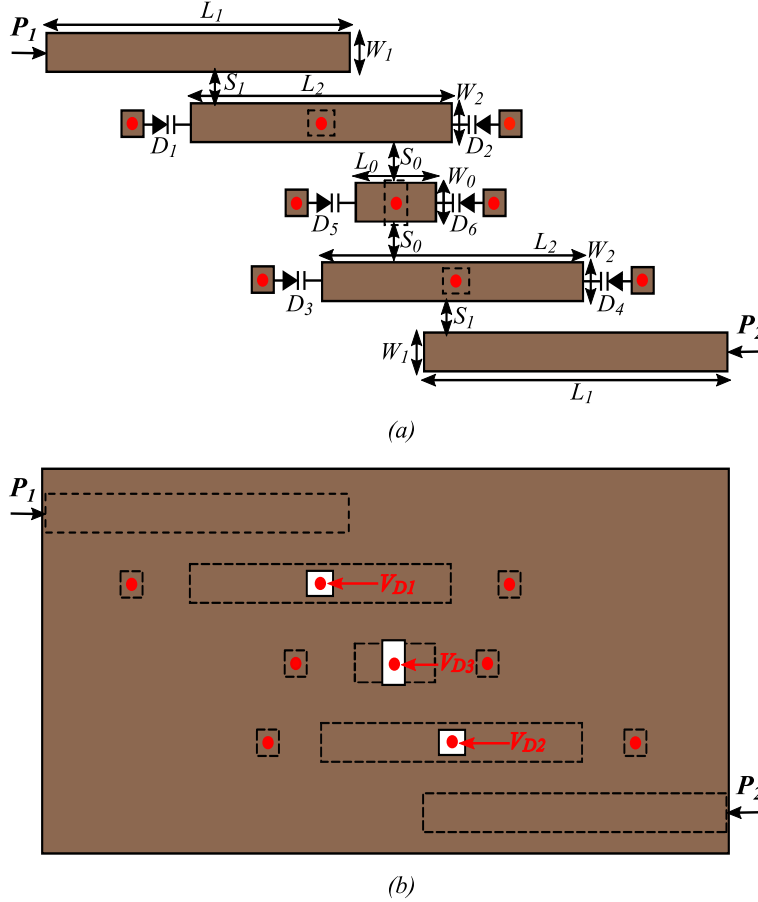
Figure 4.2: Second order filter layout (a) top view (b) bottom view

that employs half-wavelength planar resonators, is utilized for this design. Authors in [93] proposed biasing the half-wavelength resonators at the central null point by connecting bias lines from the top of the substrate. Since the electric fields are minimum at the central point of a half-wavelength resonator, there is no requirement of a DC-blocking circuitry. This work utilizes via holes of 0.4 mm drilled at the central null point of the resonators as well as NI transmission line and DC bias lines are connected from the bottom of the substrate. Figure 4.2(b) shows vias from the top going to the bottom layer where small windows are created by etching the copper from the substrate to connect the DC bias lines V_{D1}, V_{D2} and V_{D3}. The biasing mechanism eliminates the use of complicated DC biasing circuitry comprising of fixed DC capacitance, DC pads and RF chokes and reduces the board space required for the biasing circuit.

MA46H120 varactor diodes($Ct \sim 0.14 - 1$ pF, Rs = 0.8 ohms) from MACOM technology solutions are utilized to implement all the diodes D_1, D_2, D_3, D_4, D_5 and D_6 [94]. A bias resistance of 10 Kilo-ohms is used to connect DC power supply. The central vias on the

resonators and on the NI act as RF chokes because of their inductive nature. The 10 Kilo-ohms resistance act as an additional RF choke.

4.1.2 Second order filter measurements
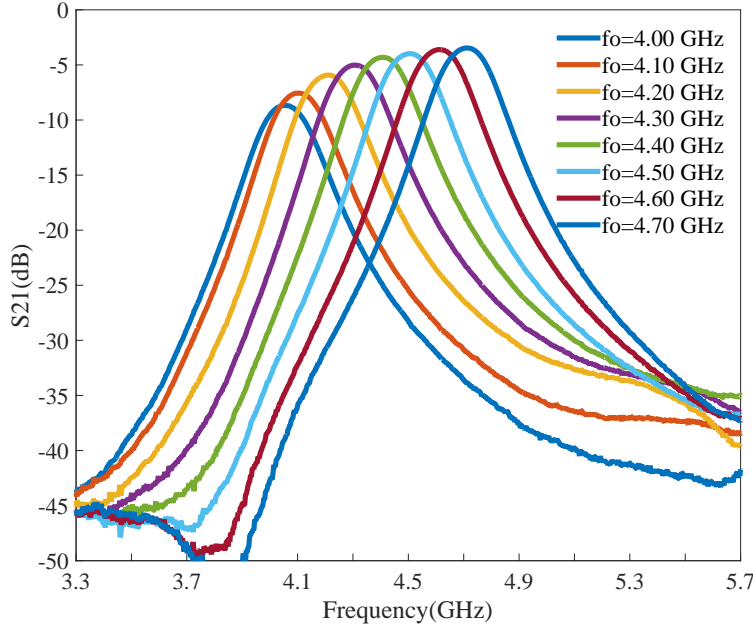
(a) Measured S_{21} (dB) vs frequency (GHz) plot
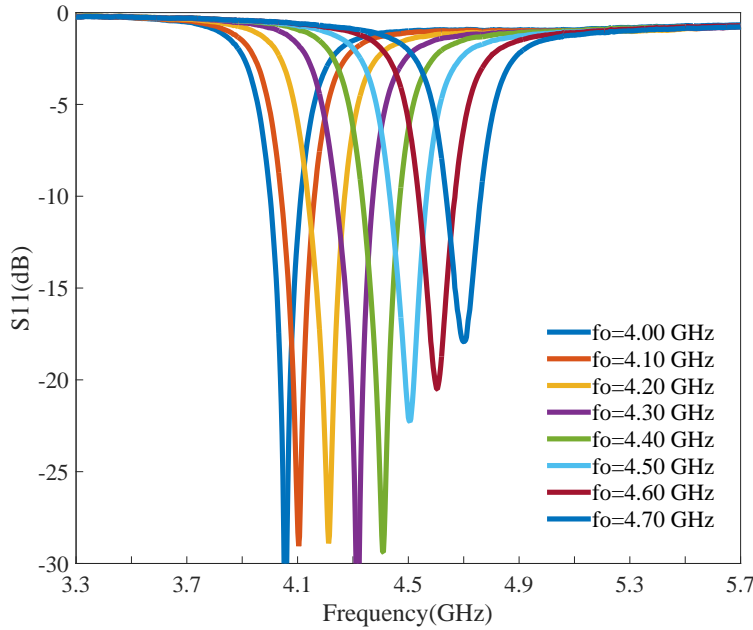
(b) Measured S_{11} (dB) vs frequency (GHz) plot

Figure 4.3: Second order filter measurement plot

The centre frequency of the filter is tuned from 4 to 4.7 GHz by utilizing diodes connected to the resonators $D_1 - D_4$. Diodes $D_1 - D_4$ are provided a DC bias voltage through $V_{D1} - V_{D2}$ in the range 0-12 V. A constant absolute bandwidth of 200 MHz is maintained across the entire frequency tuning range by controlling the inter-resonator

(a) S_{11} (dB) vs frequency (GHz) measurement plot for BW variation
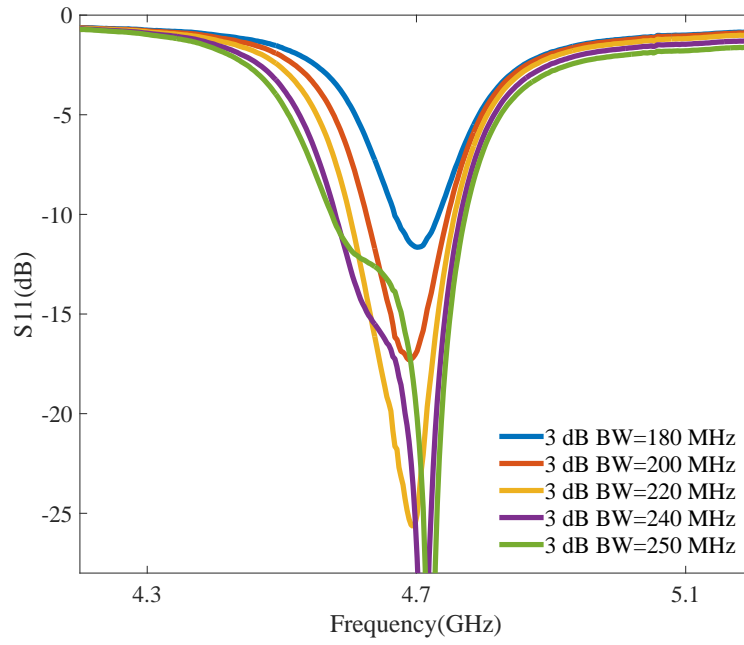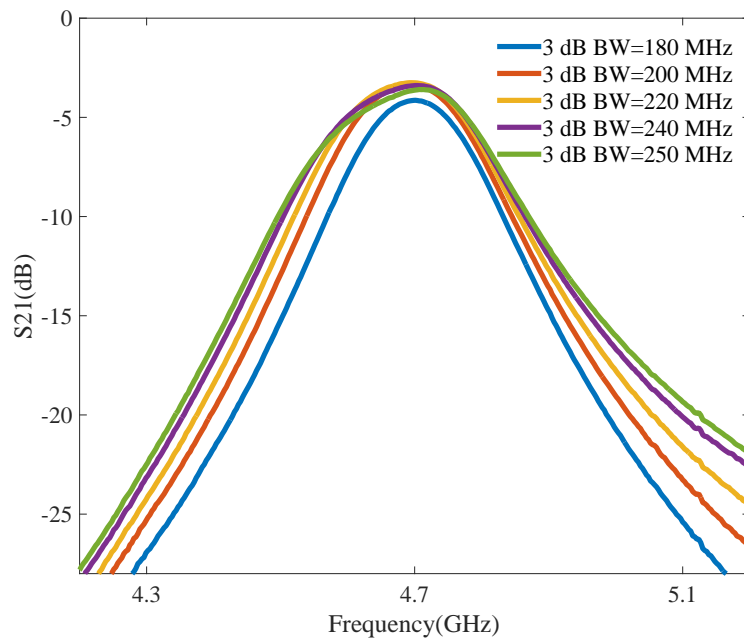

(b) S_{21} (dB) vs frequency (GHz) measurement plot for BW variation

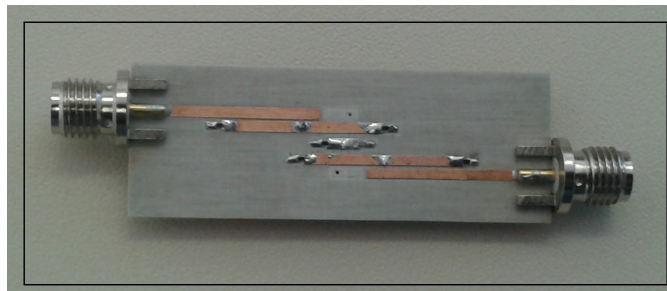Figure 4.4: Second order filter measurement results for bandwidth variation at 4.7 GHz

Figure 4.5: Fabricated second order filter

coupling using diodes $D_5 - D_6$ connected to the non-resonant node inverter (NI). Diodes $D_5 - D_6$ are biased through voltage V_{D3} between 0-12 V . The measured insertion loss is in the range 8.60-3.45 dB. Figure 4.3(a) shows the insertion loss (S_{21}) measurement plots while figure 4.3(b) shows the return loss (S_{11}) measurement plots. The insertion loss is dominated by the varactor Q as shown in figure 4.3(a). An approximate 200 MHz constant bandwidth is maintained across the entire centre frequency tuning range by varying voltage V_{D3} as shown in figure 4.3.

The filter has the added functionality of a fixed centre frequency and variable bandwidth. The 3 dB bandwidth is tuned for a centre frequency of 4.7 GHz. Figure 4.4(a) shows S_{11} plots while figure 4.4(b) shows the S_{21} plots for a -3 dB bandwidth variation from 180 MHZ to 250 MHz. A deviation of 28 % in bandwidth is achieved with insertion loss minimizing from -4.4 dB to -3.74 dB while return loss improving from -12 dB to -25 dB as the bandwidth is tuned from 180 MHz to 250 MHz. As the bandwidth is tuned, there is negligible change in the filter centre frequency. Figure 4.5 shows the fabricated second order filter.

4.2   Third Order Filter Without EX-Q Tuning Using NI

4.2.1   Third order filter design

Using the synthesis design steps presented in section 3.4.1, a third order filter is designed at a centre frequency f_0 of 4.6 GHz with fractional bandwidth of 5% on a Chebyshev function with 0.1 dB ripple.

1. Using design step 1, the following values are calculated $k_{12} = 0.04595$, $k_{23} = 0.04595$, $Q_e = 20.632$.

2. Using design step 2 and utilizing susceptance slope parameter $\beta = 0.0314$ mhos, pi-admittance inverter constants $B_{12} = 0.001422$ and $B_{23} = 0.001422$ are calculated.

3. Choosing $Y_0 = 0.02$ mhos (corresponding to 50 ohm line), utilizing design equation 3.16, $B'_{12} = 0.0055$ and $B'_{23} = 0.0055$ are calculated.

4. Using design equation 3.11, parameters $\theta_{12} = 74.62°$ and $\theta_{23} = 74.62°$ are calculated.

5. As discussed previously, synthesized electrical length θ is sum of node length θ' and initial variable susceptance $B_{var} = \omega_0 C_{var}$ offered by the varactor diodes. Utilizing the values of the derived parameters in the earlier steps and choosing $Y'_0 = 0.02$ mhos (corresponding to 50 ohm), design parameters θ' and C_{var} required for the coupling coefficient k are plotted using equation 3.22 as shown in the graph of figure 4.6. The graph of figure 4.6 gives values of θ' and initial capacitance C_{var} offered by varactor diodes which can be utilized to implement the required $k_{12} = 0.04595$. Skyworks SMV 1405 varactor diodes ($Ct \sim 0.63 - 2.67$ pF, Rs $= 0.8$ ohms) from Skyworks are utilized to implement variable capacitances C_{var} attached to the NI. For initial capacitance of $C_{var} = 0.63$ pF offered by Skyworks SMV 1405 varactor diodes, $\theta'_{12} = 20°$ and $\theta'_{23} = 20°$ is selected to implement the NI using figure 4.6.

With this step, the design of an equivalent NI inverter to be implemented in a half-wavelength microstrip resonator based third order filter is complete.

The layout of the filter is shown in figure 4.7. The filter is fabricated on Rogers RO 4003C substrate with relative dielectric constant $\varepsilon_r = 3.38$ and loss tangent $\tan\delta$ of 0.0027. The substrate thickness is 0.508 mm. In order to utilize the complete tuning range of the varactor diodes, all the varactors in the filter design, either on the resonators or on the NI are simulated at their minimum initial capacitance value. The calculated parameter values using circuit model are utilized and parameter sweeps are performed to calculate the filter dimensions for the desired filter response. The finalized filter design parameters are $L_1 = 28$ mm, $W_1 = 1.1558$ mm, $S_1 = 0.2$ mm, $L_2 = 16.86$ mm, $W_2 = 1.155$ mm, $L_3 = L_4 = 2$ mm, $W_3 = W_4 = 1.15$ mm and $S_2 = S_3 = 0.2568$ mm. The dimensions of the filter are 18x44 mm. The electromagnetic model of the filter is developed in CST while ADS is used to add the spice parameters of the varactor diodes in order to consider all the parasitic effects and losses.
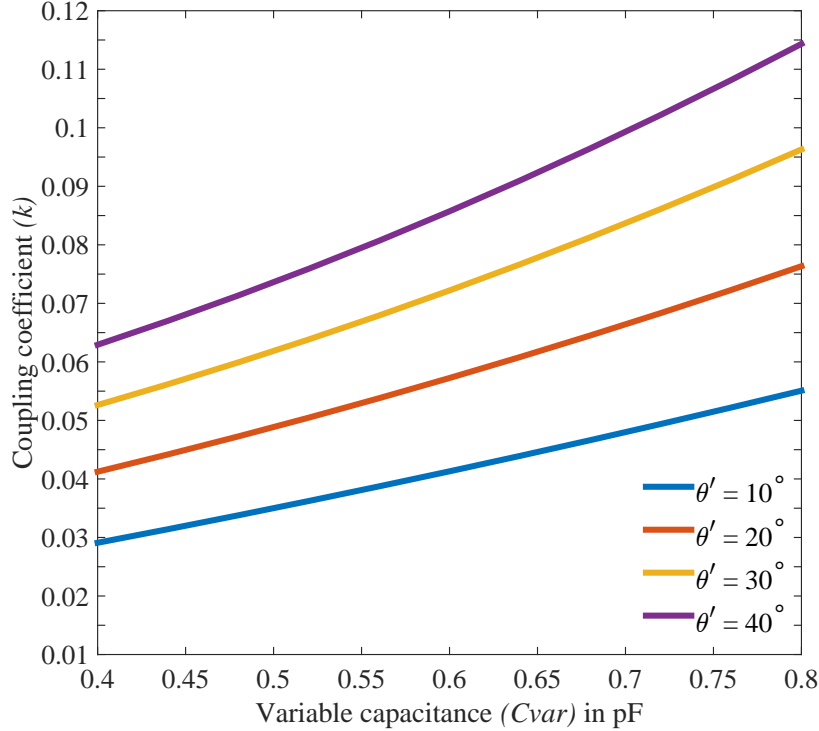
Figure 4.6: NI parameters for the third order filter $B' = 0.0055$

MA46H120 varactor diodes ($Ct \sim 0.14-1$ pF, Rs = 0.8 ohms) from MACOM technology solutions are utilized to implement diodes D_1, D_2, D_3, D_4, D_5 and D_6 while Skyworks SMV 1405 varactor diodes ($Ct \sim 0.63-2.67$ pF, Rs = 0.8 ohms) are utilized to implement diodes D_7-D_{10} [95]. Spatial biasing with 0.4 mm vias and bias resistance of 10 Kilo-ohms is used to connect the DC power supply. The central vias on the resonators and on the NI act as RF chokes because of their inductive nature. The 10 Kilo-ohms resistance act as an additional RF choke.
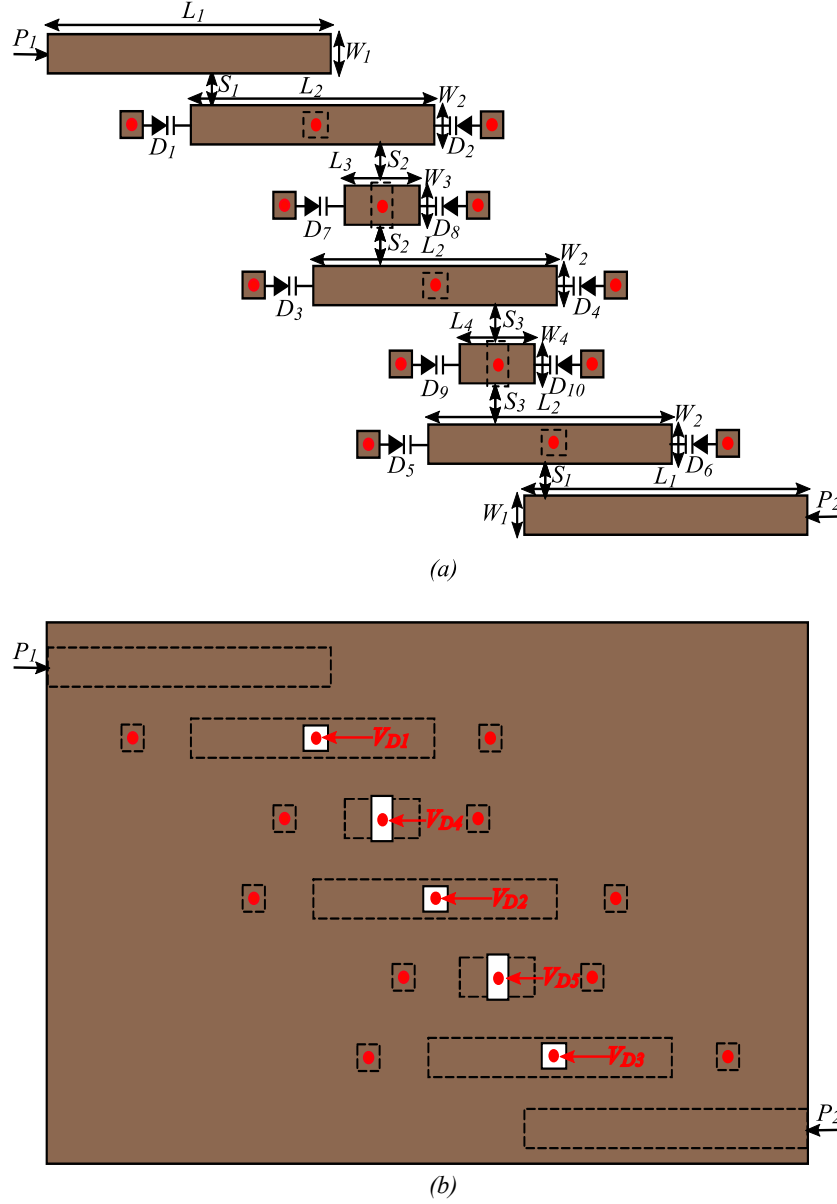
Figure 4.7: Third order filter (a) top view (b) bottom view

4.2.2   Third order filter measurements

The centre frequency of the filter is tuned from 3.54 to 4.54 GHz utilizing diodes $D_1 - D_6$ by providing the bias voltage $V_{D1} - V_{D3}$ in the range 0-12 V. Figure 4.8(a) shows the S_{21} measurement plots while 4.8(b) shows the S_{11} measurement plots. A constant absolute bandwidth of 210 MHz is maintained across the entire frequency tuning range by controlling the inter-resonator coupling using diodes $D_7 - D_{10}$ operating through $V_{D4} - V_{D5}$ between 0-20 V. The measured insertion loss is in the range 11.319 - 4.94 dB. The insertion loss is dominated by the varactor Q.

The filter has the added functionality of variable bandwidth at a fixed centre frequency. The 3 dB bandwidth is tuned for a fixed centre frequency of 5.2 GHz. Figure 4.9 shows S_{11} plots for a bandwidth variation from 207.6 MHZ to 281.81 MHz. A deviation of 26 % in bandwidth is achieved with improvement in both return loss and insertion loss. For

the bandwidth tuning as discussed, the varactor diodes on the resonators were removed specifically to study the change in the filter centre frequency while tuning the bandwidth. It can be observed from figure 4.9 that as the bandwidth is tuned, there is negligible change in the filter centre frequency giving independent control of the bandwidth. Figure 4.10 shows the fabricated third order filter.
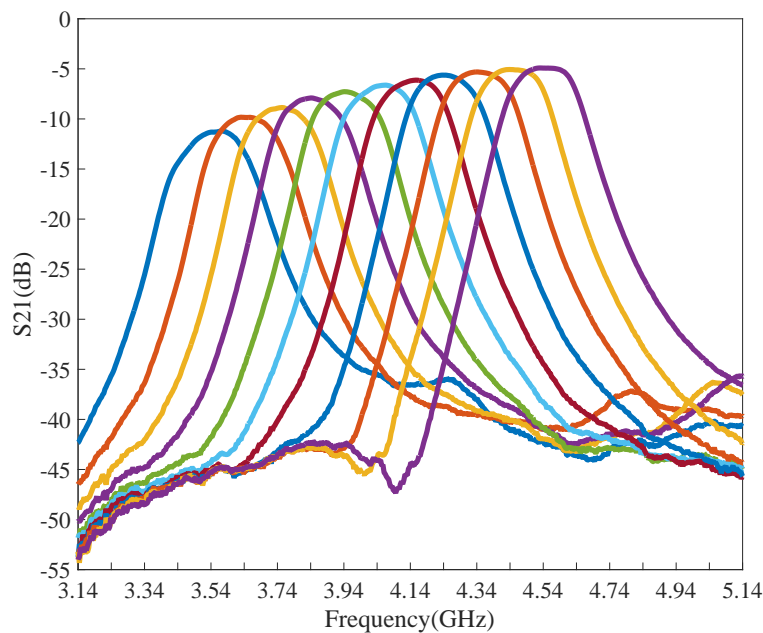
(a) Third order filter S_{21} (dB) vs frequency (GHz) measurements
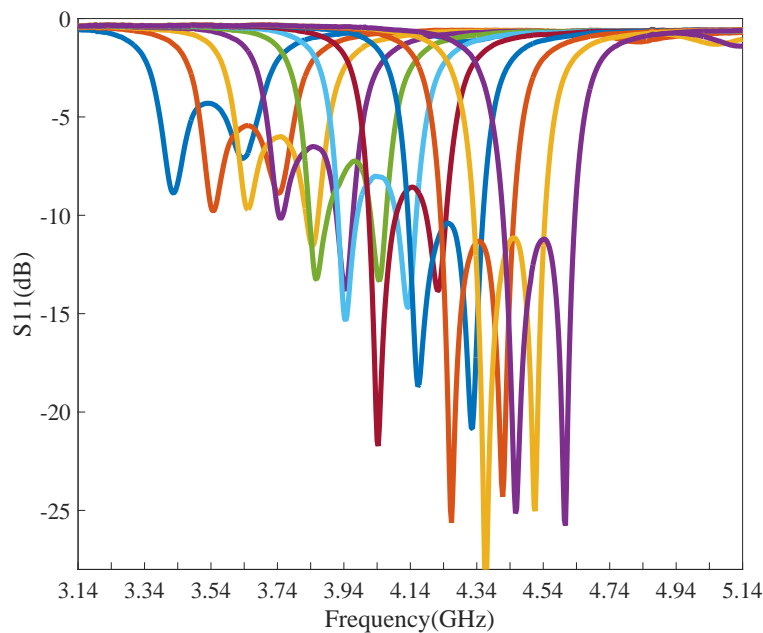
(b) Third order filter S_{11} (dB) vs frequency (GHz) measurements

Figure 4.8: Third order filter measurements
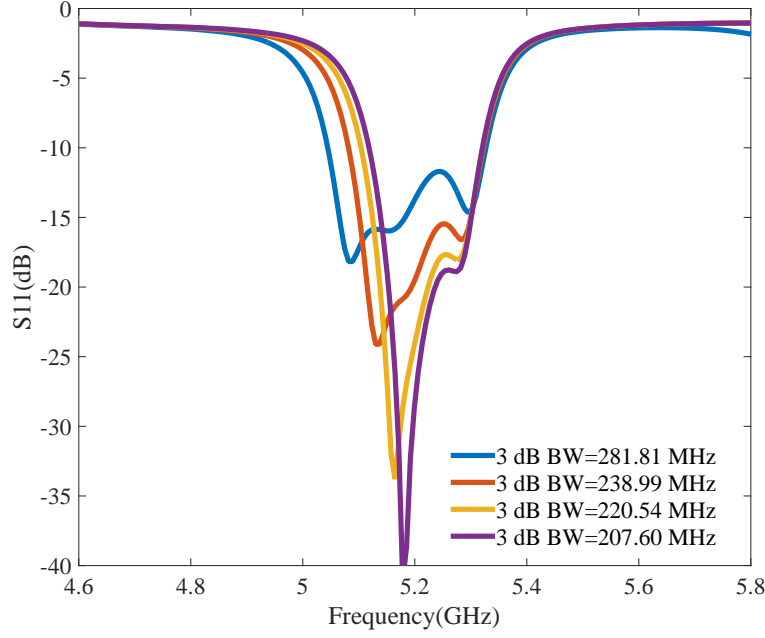
Figure 4.9: Third order filter bandwidth variation at the centre frequency of 5.2 GHz
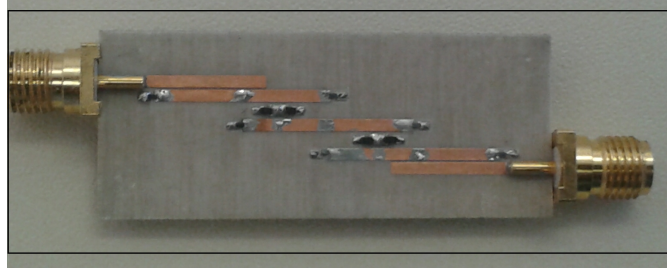
Figure 4.10: Fabricated third order filter

4.3   Third Order Filter With EX-Q Tuning Using NI

4.3.1   Third order filter with EX-Q design

As shown in figure 4.8(a) and 4.8(b), both insertion loss and return loss degrades towards the lower end of the tuning range, though a constant absolute bandwidth is maintained using non-resonant node based inverters (NI). To further investigate the possibility of maintaining a constant return loss and insertion loss response of the filter, the following analysis is performed.

From the coupled resonator filter theory, the external quality factor for filters at the source and the load end is given by

$$Q_e = \frac{g_0 g_1}{\Delta} = \frac{g_n g_{n+1}}{\Delta} \tag{4.1}$$

where g_0, g_1, g_n and g_{n+1} are lowpass prototype element values and Δ is the fractional bandwidth given as,

$$\Delta = \frac{\omega_2 - \omega_1}{\omega_0} = \frac{CBW}{f_0} \tag{4.2}$$

CBW refers to the constant absolute bandwidth and f_0 refers to the centre frequency of the operation of the filter. Considering source end and writing equation 4.1 using equation
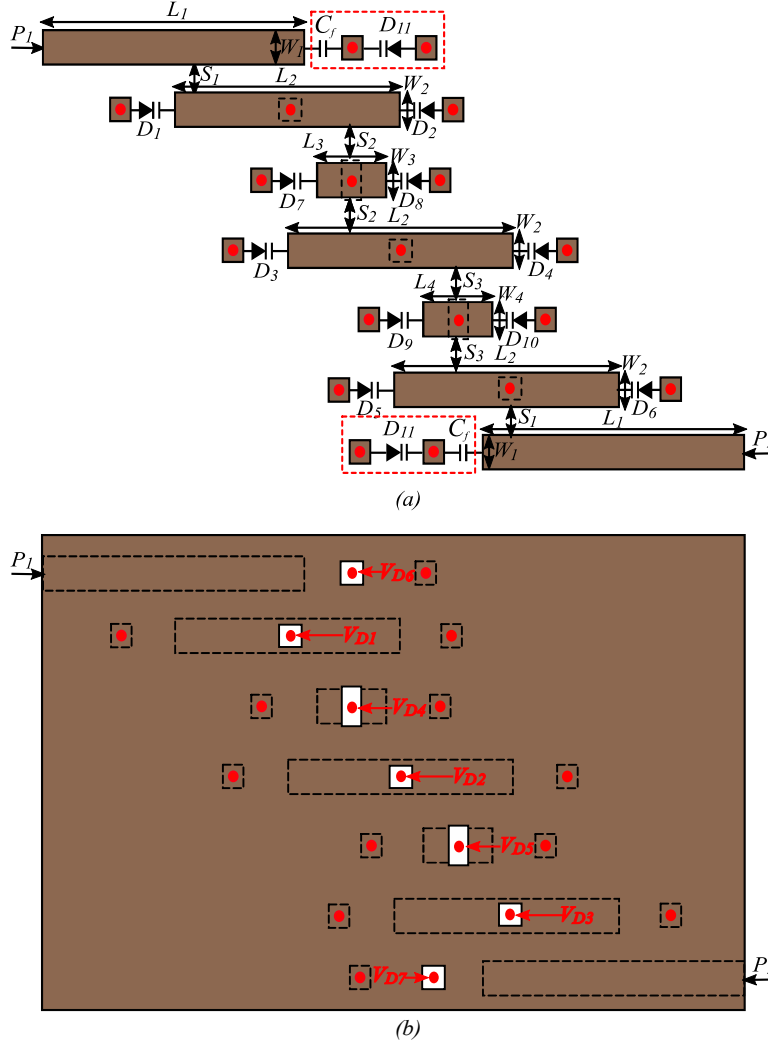
Figure 4.11: Third order filter with Q_e tuning layout (a) Top layout (b) Bottom layout

4.2,

$$Q_e = \frac{g_0 g_1 \omega_0}{CBW} \tag{4.3}$$

External quality factor Q_e can also be written as,

$$Q_e = \frac{\beta}{J_{01}^2/Re(Y_L)} = \frac{\beta Re(Y_L)}{J_{01}^2} \tag{4.4}$$

In the above equation, J_{01} is the input inverter constant between the source port and the first resonator, β refers to the susceptance slope parameter while $Re(Y_L)$ refers to the real part of the terminating port admittance.

To vary the centre frequency of the filter, as the capacitance offered by the varactor diodes attached to the resonators is increased, the centre frequency f_0 of the filter is decreased. From equation 4.3, it can be observed that $Q_e \propto f_0$ while $Q_e \propto 1/CBW$. Towards the lower end of the frequency tuning range, as the centre frequency f_0 is decreased, to maintain a constant absolute bandwidth (CBW), Q_e needs to be decreased. From equation 4.4, it can be further observed that decreased Q_e corresponds to increased external coupling J_{01}. To summarize, towards the lower end of the tuning range, to maintain a constant

absolute bandwidth, there is a need to increase the external coupling between the source port and the first resonator. Similarly, there is a need to increase the external coupling between the load port and the last resonator. In order to increase the external coupling, additional external Q_e tuning circuitry is attached to the designed third order filter as shown by the red dashed box in figure 4.11. The Q_e tuning circuitry comprises of a fixed DC block capacitor C_f and varactor diode. The DC block capacitor has capacitance $C_f = 39$ pF and the varactor diodes MA46H120 ($Ct \sim 0.14 - 1$ pF, Rs = 0.8 ohms) from MACOM are utilized to implement diode D_{11}. Due to the voltage and current distribution on the feed lines, the variable capacitance offered by the varactor diodes D_{11} makes the feed lines appear longer as the capacitance is increased. Towards lower end of the tuning range, by increasing the capacitance offered by varactor diodes D_{11} connected to the feed lines, external coupling can be varied resulting in improved in-band response of the filter.

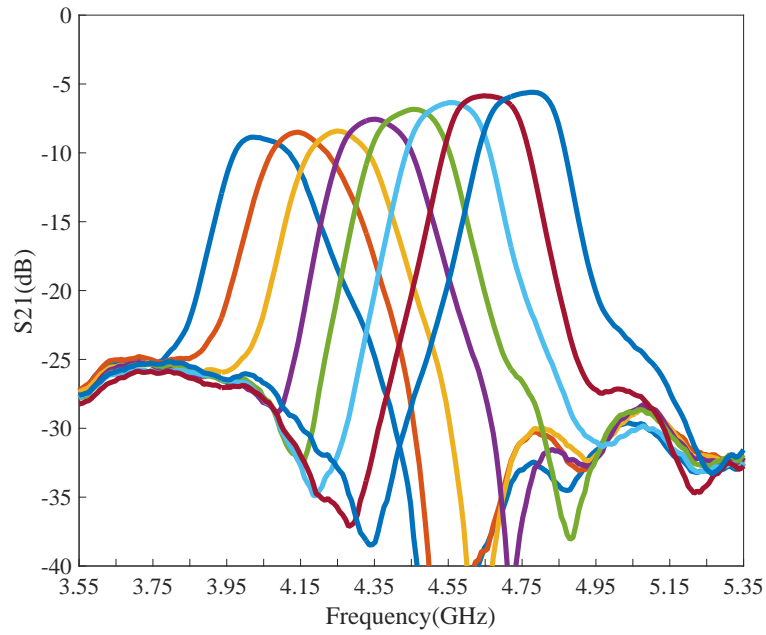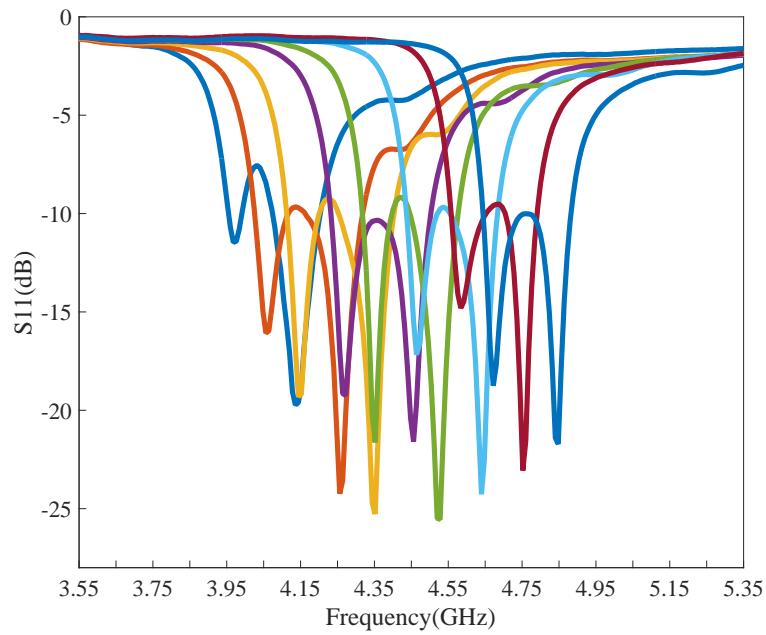### 4.3.2   Third order filter with EX-Q measurements

The additional external quality factor tuning circuit makes the feed lines appear longer due to the initial capacitance offered by the varactor diodes D_{11} and hence a change in the centre frequency f_0 of the filter to 4.75 GHz is observed. The centre frequency of the filter is tuned from 4.05 to 4.75 GHz utilizing diodes $D_1 - D_6$ by providing the bias voltage $V_{D1} - V_{D3}$ in the range 0-20 V. A constant absolute bandwidth of 210 MHz is maintained across the entire centre frequency tuning range by controlling the inter-resonator coupling using diodes $D_7 - D_{10}$ operating through voltages $V_{D4} - V_{D5}$ between 0-25 V. The measured insertion loss is in the range 8.9-5.6 dB as shown by figure 4.12(a). The insertion loss is dominated by the varactor Q. Figure 4.12(b) shows the return loss measurement plots and a constant return loss of -10 dB is maintained across the entire tuning range, as shown in figure 4.12(b).

The wideband measurement plots for the filter are shown in figure 4.13. It can be observed that the presence of the out of band resonance peak observed in simulation results in section 3.3.1 is attenuated. The losses due to quality factor of the varactor diodes and substrate losses attenuates the out of band peak and does not effect the in-band response.

The filter has the added functionality of a fixed centre frequency and a variable bandwidth. The 3 dB bandwidth is tuned for a centre frequency of 4.65 GHz. Figure 4.14 shows S_{11} plots for a bandwidth variation from 170 MHz to 230 MHz. A constant return loss of -10 dB is maintained using the external Q_e tuning circuit as the bandwidth of the filter is varied. The fabricated filter is shown in figure 4.15.

4.4   Conclusion

In this chapter, the theory developed to design microstrip filters using NI is utilized to design filter prototypes. The fabricated filters with integrated varactor diodes are measured using a vector network analyzer (VNA). The measured results validates the developed design technique. In the following chapter, final conclusions of the dissertation are presented with recommendations for the future work.

(a) S_{21} (dB) vs frequency (GHz) measurements with Q_e tuning

(b) S_{11} (dB) vs frequency (GHz) measurements with Q_e tuning

Figure 4.12: Measurement plots for the third order filter with Q_e tuning
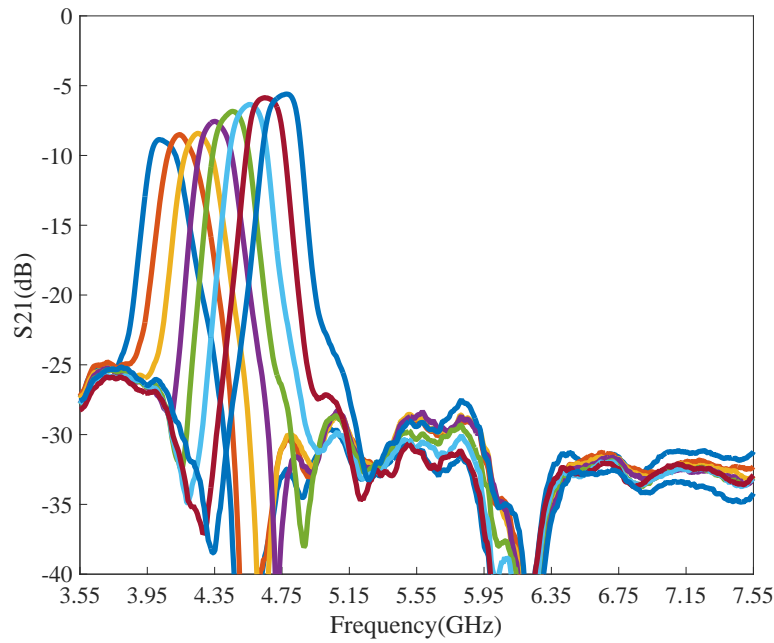
(a) S_{21} (dB) vs frequency (GHz) measurements with Q_e tuning
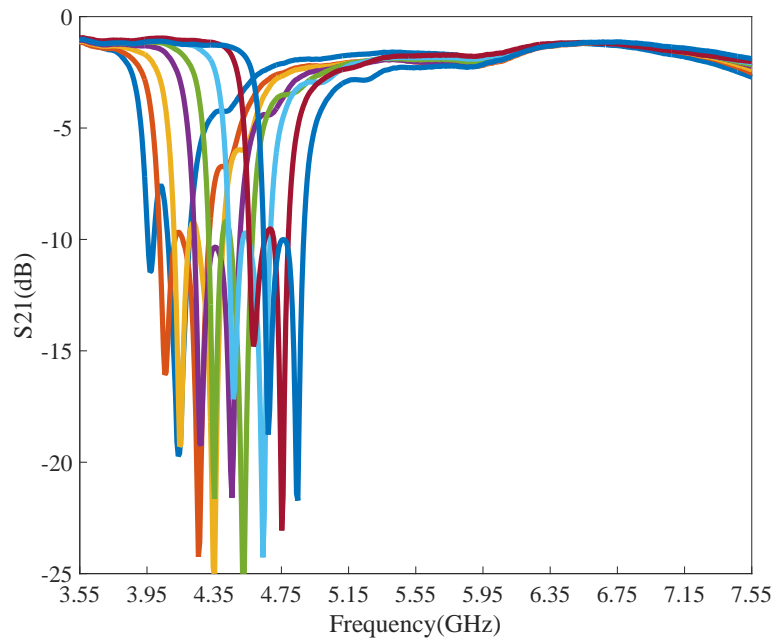
(b) S_{11} (dB) vs frequency (GHz) measurements with Q_e tuning

Figure 4.13: Measurement plots for the third order filter with Q_e tuning (wideband measurements)

Figure 4.14: Third order filter with Q_e tuning bandwidth variation at 4.65 GHz

Figure 4.15: Fabricated third order filter with Q_e tuning

Chapter 5

Conclusion

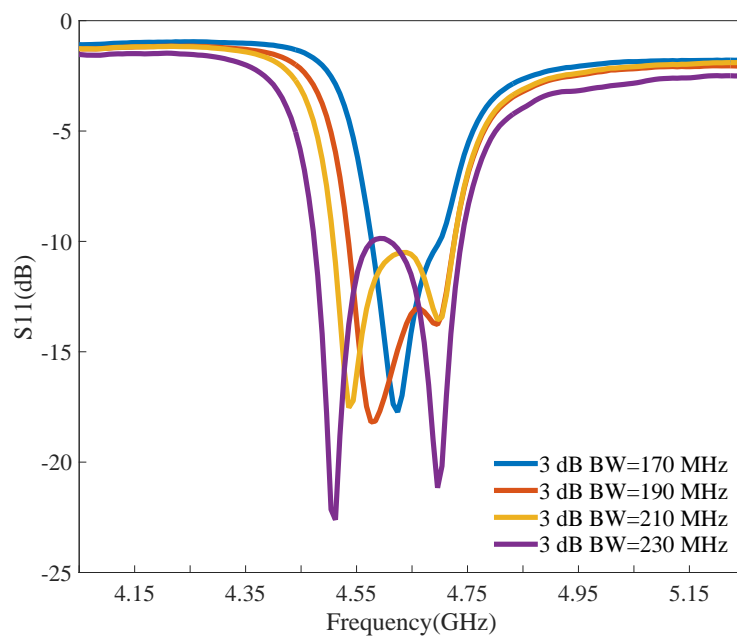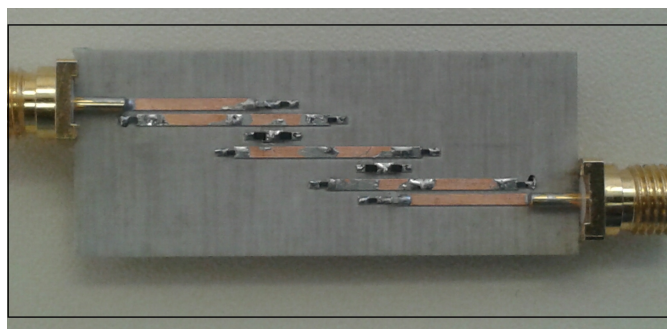In this dissertation, the functionality of non-resonant nodes are investigated and extended for the purpose of controlling the inter-resonator couplings. A novel tunable non-resonant inverter (NI) is presented to design filters with bandwidth control. Systematic design procedures are illustrated with examples in order to design tunable filters based on NI in microstrip and substrate integrated waveguide technologies.

A complete synthesis method is proposed for microstrip implementation of tunable filters with NI. The synthesis method provides filter dimensional parameters for a required filter specification. Design steps are proposed and followed to design three reconfigurable microstrip filters. A second order filter based on NI with constant absolute bandwidth of 200 MHz across centre frequency tuning range of 700 MHz is designed and measured with acceptable ranges of insertion and return losses. A third order filter based on NI with constant absolute bandwidth of 210 MHz with centre frequency tuning range of 1 GHz is designed and measured with acceptable ranges of insertion and return losses. A third order filter based on NI with a circuitry to maintain constant return loss is designed and measured. The filter maintains a constant bandwidth of 210 MHz across centre frequency tuning range of 700 MHz with constant return loss of -10 dB. The proposed NI is further illustrated in substrate integrated waveguide (SIW) technology. A T-ridge pedestal resonator SIW based filter topology is chosen for implementation. Design steps are proposed and a second order T-ridge pedestal SIW filter with bandwidth control is designed and simulated. A bandwidth increase of 31% (200 MHz-262 MHz) is observed at centre frequency of 5.1 GHz, validating the design technique.

The proposed technique offers significant advantages as compared to other design techniques. Most of the reconfigurable filter designs in the present state-of-the-art follow a design through optimization process. The filter dimensional parameters are fixed through optimization iterations for a given filter specification. For a different filter specification, the optimization cycle needs to be followed again. In this dissertation, an attempt is made to provide filter designers with analytical tools in terms of design equations and design charts in order to have an estimate of dimensional requirements to design tunable filters based on NI. This beforehand information would help in reducing the design effort, computational costs and design time. The designed and measured filter prototypes demonstrate the advantage of negligible frequency deviation as the bandwidth is tuned.

The bandwidth control circuitry is completely separated from frequency tuning circuitry which minimizes the losses due to the loading of resonators. In addition, with the use of spatial biasing the need for additional biasing circuitry is eliminated, thus, simplifying the complexity of the design.

The proposed design technique depicts a limitation of an out of band resonance peak. This out of band resonance peak is observed in simulated filters in both microstrip and substrate integrated waveguide (SIW) technologies. The out of band resonance peak is due to the non-resonant node and the ideal capacitor used to simulate the effect of the tuning varactor diodes. However, a significant variation in bandwidth can be achieved by keeping the out of band resonance peak far away from the passband as demonstrated in simulated results. In the same manner, a constant absolute bandwidth can be easily maintained across the entire centre frequency tuning range by keeping the resonance peak far away from filter passband. In the final measurements performed for the prototypes of the designed filters, it is observed that the effect of the out of band peak is negligible because of the losses due to the quality factor of the varactor diodes and substrate losses. The design technique is validated through measured results and can be integrated in practical filter designs.

Future expansion of the current work may include the following:

1. Research efforts can be made in the direction of completely eliminating the out of band resonance peak.

2. The presented filter designs can be expanded to introduce transmission zeros in the stopband for better roll off characteristics.

3. The functionality of the NI can be explored to design filters with adjustable transmission zeros.

4. The proposed NI can be investigated to change the cross couplings i.e. couplings between non-adjacent resonators.

5. Integration of NI based filters in tunable filter banks or tunable multiplexers can be explored.

6. The NI based filter designed in T-ridge SIW topology can be further expanded for simultaneous frequency and bandwidth tuning.

7. Implementation of the proposed NI in different technologies like coaxial, waveguide etc. can be investigated.

Bibliography

[1] S. Courreges, Z. Zhao, K. Choi, A. Hunt, and J. Papapolymerou, "A quasi-elliptic ferroelectric tunable filter for X-band applications," in *2009 European Microwave Conference (EuMC)*, Sept 2009, pp. 1409–1412.

[2] W. Tang and J. S. Hong, "Varactor-Tuned Dual-Mode Bandpass Filters," *IEEE Transactions on Microwave Theory and Techniques*, vol. 58, no. 8, pp. 2213–2219, Aug 2010.

[3] P. W. Wong and I. Hunter, "Electronically Tunable Filters," *IEEE Microwave Magazine*, vol. 10, no. 6, pp. 46–54, Oct 2009.

[4] R. Gomez-Garcia, M. A. Sanchez-Soriano, K. W. Tam, and Q. Xue, "Flexible Filters: Reconfigurable-Bandwidth Bandpass Planar Filters with Ultralarge Tuning Ratio," *IEEE Microwave Magazine*, vol. 15, no. 5, pp. 43–54, July 2014.

[5] J. s. Hong, "Reconfigurable planar filters," *IEEE Microwave Magazine*, vol. 10, no. 6, pp. 73–83, Oct 2009.

[6] Y. H. Chun and J. S. Hong, "Electronically Reconfigurable Dual-ModeMicrostrip Open-Loop Resonator Filter," *IEEE Microwave and Wireless Components Letters*, vol. 18, no. 7, pp. 449–451, July 2008.

[7] G. M. Rebeiz, K. Entesari, I. C. Reines, S. j. Park, M. A. El-tanani, A. Grichener, and A. R. Brown, "Tuning in to RF MEMS," *IEEE Microwave Magazine*, vol. 10, no. 6, pp. 55–72, Oct 2009.

[8] M. Sanchez-Renedo, "High-Selectivity Tunable Planar Combline Filter With Source/Load-Multiresonator Coupling," *IEEE Microwave and Wireless Components Letters*, vol. 17, no. 7, pp. 513–515, July 2007.

[9] M. A. El-Tanani and G. M. Rebeiz, "High-Performance 1.5-2.5-GHz RF-MEMS Tunable Filters for Wireless Applications," *IEEE Transactions on Microwave Theory and Techniques*, vol. 58, no. 6, pp. 1629–1637, June 2010.

[10] J. Nath, D. Ghosh, J. P. Maria, A. I. Kingon, W. Fathelbab, P. D. Franzon, and M. B. Steer, "An electronically tunable microstrip bandpass filter using thin-film Barium-Strontium-Titanate (BST) varactors," *IEEE Transactions on Microwave Theory and Techniques*, vol. 53, no. 9, pp. 2707–2712, Sept 2005.

[11] P. W. Wong and I. C. Hunter, "A New Class of Low-Loss High-Linearity Electronically Reconfigurable Microwave Filter," *IEEE Transactions on Microwave Theory and Techniques*, vol. 56, no. 8, pp. 1945–1953, Aug 2008.

[12] L. Athukorala and D. Budimir, "Compact Second-Order Highly Linear Varactor-Tuned Dual-Mode Filters With Constant Bandwidth," *IEEE Transactions on Microwave Theory and Techniques*, vol. 59, no. 9, pp. 2214–2220, Sept 2011.

[13] P. W. Wong and I. C. Hunter, "Electronically Reconfigurable Microwave Bandpass Filter," *IEEE Transactions on Microwave Theory and Techniques*, vol. 57, no. 12, pp. 3070–3079, Dec 2009.

[14] I. Reines, A. Brown, M. El-Tanani, A. Grichener, and G. Rebeiz, "1.6-2.4 GHz RF MEMS tunable 3-pole suspended combline filter," in *2008 IEEE MTT-S International Microwave Symposium Digest*, June 2008, pp. 133–136.

[15] X. Y. Zhang and Q. Xue, "High-Selectivity Tunable Bandpass Filters With Harmonic Suppression," *IEEE Transactions on Microwave Theory and Techniques*, vol. 58, no. 4, pp. 964–969, April 2010.

[16] I. Lockerbie and S. Kumar, "A broadband tunable combline filter using active devices," in *IEEE WESCANEX 93 Communications, Computers and Power in the Modern Environment - Conference Proceedings*, 1993, pp. 196–200.

[17] S. R. Chandler, I. C. Hunter, and J. G. Gardiner, "Active varactor tunable bandpass filter," *IEEE Microwave and Guided Wave Letters*, vol. 3, no. 3, pp. 70–71, March 1993.

[18] C. Rauscher, "Varactor-tuned active notch filter with low passband noise and signal distortion," *IEEE Transactions on Microwave Theory and Techniques*, vol. 49, no. 8, pp. 1431–1437, Aug 2001.

[19] H. Trabelsi and C. Cruchon, "A varactor-tuned active microwave bandpass filter," *IEEE Microwave and Guided Wave Letters*, vol. 2, no. 6, pp. 231–232, June 1992.

[20] C. Y. Chang and T. Itoh, "Microwave active filters based on coupled negative resistance method," *IEEE Transactions on Microwave Theory and Techniques*, vol. 38, no. 12, pp. 1879–1884, Dec 1990.

[21] Y. C. Chiou and G. M. Rebeiz, "A Quasi Elliptic Function 1.75-2.25 GHz 3-Pole Bandpass Filter With Bandwidth Control," *IEEE Transactions on Microwave Theory and Techniques*, vol. 60, no. 2, pp. 244–249, Feb 2012.

[22] ——, "A Tunable Three-Pole 1.5-2.2-GHz Bandpass Filter With Bandwidth and Transmission Zero Control," *IEEE Transactions on Microwave Theory and Techniques*, vol. 59, no. 11, pp. 2872–2878, Nov 2011.

[23] B.-W. Kim and S.-W. Yun, "Varactor-tuned combline bandpass filter using step-impedance microstrip lines," *IEEE Transactions on Microwave Theory and Techniques*, vol. 52, no. 4, pp. 1279–1283, April 2004.

[24] X. G. Wang, Y. H. Cho, and S. W. Yun, "A Tunable Combline Bandpass Filter Loaded With Series Resonator," *IEEE Transactions on Microwave Theory and Techniques*, vol. 60, no. 6, pp. 1569–1576, June 2012.

[25] M. Sanchez-Renedo, R. Gomez-Garcia, J. I. Alonso, and C. Briso-Rodriguez, "Tunable combline filter with continuous control of center frequency and bandwidth," *IEEE Transactions on Microwave Theory and Techniques*, vol. 53, no. 1, pp. 191–199, Jan 2005.

[26] M. A. El-Tanani and G. M. Rebeiz, "Corrugated Microstrip Coupled Lines for Constant Absolute Bandwidth Tunable Filters," *IEEE Transactions on Microwave Theory and Techniques*, vol. 58, no. 4, pp. 956–963, April 2010.

[27] S. J. Park and G. M. Rebeiz, "Low-Loss Two-Pole Tunable Filters With Three Different Predefined Bandwidth Characteristics," *IEEE Transactions on Microwave Theory and Techniques*, vol. 56, no. 5, pp. 1137–1148, May 2008.

[28] F. Lin and M. R. Zadeh, "Continuously Tunable 0.55-1.9-GHz Bandpass Filter With a Constant Bandwidth Using Switchable Varactor-Tuned Resonators," *IEEE Transactions on Microwave Theory and Techniques*, vol. 65, no. 3, pp. 792–803, March 2017.

[29] S. Arain, P. Vryonides, M. A. B. Abbasi, A. Quddious, M. A. Antoniades, and S. Nikolaou, "Reconfigurable Bandwidth Bandpass Filter With Enhanced Out-of-Band Rejection Using pi -Section-Loaded Ring Resonator," *IEEE Microwave and Wireless Components Letters*, vol. 28, no. 1, pp. 28–30, Jan 2018.

[30] Z. Zhao, J. Chen, L. Yang, and K. Chen, "Three-Pole Tunable Filters With Constant Bandwidth Using Mixed Combline and Split-Ring Resonators," *IEEE Microwave and Wireless Components Letters*, vol. 24, no. 10, pp. 671–673, Oct 2014.

[31] T. Cheng and K. W. Tam, "A Wideband Bandpass Filter With Reconfigurable Bandwidth Based on Cross-Shaped Resonator," *IEEE Microwave and Wireless Components Letters*, vol. 27, no. 10, pp. 909–911, Oct 2017.

[32] C. Schuster, A. Wiens, F. Schmidt, M. Nickel, M. Schubler, R. Jakoby, and H. Maune, "Performance Analysis of Reconfigurable Bandpass Filters With Continuously Tunable Center Frequency and Bandwidth," *IEEE Transactions on Microwave Theory and Techniques*, vol. 65, no. 11, pp. 4572–4583, Nov 2017.

[33] V. Sekar, M. Armendariz, and K. Entesari, "A 1.2 -1.6-GHz Substrate-Integrated-Waveguide RF MEMS Tunable Filter," *IEEE Transactions on Microwave Theory and Techniques*, vol. 59, no. 4, pp. 866–876, April 2011.

[34] C. Arnold, J. Parlebas, and T. Zwick, "Reconfigurable Waveguide Filter with Variable Bandwidth and Center Frequency," *IEEE Transactions on Microwave Theory and Techniques*, vol. 62, no. 8, pp. 1663–1670, Aug 2014.

[35] H. Joshi, H. H. Sigmarsson, S. Moon, D. Peroulis, and W. J. Chappell, "High-Q Fully Reconfigurable Tunable Bandpass Filters," *IEEE Transactions on Microwave Theory and Techniques*, vol. 57, no. 12, pp. 3525–3533, Dec 2009.

[36] K. Kawai, H. Okazaki, and S. Narahashi, "Center frequency and bandwidth independently tunable filter using MEMS digitally tunable capacitors," in *2014 XXXIth URSI General Assembly and Scientific Symposium (URSI GASS)*, Aug 2014, pp. 1–4.

[37] ——, "Ring resonators for bandwidth and center frequency tunable filter," in *2007 European Microwave Conference*, Oct 2007, pp. 298–301.

[38] C. Lugo, D. Thompson, and J. Papapolymerou, "Reconfigurable Bandpass Filter with Variable Bandwidth at 5.8 GHz Using a Capacitive Gap Variation Technique," in *2003 33rd European Microwave Conference*, Oct 2003, pp. 923–926.

[39] A. Miller and J. S. Hong, "Wideband Bandpass Filter With Reconfigurable Bandwidth," *IEEE Microwave and Wireless Components Letters*, vol. 20, no. 1, pp. 28–30, Jan 2010.

[40] C. Rauscher, "Reconfigurable bandpass filter with a three-to-one switchable passband width," *IEEE Transactions on Microwave Theory and Techniques*, vol. 51, no. 2, pp. 573–577, Feb 2003.

[41] Y. B. Zhang, F. L. Yu, and X. Y. Zhang, "Design of center frequency and bandwidth tunable bandpass filter," in *2012 International Conference on Microwave and Millimeter Wave Technology (ICMMT)*, vol. 5, May 2012, pp. 1–4.

[42] M. Ninic, B. Jokanovic, and P. Meyer, "Reconfigurable Multi-State Composite Split-Ring Resonators," *IEEE Microwave and Wireless Components Letters*, vol. 26, no. 4, pp. 267–269, April 2016.

[43] A. I. Abunjaileh and I. C. Hunter, "Tunable Bandpass and Bandstop Filters Based on Dual-Band Combline Structures," *IEEE Transactions on Microwave Theory and Techniques*, vol. 58, no. 12, pp. 3710–3719, Dec 2010.

[44] R. Cameron, R. Mansour, and C. Kudsia, *Microwave Filters for Communication Systems: Fundamentals, Design and Applications*. Wiley, 2007. [Online]. Available: https://books.google.co.za/books?id=GyVTAAAAMAAJ

[45] J. Rhodes, *Theory of Electrical Filters*, ser. A Wiley-Interscience Publication. Wiley, 1976. [Online]. Available: https://books.google.co.za/books?id=DsSaQgAACAAJ

[46] I. Hunter, *Theory and Design of Microwave Filters*, ser. Electromagnetics and Radar Series. Institution of Engineering and Technology, 2001. [Online]. Available: https://books.google.co.za/books?id=4dOYvsZ6uDQC

[47] R. J. Cameron, "General coupling matrix synthesis methods for Chebyshev filtering functions," *IEEE Transactions on Microwave Theory and Techniques*, vol. 47, no. 4, pp. 433–442, Apr 1999.

[48] L. Weinberg, "Additional tables for design of optimum ladder networks," *Journal of the Franklin Institute*, vol. 264, no. 1, pp. 7 – 23, 1957. [Online]. Available: http://www.sciencedirect.com/science/article/pii/0016003257908438

[49] A. Zverev, *Handbook of filter synthesis.* Wiley, 1967. [Online]. Available: https://books.google.co.za/books?id=8SBTAAAAMAAJ

[50] G. Matthaei, L. Young, and E. Jones, *Microwave Filters, Impedance-matching Networks, and Coupling Structures*, ser. Artech House microwave library. Artech House Books, 1980. [Online]. Available: https://books.google.co.za/books?id=cRMoAQAAMAAJ

[51] J. Hong, *Microstrip Filters for RF / Microwave Applications*, ser. Wiley Series in Microwave and Optical Engineering. Wiley, 2011. [Online]. Available: https://books.google.co.za/books?id=Z4sZCf97j_0C

[52] D. R. Jachowski, "Compact, frequency-agile, absorptive bandstop filters," in *IEEE MTT-S International Microwave Symposium Digest, 2005.*, June 2005, pp. 4 pp.–.

[53] K. K. M. Cheng and M. C. J. Chik, "A Frequency-Compensated Rat-Race Coupler With Wide Bandwidth and Tunable Power Dividing Ratio," *IEEE Transactions on Microwave Theory and Techniques*, vol. 61, no. 8, pp. 2841–2847, Aug 2013.

[54] F. A. Miranda, G. Subramanyam, F. W. van Keuls, R. R. Romanofsky, J. D. Warner, and C. H. Mueller, "Design and development of ferroelectric tunable microwave components for Kuand K-band satellite communication systems," *IEEE Transactions on Microwave Theory and Techniques*, vol. 48, no. 7, pp. 1181–1189, Jul 2000.

[55] P. M. Suherman, T. J. Jackson, Y. Y. Tse, I. P. Jones, R. I. Chakalova, M. J. Lancaster, and A. Porch, "Microwave properties of Ba0.5Sr0.5TiO3 thin film coplanar phase shifters," *Journal of Applied Physics*, vol. 99, no. 10, p. 104101, 2006. [Online]. Available: https://doi.org/10.1063/1.2198933

[56] Y.-H. Chun, J.-S. Hong, P. Bao, T. J. Jackson, and M. J. Lancaster, "BST varactor tuned bandstop filter with slotted ground structure," in *2008 IEEE MTT-S International Microwave Symposium Digest*, June 2008, pp. 1115–1118.

[57] G. Rebeiz, *RF MEMS: Theory, Design, and Technology.* Wiley, 2004. [Online]. Available: https://books.google.co.za/books?id=A7728XHtmzAC

[58] D. Peroulis, S. Pacheco, K. Sarabandi, and L. P. B. Katehi, "Tunable lumped components with applications to reconfigurable MEMS filters," in *2001 IEEE MTT-S International Microwave Sympsoium Digest (Cat. No.01CH37157)*, vol. 1, May 2001, pp. 341–344 vol.1.

[59] B. Zabdiel, L. Ignacio, and P. Lluis, "Precise frequency and bandwidth control of microstrip switchable bandstop filters," *Microwave and Optical Technology Letters*, vol. 51, no. 11, pp. 2573–2578. [Online]. Available: https://onlinelibrary.wiley.com/doi/abs/10.1002/mop.24679

[60] J. D. Rhodes, "The Generalized Direct-Coupled Cavity Linear Phase Filter," *IEEE Transactions on Microwave Theory and Techniques*, vol. 18, no. 6, pp. 308–313, Jun 1970.

[61] S. A. Alseyab, "A Novel Class of Generalized Chebyshev Low-Pass Prototype for Suspended Substrate Stripline Filters," *IEEE Transactions on Microwave Theory and Techniques*, vol. 30, no. 9, pp. 1341–1347, Sep 1982.

[62] J. D. Rhodes and R. J. Cameron, "General Extracted Pole Synthesis Technique with Applications to Low-Loss TE011 Mode Filters," *IEEE Transactions on Microwave Theory and Techniques*, vol. 28, no. 9, pp. 1018–1028, Sep 1980.

[63] G. Macchiarella, "Synthesis of prototype filters with triplet sections starting from source and load," *IEEE Microwave and Wireless Components Letters*, vol. 12, no. 2, pp. 42–44, Feb 2002.

[64] ——, "Synthesis of an in-line prototype filter with two transmission zeros without cross couplings," *IEEE Microwave and Wireless Components Letters*, vol. 14, no. 1, pp. 19–21, Jan 2004.

[65] G. Macchiarella and M. Fumagalli, "Inline comb filters with one or two transmission zeros," in *2004 IEEE MTT-S International Microwave Symposium Digest (IEEE Cat. No.04CH37535)*, vol. 2, June 2004, pp. 1085–1088 Vol.2.

[66] S. Amari and U. Rosenberg, "Synthesis and design of novel in-line filters with one or two real transmission zeros," *IEEE Transactions on Microwave Theory and Techniques*, vol. 52, no. 5, pp. 1464–1478, May 2004.

[67] S. Amari, U. Rosenberg, and J. Bornemann, "Singlets, cascaded singlets, and the nonresonating node model for advanced modular design of elliptic filters," *IEEE Microwave and Wireless Components Letters*, vol. 14, no. 5, pp. 237–239, May 2004.

[68] Y. H. Cho and G. M. Rebeiz, "Two- and Four-Pole Tunable 0.7-1.1-GHz Bandpass-to-Bandstop Filters With Bandwidth Control," *IEEE Transactions on Microwave Theory and Techniques*, vol. 62, no. 3, pp. 457–463, March 2014.

[69] D. Pozar, *Microwave Engineering*. Wiley, 2004. [Online]. Available: https://books.google.co.za/books?id=4wzpQwAACAAJ

[70] J. B. Ness, "A unified approach to the design, measurement, and tuning of coupled-resonator filters," *IEEE Transactions on Microwave Theory and Techniques*, vol. 46, no. 4, pp. 343–351, Apr 1998.

[71] Y. Cassivi, L. Perregrini, P. Arcioni, M. Bressan, K. Wu, and G. Conciauro, "Dispersion characteristics of substrate integrated rectangular waveguide," *IEEE Microwave and Wireless Components Letters*, vol. 12, no. 9, pp. 333–335, Sept 2002.

[72] Y. Cassivi, L. Perregrini, K. Wu, and G. Conciauro, "Low-Cost and High-Q Millimeter-Wave Resonator Using Substrate Integrated Waveguide Technique," in *2002 32nd European Microwave Conference*, Sept 2002, pp. 1–4.

[73] J. R. Bray and L. Roy, "Resonant frequencies of post-wall waveguide cavities," *IEE Proceedings - Microwaves, Antennas and Propagation*, vol. 150, no. 5, pp. 365–368, Oct 2003.

[74] D. Deslandes and K. Wu, "Millimeter-wave substrate integrated waveguide filters," in *CCECE 2003 - Canadian Conference on Electrical and Computer Engineering. Toward a Caring and Humane Technology (Cat. No.03CH37436)*, vol. 3, May 2003, pp. 1917–1920 vol.3.

[75] K. Wu, D. Deslandes, and Y. Cassivi, "The substrate integrated circuits - a new concept for high-frequency electronics and optoelectronics," in *6th International Conference on Telecommunications in Modern Satellite, Cable and Broadcasting Service, 2003. TELSIKS 2003.*, vol. 1, Oct 2003, pp. P–III–P–X vol.1.

[76] F. Xu and K. Wu, "Guided-wave and leakage characteristics of substrate integrated waveguide," *IEEE Transactions on Microwave Theory and Techniques*, vol. 53, no. 1, pp. 66–73, Jan 2005.

[77] Y. L. Zhang, W. Hong, K. Wu, J. X. Chen, and H. J. Tang, "Novel substrate integrated waveguide cavity filter with defected ground structure," *IEEE Transactions on Microwave Theory and Techniques*, vol. 53, no. 4, pp. 1280–1287, April 2005.

[78] Z. C. Hao, W. Hong, J. X. Chen, X. P. Chen, and K. Wu, "Planar diplexer for microwave integrated circuits," *IEE Proceedings - Microwaves, Antennas and Propagation*, vol. 152, no. 6, pp. 455–459, Dec 2005.

[79] T.-S. Yun, H. Nam, K.-B. Kim, and J.-C. Lee, "Iris waveguide bandpass filter using substrate integrated waveguide (SIW) for satellite communication," in *2005 Asia-Pacific Microwave Conference Proceedings*, vol. 1, Dec 2005, pp. 4 pp.–.

[80] D. Deslandes and K. Wu, "Accurate modeling, wave mechanisms, and design considerations of a substrate integrated waveguide," *IEEE Transactions on Microwave Theory and Techniques*, vol. 54, no. 6, pp. 2516–2526, June 2006.

[81] J. C. Bohorquez, B. Potelon, C. Person, E. Rius, C. Quendo, G. Tanne, and E. Fourn, "Reconfigurable Planar SIW Cavity Resonator and Filter," in *2006 IEEE MTT-S International Microwave Symposium Digest*, June 2006, pp. 947–950.

[82] F. Mira, A. A. S. Blas, V. E. Boria, and B. Gimeno, "Fast and accurate analysis and design of substrate integrated waveguide (SIW) filters," in *2007 European Microwave Conference*, Oct 2007, pp. 170–173.

[83] C. T. Bui, P. Lorenz, M. Saglam, W. Kraemer, and R. H. Jansen, "Investigation of Symmetry Influence in Substrate Integrated Waveguide (SIW) Band-Pass Filters using Symmetric Inductive Posts," in *2008 38th European Microwave Conference*, Oct 2008, pp. 492–495.

[84] X.-P. Chen and K. Wu, "Accurate and efficient design approach of substrate integrated waveguide filter using numerical TRL calibration technique," in *2008 IEEE MTT-S International Microwave Symposium Digest*, June 2008, pp. 1231–1234.

[85] M. Armendariz, V. Sekar, and K. Entesari, "Tunable SIW bandpass filters with PIN diodes," in *The 40th European Microwave Conference*, Sept 2010, pp. 830–833.

[86] M. Salehi and E. Mehrshahi, "A Closed-Form Formula for Dispersion Characteristics of Fundamental SIW Mode," *IEEE Microwave and Wireless Components Letters*, vol. 21, no. 1, pp. 4–6, Jan 2011.

[87] W. Shen, W. Y. Yin, and X. W. Sun, "Miniaturized Dual-Band Substrate Integrated Waveguide Filter With Controllable Bandwidths," *IEEE Microwave and Wireless Components Letters*, vol. 21, no. 8, pp. 418–420, Aug 2011.

[88] S. Adhikari, A. Ghiotto, and K. Wu, "Simultaneous Electric and Magnetic Two-Dimensionally Tuned Parameter-Agile SIW Devices," *IEEE Transactions on Microwave Theory and Techniques*, vol. 61, no. 1, pp. 423–435, Jan 2013.

[89] X. P. Chen and K. Wu, "Substrate Integrated Waveguide Filters: Practical Aspects and Design Considerations," *IEEE Microwave Magazine*, vol. 15, no. 7, pp. 75–83, Nov 2014.

[90] K. Entesari, A. P. Saghati, V. Sekar, and M. Armendariz, "Tunable SIW Structures: Antennas, VCOs, and Filters," *IEEE Microwave Magazine*, vol. 16, no. 5, pp. 34–54, June 2015.

[91] K. Dhwaj, X. Li, Z. Shen, and S. Qin, "Cavity Resonators Do the Trick: A Packaged Substrate Integrated Waveguide, Dual-Band Filter," *IEEE Microwave Magazine*, vol. 17, no. 1, pp. 58–64, Jan 2016.

[92] S. O. Nassar and P. Meyer, "Pedestal substrate integrated waveguide resonators and filters," *IET Microwaves, Antennas Propagation*, vol. 11, no. 6, pp. 804–810, 2017.

[93] E. Botes and P. Meyer, "Spatially decoupled varactor biasing for a tunable staircase filter," *IET Microwaves, Antennas Propagation*, vol. 11, no. 1, pp. 10–16, 2017.

[94] *MA46H120 GaAs varactor diode data sheet*, MACOM Technologies.

[95] *SMV1405 to SMV1430 Series Plastic Packaged Abrupt Junction Tuning Varactorst data sheet*, Skyworks Solutions Inc.